Investigation of the Ca^{2+}-inducible mitochondrial permeability transition pore and Bongkrekate sensitivity in distantly related animal species

Ph.D Thesis

Csaba Konrád, Pharm.D

Semmelweis University
János Szentágothai Doctoral School of Neurosciences

Supervisor:	Dr. Christos Chinopoulos, Associate Professor, Ph.D.
Official reviewers:	Dr. Csaba Sőti, Associate Professor, Ph.D. Dr. Beáta Sperlágh, Deputy Director, Head of Laboratory, Ds.C.
Chairman of the comittee:	Dr. József Mandl, Head of Depratment, Ds.C.
Members of the comittee:	Dr. Tibor Zelles, Associate Professor, Ph.D. Dr. Erzsébet Ligeti, Deputy Head of Depratment, DsC. Dr. László Drahos, Senior Research Fellow, Ph.D.

Budapest
2014

1. List of contents

2. Abbreviations

AD:	Alzheimer’s disease
ADP:	adenosine diphosphate
ALM:	alamethicin
ALS:	Amyothropic lateral sclerosis
ANT:	adenine nucleotide translocator
AP_5A:	diadenosine pentaphosphate
ATP:	adenosine triphosphate
BCECF:	2',7'-Bis-(2-Carboxyethyl)-5-(and-6)-Carboxyfluorescein
BKA:	Bongkrekik acid
BSA:	bovine serum albumin
CaGr 5N:	Calcium Green 5N
cATR:	carboxy-atractyloside
CSA:	cyclosporine A
CypD:	cyclophillin D
DMSO:	dimethyl-sulfoxide
DNP:	2,4-Dinitrophenol
EDTA:	ethylene-diamine-tetraacetic acid
EFTEM:	energy-filtered transmission electron microscopy
EGTA:	ethylene-glycol-tetraacetic acid
ER:	endoplasmatic reticulum
FCCP:	Trifluorocarbonylcyanide Phenylhydrazone
FKBP:	FK506 binding protein
HEPES:	4-(2-hydroxyethyl)-1-piperazineethanesulfonic acid
IMM:	inner mitochondrial membrane
KO:	knock-out
MgGr 5N:	Magnesium Green 5N

mHTT:	Mutated huntingtin protein
$NAD(P)^+$:	nicotinamide-adenine dinucleotide (phosphate)
NMDA:	N-methyl-D-aspartate receptor
OMM:	outer mitochondrial membrane
PGC-1α:	peroxisome proliferator-activated receptor gamma co-activator 1α
pH_{in}:	mitochondrial matrix pH
pH_o:	extramitochondrial pH
P_i:	inorganic phosphate
pmf:	proton-motive force
PT:	permeability transition
PTP:	permeability transition pore
ROS:	reactive oxygen species
SF 6847:	(Tyrphostin 9, RG-50872, Malonaben): 2-[[3,5-bis(1,1-dimethylethyl)-4-hydroxyphenyl]methylene]-propanedinitrile
SOD1:	superoxide dismutase 1, Cu-Zu superoxide dismutase
TEM:	transmission electron microscopy
TSPO:	18 kDa translocator protein
VDAC:	voltage-dependent anion channel
WT:	wild type
ΔpH:	pH gradient across the inner mitochondrial membrane
$\Delta\mu H^+$:	proton electrochemical potential gradient
ΔΨm:	membrane potential

3. Introduction

3.1. General aspects of mitochondria

Mitochondria are the prime source of ATP in the majority of eukaryotes. The energy requirement of the endothermic reaction of converting ADP + P_i to ATP is covered by an electrochemical gradient across the inner mitochondrial membrane (IMM). This electrochemical gradient is maintained by the electron transport chain, which converts the energy from the oxidation of reducing equivalents (NADH + H^+, $FADH_2$) into a proton gradient through pumping mechanisms, from the mitochondrial matrix to the intermembrane space. The electrons finally reduce molecular oxygen, thus the name, terminal oxidation. The consumption of oxygen by mitochondria is termed respiration. The respiratory chain consists of four complexes. Complexes I, III, and IV function as proton pumps, acting as a sequential path for the electron flux. The fall in redox potential of the electrons passing through these complexes is used to generate a proton electrochemical potential gradient, $\Delta\mu_{H+}$, usually expressed in electrical potential units of mV as the proton-motive force (Δp, Eq.1) [1].

$$\Delta \mathrm{p}\ (\mathrm{mV}) = \Delta\psi_{\mathrm{m}} - (2.3RT/F)\Delta\mathrm{pH}.$$
$$(\mathrm{At}\ 37^{\circ}\mathrm{C},\ \Delta \mathrm{p} = \Delta\psi_{\mathrm{m}} - 60\Delta\mathrm{pH})$$

Equation 1

Where ΔΨm is the mitochondrial membrane potential and ΔpH is the pH gradient across the inner membrane (conventionally the matrix is referenced to the intermembrane space), and R, T and F refer to the gas constant (8.31 J/(mol*K)), the absolute temperature (310.15 K in human), and the Faraday constant ($9.65*10^4$ C/mol), respectively. Under most conditions, ΔΨm is the dominant component of Δp, accounting for 150–180 mV of the total proton-motive force of 200–220 mV, in energized, non-phosphorylating isolated mitochondria [3, 4]. The ΔΨm of mitochondria within cells is lower, as it is being utilized

by energy demanding processes. In cultured rat cortical neurons it follows a Gaussian distribution, ranging from -108 to -158 mV, with an average of -139 mV at rest [5].

The respiration generated proton-motive force drives the phosphorylation of ADP into ATP, in functional mitochondria by the F_oF_1-ATP synthase, residing in the IMM. This protein complex has a proton channel activity, and while allowing a flow of protons into the matrix, converts the pmf into kinetic energy by spinning a central shaft in the molecule which serves as a flexible coupling that transfers the kinetic energy causing conformational changes in the active site, and driving the endothermic reaction of phosphorylation yielding ATP. The less the consumption of the pmf by other processes is, the more tightly respiration and phosphorylation are coupled. Fig. 1 demonstrates the path of electrons and protons in the process of oxidative phosphorylation, through the respiratory complexes and the F_oF_1-ATP synthase.

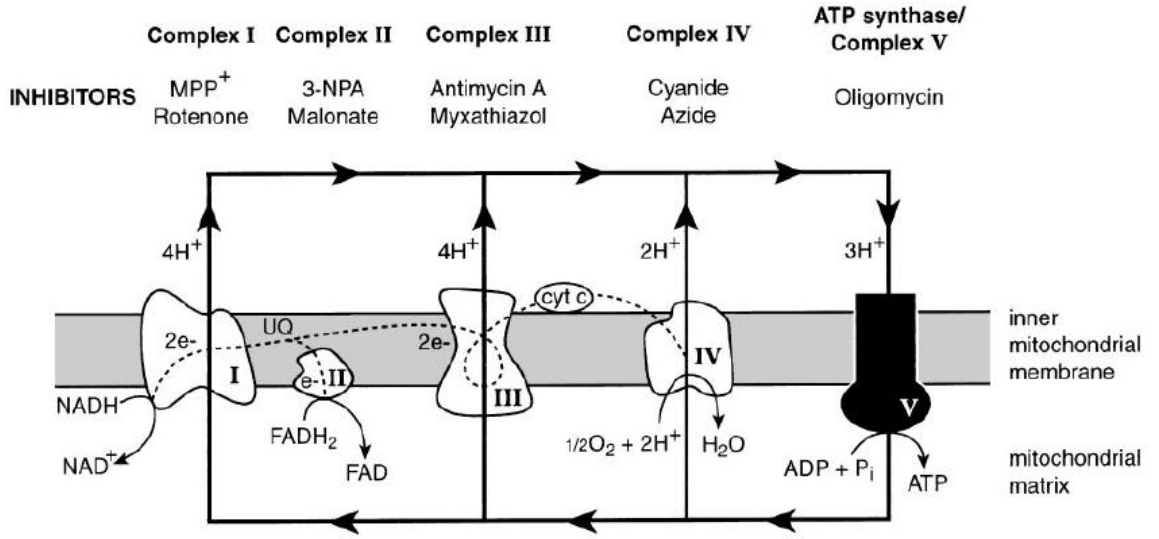

Figure 1: The flow of electrons and protons through the respiratory complexes. Reproduced from [1]; no permission required.

A variety of substances, categorized as uncouplers, such as Trifluorocarbonylcyanide Phenylhydrazone (FCCP), 2,4-Dinitrophenol (DNP) or SF6847 (Tyrphostin 9), are capable of dissipating the pmf by increasing the proton permeability of the IMM. The idea of the two reactions being coupled by an electrochemical gradient originates from Peter Mitchell,

in 1961 [6]. The coupled reaction is termed oxidative phosphorylation, and is quantified by a dimensionless number, the P/O ratio, indicating how many phosphate molecules are used for ATP synthesis per the reduction of a single oxygen atom. The utilization of $FADH_2$ in well coupled mitochondria yields a P/O ratio of ~1.5, while that of $NADH+H^+$ yields ~2.5.

The substrates of the F_oF_1-ATP synthase are inorganic phosphate (P_i) and ADP, which need to be imported across the IMM for ATP production. P_i is transported by the $H_2PO_3^-/OH^-$ antiporter. Cytosolic ADP^{3-} is exchanged for matrix ATP^{4-} in a 1:1 stoichiometry, by the adenine nucleotide translocator (ANT). The F_oF_1-ATP synthase utilizes 3 H^+ to produce a matrix ATP from ADP. The P_i import causes the decrease of the ΔpH, while the exchange of ADP for ATP results in a loss of a charge, leading to the decrease of the ($\Delta\Psi m$). Therefore the production of a cytosolic ATP costs a total of 4 H^+ flowing back into the matrix.

3.2. Mitochondrial Ca^{2+} management

3.2.1. Mitochondrial Ca^{2+} sequestration

The mitochondrion is a major player in regulating and shaping cellular Ca^{2+} levels. Mitochondrial Ca^{2+} handling has become a re-emerging topic in recent years (for an extensive review see [2]). Mitochondria from all tissues of mammals possess the ability to sequester divalent cations, like Ca^{2+}, Sr^{2+} and Ba^{2+}, but Ca^{2+} is the only one having physiological relevance. Mitochondrial Ca^{2+} uptake is not only important for buffering transient cytosolic Ca^{2+} loads, but sequestered Ca^{2+} is also an activator pyruvate-dehydrogenase, isocitrate-dehydrogenase and α-ketoglutarate-dehydrogenase, regulating the production of reducing equivalents for the energy-demanding uptake of Ca^{2+} (for review see [7]).

Mitochondria both bind and sequester Ca^{2+}, however the quantity of Ca^{2+} specifically binding to uptake regulatory sites and substrate transporters, plus the aspecifically binding to membranes is miniscule compared to the uptake capacity. The uptake capacity varies between different tissues, and in the brain, even between mitochondria from different regions [8].

The driving force for Ca^{2+} uptake is the high electrical potential across the IMM [9, 10]. Indeed, for a $\Delta\Psi m$ of −180 mV, the Nernst equation would predict at equilibrium a mitochondrial $[Ca^{2+}]_{in}/[Ca^{2+}]_{out}$ ratio of about 10^6 fold, *i.e.*, given a cytosolic Ca^{2+} concentration of 100 nM at rest, the mitochondrial matrix $[Ca^{2+}]$ should be as high as 0.1 M [11]. In reality such extreme concentrations of free matrix $[Ca^{2+}]$ are never reached, due to the formation of Ca^{2+} containing precipitates, above 100 nM of $[Ca^{2+}]$, which stabilize matrix $[Ca^{2+}]$ at 1-5 µM. Counter-ions for Ca^{2+} are primarily P_i, provided by the $H_2PO_3^-/OH^-$ antiporter and OH^-.

Ca^{2+} uptake by isolated mitochondria has a relatively low affinity: half maximal uptake speed is achieved at µMs of $[Ca^{2+}]$ [12, 13]. This fact was the main reason for abandoning mitochondrial Ca^{2+} handling for many years, as cytosolic $[Ca^{2+}]$ are within the mid nM

concentrations. The field regained interest when mitochondrial [Ca^{2+}] was measured directly during stimulus. It was done by the transfection of the Ca^{2+} sensitive photoprotein aequorin, which was fused in frame with a mitochondrial presequence [14].

Mitochondrial Ca^{2+} uptake can be selectively blocked by Ru 360, the active compound of Ruthenium Red, which is an inorganic dye originally used to stain mucopolysaccharides [15, 16]. The machinery residing in the inner mitochondrial membrane and responsible for Ca^{2+} uptake was named the calcium uniporter. It has been only until recently, that its proper electrophysiological characterization has been made and its molecular identity has been revealed [17].

The idea that the uniporter is a gated ion channel was first proposed by Bragadin in 1979, on the basis of the dependence characteristics of mitochondrial Ca^{2+} kinetics on temperature [18]. For decades no major advances were made in identifying the uniporter, until 2004, when direct methods proved his' theory to be correct. Electrophysiological experiments were carried out on mitoplasts, small derivates of mitochondria devoid of the OMM. A highly selective ion channel, with an affinity for Ca^{2+} of 2 nM, which accounts for the properties of the uniporter was successfully identified. Its relative divalent ion conductance was $Ca^{2+} \approx Sr^{2+} >> Mn^{2+} \approx Ba^{2+}$, however it was completely impermeable to Mg^{2+} and monovalent cations, except Na^{+} at extremely low [Ca^{2+}]. It was also found that it is forwardly rectifying and sensitive to nanomolar concentrations of Ruthenium Red or Ru360 [17].

In 2010 a regulatory protein of Ca^{2+} uptake was identified in mitochondria. The protein has two EF-hand domains, the function of which is calcium sensing and one transmembrane domain, which does not support the notion that it could have a channel activity. Its silencing was found to affect Ca^{2+} uptake activity dramatically. The protein was named *MICU1* [19]. The successful molecular identification of the uniporter was achieved by two different groups, using similar methods: both groups highlighted candidate proteins *in silico,* one by comparing databases of mitochondrial proteins to that of *Saccharomyces cerevisiae*, in which the uniporter is naturally absent [20], and the other by finding proteins

that could be related to the *MICU1* [21]. Search results yielded a handful of proteins, of which one, an IMM protein, with two transmembrane regions, plus an intervening loop enriched in acidic residues and with no known function, was further investigated. siRNA and overexpression experiments showed the protein to have a great influence on Ca^{2+} uptake both *in vitro* and *in vivo*. Fluorescent tagging of the protein verified expression in mitochondria. Finally the purified protein was reconstituted in lipid bilayers, for electrophysiological investigation, the results of which are in line with the properties of the uniporter. All these results support, that the 40-kDa protein identified is in fact the mitochondrial calcium uniporter.

3.2.2. The nature of Ca^{2+} precipitates in the mitochondrial matrix

The phenomenon of precipitation allows an approximately 1 M of $[Ca^{2+}]_{total}$ to be sequestered by mitochondria inside their matrix [22]. Precipitates in mitochondria loaded with Ca^{2+} can be observed on electron-microscopic images, as amorphous electron-dense granules or ring-like structures. Thread- or needle-like formations were reported in rabbit heart mitochondria, in media devoid of Mg^{2+} [23], and *Artemia franciscana* (see below). Chemical and X-ray diffraction analysis in early studies showed the inorganic content of the precipitates to resemble a mixture hydroxyapatite ($Ca_{10}(PO_4)_6OH_2$) and whitlockite ($Ca_3(PO_4)_2$). Mg^{2+} and CO_3^{2-} were present in significant quantities, furthermore organic compounds like ADP, ATP and proteins were also found [24]. Recent observations, using more advanced techniques conclude, that stoichiometry between Ca^{2+} and P_i can vary greatly depending on conditions of Ca^{2+} sequestration, inhibitors used and the tissue mitochondria originate from [25].

Several anions serve as counter ions for Ca^{2+}, however the most abundant are P_i and OH^-. The uptake of ADP or ATP is also necessary [26]. Lack of rapid Ca^{2+} sequestration by isolated mitochondria incubated in media, in which P_i is absent, demonstrates its relevance in the process [13, 27, 28]. Acidification of the matrix effects precipitate formation, which can be due to the loss of the ΔpH or also, as the ΔpH is constant, due to acidification of the cytosol. The slightly alkaline nature of the matrix favors precipitation, as hydroxide

concentration is higher, and also, the dissociation constants of calcium-phosphate salts are pH dependent. During acidification the concentration of hydroxide is decreased and the dissociation constants of calcium-phosphate salts are increased. Furthermore, P_i is imported into mitochondria in exchange for OH^-, which leads to a decrease in free P_i when the matrix is acidified [22]. Our laboratory has found however, that even though matrix acidification is an important contributor, it is not a major player in Ca^{2+} release under the collapse of the ΔpH, induced by uncouplers [29].

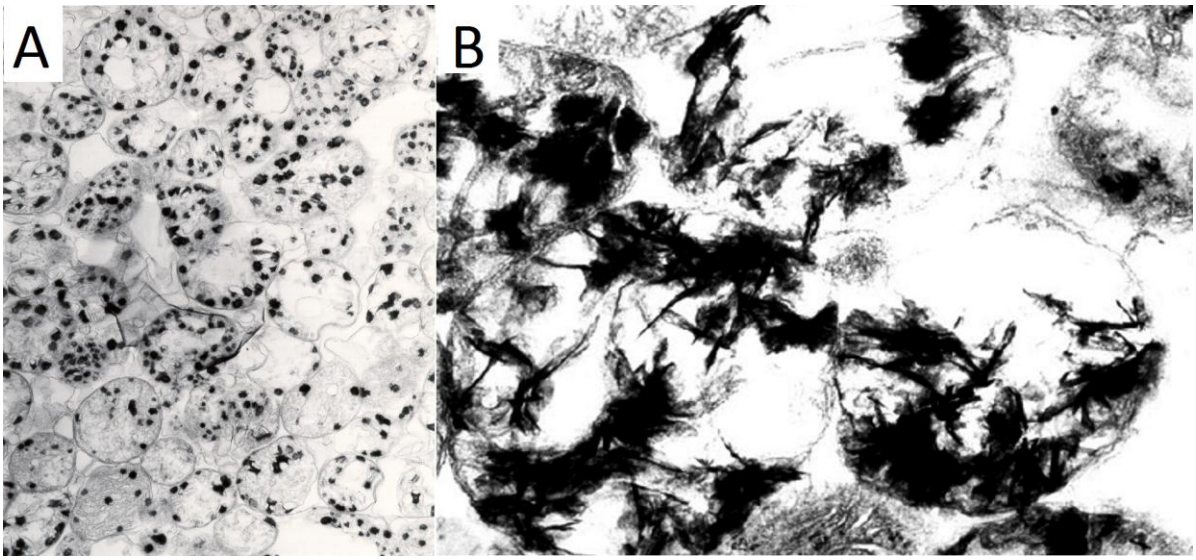

Figure 2: Electron microscopic images of Ca^{2+} precipitate morphology. A) rat cortical mitochondria fixed after active Ca^{2+} uptake, 12 000x magnification. B)Rabbit cardiac mitochondria fixed after active Ca^{2+} uptake in the absence of Mg^{2+}. Reproduced from [2]; no permission required.

Precipitates also contain a significant amount of protein. The role of proteins and their functions remains unknown, and rise numerous questions regarding mitochondrial Ca^{2+} precipitation. It has been suggested these proteins are regulators or base points of precipitate formation. Interestingly, there have been no Ca^{2+} binding proteins reported in mitochondria, that would be analogous to proteins, such as calsequestrin, calreticulin or Bip in the endoplasmic reticulum [11].

Another open question is the role of hydroxyapatite and whitlockite forming amorphous precipitates instead of normal crystalline structures. A hypothesis is the presence of lattice

breaker compounds present in mitochondria. A known lattice breaker, phosphocitrate, might be responsible for this feature [30, 31]. It was shown to be present in cell homogenates [32] and also mitochondria [33].

3.2.3. Release mechanisms of sequestered Ca^{2+}

It was described in the late 1970s, that mitochondria loaded with Ca^{2+} prior to addition of ruthenium red demonstrate a slow Ca^{2+} release. Furthermore Na^{+} enhanced release in mitochondria from specific tissues [34-36]. Release of Ca^{2+} is a slow process, compared to uptake. As they are thermodynamically unfavorable, due to the high electrochemical potential for Ca^{2+} provided by the $\Delta\Psi m$ and low free matrix Ca^{2+}caused by precipitate formation, these mechanisms are required to be coupled to other electrochemical gradients [37]. Ca^{2+} release involves two antiporters: the mitochondrial Na^{+}/Ca^{2+} exchanger and the Ca^{2+}/H^{+} exchanger, both of which reside in the IMM. The Ca^{2+}/H^{+} exchanger dissipates pmf directly, while the low matrix Na+ required by the Na^{+}/Ca^{2+} exchanger is maintained by the Na^{+}/H^{+} exchanger. The energy required to extrude one atom of Ca^{2+} can be supplied by the exchange of at least two protons or two Na^{+} ions. The primarily pathway of Ca^{2+} release in excitable tissues i.e. heart, brain, skeletal muscle is Na^{+} dependent Ca^{2+} efflux, while in liver, kidney, lung and smooth muscle, the Na^{+}/Ca^{2+} exchanger is not expressed and Ca^{2+} release is slower and Na^{+} independent. Characterization of the Ca^{2+} efflux in excitable tissues showed that the rate of Ca^{2+} efflux by the Na^{+}/Ca^{2+} exchanger remains unchanged if Na^{+} is substituted by Li^{+}, furthermore the antiporter is sensitive to inhibition by CGP-37157.

The molecular identity of the mitochondrial Na^{+}/Ca^{2+} exchanger is known: the NCLX, which was first described in the plasma membrane, however its unique phylogenetic and functional properties triggered the attention of the group of Sekler. Overexpression, silencing, western blot and immune-electron microscopic experiments confirmed the NCLX to be the Na^{+}/Ca^{2+} antiporter in mitochondria [38]. The characterization of the NCLX is yet incomplete, with the most pressing question still being the exchange stoichiometry. The molecular identity of the Na^{+}/H^{+} antiporter remains unknown.

Another player in Ca^{2+} efflux is a H^{+}/Ca^{2+} antiport mechanism. A mitochondrial protein, Letm1 was proposed to be the H^{+}/Ca^{2+} antiporter, however these findings are debated, as Letm1 was previously described as a K^{+}/H^{+} exchanger [39], which is sensitive to

Ruthenium Red and insensitive to CGP-37157 [40]. By immobilized calcium affinity chromatography, the partially purified protein fraction at 66 kDa showed H^+/Ca^{2+} antiport activity when reconstituted in lipid bilayers [41]. Similarly to the Na^+/Ca^{2+} exchanger, there is no consensus in exchange stoichiometry.

Also, the flickering of the mitochondrial permeability transition pore (PTP) could be yet another efflux mechanism, on which phenomena this thesis focuses in later chapters.

Furthermore, a diacylglycerol induced release mechanism was reported, which was unaffected by Ruthenium Red, CGP-37157 or PTP inhibition. The phenomenon could not be demonstrated on mitochondria from sweet potato (*Ipomoea batatas*), indicating biodiversity, and suggesting it is unlikely to be an artifact [42].

3.2.4. Physiological relevance of mitochondrial Ca^{2+} handling

Mitochondria couple cellular metabolic state with Ca^{2+} transport processes. They therefore control not only their own intra-organelle [Ca^{2+}], but also influence the entire cellular network of Ca^{2+} signaling, including the endoplasmic reticulum, the plasma membrane, and the nucleus [43]. Close interactions with other organelles create so-called microdomains, which can have properties different from that of the cytosol, when rapid changes occur, due to diffusion barriers. The first report of close contacts between mitochondria and the ER was on the basis of overlapping of fluorophores, specific to these organelles, by confocal microscopy [44]. In these regions the Ca^{2+} concentration can elevate to levels where mitochondrial uptake is active. Lately an elegant method was developed, to directly visualize organelle contacts. The approach used an FKBP-FRB heterodimerization system, targeting the FKBP to the OMM and the FRB to the ER. Introduction of rapamycin was used to cause heterodimerization where FKBP and FRB were close, and close contacts were visualized by FRET [45].

The microdomains between organelles are essential for their coordinated action. Mitochondrial Ca^{2+} uptake limits the rapid rise of Ca^{2+} in these microdomains, otherwise flooded by reticular stores or extracellular Ca^{2+}. Mitochondrial Ca^{2+} release prolongs the

recovery from the Ca^{2+} stimulus [46]. The microdomains between mitochondria and the endoplasmic reticulum (ER) or the plasma membrane explain the Ca^{2+} buffering ability of mitochondria *in vivo*, despite the low affinity of the uptake machinery, as high enough Ca^{2+} concentrations are reached in these subcellular regions [14].

Early experiments by polarographic Clark electrodes demonstrated mitochondria to take up Ca^{2+} completely prior to phosphorylating ADP, when challenged with both [13]. However the maintenance of ATP levels is crucial during transients of Ca^{2+}, because the restoration of the ion balance of the cytosol by the ER and the plasmamembrane has a high energy demand. Normal restoration of reticular Ca^{2+} stores cannot be achieved in experimental conditions where oxidative phosphorylation is blocked and high ATP is made available by permeabilization of cells which supports the importance of high ATP concentration in microdomains between the mitochondria and the ER [47].

The matching of energy production to requirements of the pumping mechanisms is due to the regulatory effect of Ca^{2+} in the mitochondrial matrix. Ca^{2+} activates the citric acid cycle in mitochondria by stimulating the pyruvate dehydrogenase complex through the pyruvate dehydrogenase phosphatase, the isocitrate dehydrogenase and the α-ketoglutarate dehydrogenase (for review see [7]). These enzymes all have high flux control coefficients. A flux control coefficient is a relative measure of how much an infinitely small perturbation of a system parameter affects a system variable: enzymes with a high (close to one) flux control coefficient have a great impact on the rate of an enzymatic pathway. An increase in NADH autofluorescence can be detected for several minutes upon depolarization of excitable cells, like neurons [48]. This increase in reducing equivalents helps maintaining membrane potential during Ca^{2+} sequestration.

Furthermore organelle interactions is further complicated their motility. The relevance of morphology and dynamics regarding signaling with other organelles has been acknowledged in recent years. The advances mainly in fluorescent microscopic imagery revealed the mitochondria being under constant movement, fusion and fission in the cell. Elevation in the cytoplasmic [Ca^{2+}] induces translocation of the dynamin-like DRP-1 to the

OMM, which is responsible for mitochondrial fission [49]. Also, Rho GTPases (Miro 1 and 2) were found to effect mitochondrial homeostasis, most likely through the mitochondrial trafficking apparatus, as they connect mitochondria to the microtubular network. These proteins exhibit EF-hand domains, the mutation of which influences mitochondrial morphology and distribution in the cell [50].

3.2.5. Pathological effects of Ca^{2+} involving mitochondria

Ca^{2+} is implicated in mitochondrial pathologies by two different mechanisms: the mitochondrial permeability transition, on which this thesis focuses and reactive oxygen species (ROS) generation. ROS are the byproducts of mitochondrial respiration and have been implicated in aging and in the pathophysiology of a wide variety of diseases, ranging from diabetes to neurodegeneration. To avoid the malignant effects of ROS, the cell is equipped with scavengers of ROS, such as superoxide-dismutase, catalase, glutathione oxidase, thioredoxin and peroxiredoxin [51].

The effect of Ca^{2+} on ROS production is controversial: increased [52-55], decreased [56-58] and unaffected ROS production [59-61] were all reported upon Ca^{2+} stimulation. Measured ROS production and elimination of isolated mitochondria in vitro depends on many factors, e.g. substrates, the presence of adenine nucleotides, $NADH/NAD^{+}$ ratio, inhibitors, and $\Delta\Psi m$ (for extensive review see [51]). As discussed above, Ca^{2+} has an impact on mitochondrial parameters that have an effect ROS production, which might be an explanation for the inconsistency of the results in the field.

3.3. The mitochondrial permeability transition pore

Mammalian mitochondria can only handle a certain amount of Ca^{2+}, before a regulated permeabilization (permeability transition, PT) of the normally impermeable inner membrane occurs, on which most processes of a mitochondrion relies. The entity responsible for the phenomenon was termed the mitochondrial permeability transition pore (PTP). It is commonly associated with various types of disease, and is therefore an intensely researched field [62-71].

3.3.1. Consequences of prolonged permeability transition on mitochondrial biochemistry and signaling

Two types of permeability transition of the IMM were described in mitochondria: the low- and the high-conductance pore. The low-conductance pore allows the pmf to dissipate and Ca^{2+} to be released, but no swelling or unselective passing of small solutes is observed [70, 72]. The high conductance pore, on the other hand, has a cut-off size of 1500 kDa, allowing ions and small molecules driven by their electrochemical gradients to equilibrate between the matrix and the cytosol. An increase in ROS can be detected during permeability transition, due to the loss of glutathione, impairing ROS scavenging, and NAD^+, leaving enzymes, most importantly the α-ketoglutarate dehydrogenase complex without a co-factor to properly reduce [73, 74].

Sequestered Ca^{2+} is also released in a rapid, unregulated manner. The pmf, similarly to low conductance PTP, is dissipated. PTP opening leaves only a few mV-s of membrane potential, which is caused by the higher abundance of negatively charged proteins in the matrix, too large of size to pass freely. The mitochondrial processes relying on the pmf are therefore severely affected by the opening of the PTP.

As the mitochondrial matrix is hyperosmotic compared to the cytosol, during PT water content of the matrix increases, which is accompanied by swelling. The IMM being folded in mitochondria to form cristae, has a high surface, and can withstand the expansion of the matrix, while the OMM ruptures. This allows proteins residing in the intermembrane space

to be released to the cytosol, of which some are pro-apoptotic factors, e.g. cytochrome c, Smac/Diablo, Endonuclease G, or AIF. When a large fraction of mitochondria simultaneously open the PTP in response to stress, the resulting ATP depletion makes it impossible to coordinate the apoptotic machinery, leading to necrosis induction [75, 76]. As a result, transition from apoptosis to necrosis is possible, and the two mechanisms are not always easily distinguishable [77].

3.3.2. Effectors of permeability transition

The effect of a wide variety of chemicals, and changes in different mitochondrial parameters on the probability of PTP opening is known, most of which were documented when the phenomenon was first described. In the 1950s the ability of Ca^{2+} to cause swelling of isolated mitochondria was first noted, however presumed to be due to non-osmotic mechanisms [78]. It was only in 1976, that a reversible increase in the permeability of the IMM was discovered in beef heart mitochondria, by Hunter and Haworth [79]. Their later work gives a remarkably extensive characterization of the PTP, using swelling experiments almost exclusively [80-82].

Tables 1 and 2 [83] summarize the categories of inducers and inhibitors of permeability transition. **Ca^{2+}** alone is sufficient to trigger PT, at least in liver, heart, kidney and adrenal cortex mitochondria, but only if it can be sequestered by mitochondria; inhibition of the Ca^{2+} uniporter by Ruthenium Red or Ru360 protects mitochondria from the opening of the PTP. Likewise if the counter-ion of Ca^{2+} does not favor precipitation e.g. if **phosphate** is substituted by acetate PTP is also inhibited. By this principal, P_i considered as an inducer by many authors.

A number of **oxidizing agents** have also been reported to be PTP inducers. The mechanism of their action is likely to be identical, but they can be divided into different subgroups. Furthermore, the distinction between oxidizers and SH reagents may be inappropriate, since there is now reason to think that the effect of the various oxidizers results from the

conversion of critical SH groups to disulfide bridges (see, e.g., [84, 85]). SH reducing agents and radical scavengers can be PTP inhibitors.

The effect of **uncouplers**, like FCCP, suggests a dependence of opening probability on $\Delta\Psi m$. The PTP inducing effect of ROS was emphasized, and increased generation of ROS was later suggested to be the cause of FCCP induced PTP on mitochondria loaded with Ca^{2+} [52, 55, 86], however uncouplers trigger PTP even when ROS is eliminated with catalase [87], proving that oxidization by ROS is not responsible for the effect of uncouplers on PT. Both voltage and ROS sensing mechanisms responsible for PTP inducing is unknown.

ADP and ATP are powerful PTP inhibitors [25, 88, 89]. Agents increasing ATP/ADP ratio or decreasing adenine nucleotide content of the matrix are PTP inducers. Pyrophosphate [90] and phosphoenolpyruvate [91] are both known to deplete the matrix adenine nucleotide pool, by exchange on the ANT. Thus, they induce the PT by reducing the level of a protecting agent [83]. Oligomycin also affects nucleotide levels, as the blocking of the F_oF_1-ATP synthase results in a decrease of the matrix ATP/ADP ratio and hyperpolarization of mitochondria.

PTP opening is also strongly dependent on **matrix pH** [92]. The optimum for pore opening is pH 7.4. Opening probability decreases sharply both below pH 7.4 (through reversible protonation of critical histidyl residues that can be blocked by diethylpyrocarbonate) and above pH 7.4 (through an unknown mechanism). [93]. Inhibition could be substantially eliminated by pretreatment of the mitochondria with diethyl pyrocarbonate, which effect is most likely due to modification of histidyl residues regulating the pore open-closed probability [94, 95]. The mechanism by which alkaline pH inhibits pore formation is unknown [83].

How **Mg^{2+} and other cations** mediate their effect is unknown. Mg^{2+} was shown to potentiate the effect of both Cyclosporin A and ADP [96]. Cations might act by competitive inhibition on Ca^{2+} binding sites.

Cyclosporin A (CsA) is an immonosuppressant and its effects are caused by the Ca^{2+}-calmodulin-dependent inhibition of calcineurin (a cytosolic phosphatase) by the complex of the drug with cytosolic cyclophilin A [97]. In turn, this prevents dephosphorylation and nuclear translocation of nuclear factor of activated T cells and other transcription factors that are essential for the activation of T cells [93]. CsA also binds to cyclophillin D (CypD), in the matrix, and inhibits PTP formation. The discovery of the effect of cyclosporine A on kidney mitochondria was due to the search for its nephrotoxic adverse effect [98-100].

Table 1: inducers of the permeability transition pore

Group	**Sub-group**	**Agent**
Counterions of calcium		Phosphate
Oxidizing agents	of pyridyine nucleotides	acetoacetate oxaloacetate
	hydroperoxides:	t-butylhydroperoxide cumene hydroperoxide hydrogen peroxide
	radical-generating species	menadione alloxan allantoin and uric acid adriamycin and derivatives nitrofurantoin Fe^{2+} Fe^{3+} xanthine and xanthine oxidase 5-aminolevulinic acid GSH/GSSG and disulfide hormones ascorbate
SH reagents	heavy and transition metals and their complexes	Hg^{2+} and mercurials mersalyl Cd^{2+} Cu^{2+} Zn^{2+}
	cross-linkers and disulfide bridge formers	diamide arsenite phenylarsine oxide
	other	NEM
Adenine nucleotide translocator ligands		atractyloside and carboxyatractyloside pyridoxal-5-phosphate acyl-CoA's (and acylcarnitines)
Agents causing depletion of matrix adenine nucleotides		Pyrophosphate Phosphoenolpyruvate
Transrnembrane potential-reducing agents		uncouplers lysophospholipids fatty acids
Other		thyroxine

Its effect on Ca^{2+} uptake capacity due to its PTP blocking properties was shortly recognized, by several different groups [101-103]. NIM811 is a CsA derivate causing only PTP inhibition, which makes it unlikely that calcineurin is involved in PTP regulation [104].

P**olyamides** are documented to protect against PT [105], however the mechanism by which they effect the PTP is not well understood [83].

Inhibitors of the ANT are discussed in the chapter below.

Table 2: inhibitors of the permeability transition pore

Group	**Agent**
Inhibitors of Ca2+ uptake	Ruthenium red, Ru360
Adenine nucleotides	ADP ATP
Ligands of the ANT	Bongkrekate
Ligands of the F_oF_1-ATP synthase	Oligomycin
Divalent and trivalent cations	Mg2+ Sr2+ Mn2+ Ba2+ La3+
Competitors of Ca2+ binding	phenothiazines local anesthetics
Radical scavengers	butylhydroxytoluene
Polyamines	spermine and spermidine Carnitine and acylcarnitine
SH-reducing agents	dithiothreitol
Ligands of cyclophillin D	Cyclosporin A
Fatty acid binder	BSA
	acidic pH

3.3.3. The proteins proposed to be structural elements of the PTP

Since its discovery, more than 30 years ago, there has been tremendous effort put into identifying the structure of the PTP. The current chapter discusses the most important proteins proposed to be structural elements, and the most relevant experiments unraveling their connection with PTP (for extensive review see [93]).

3.3.3.1. The Adenine nucleotide translocator

The adenine nucleotide translocator (ANT) is the transporter responsible for the exchange of ADP and ATP in a 1:1 stoichiometry between the matrix and the cytosol. Its specificity towards its ligands is far higher, than other ATP utilizing proteins, and also in contrast to them binds the nucleotides in their fully deprotonated form (ATP^{4-}/ ADP^{3-}), without Mg^{2+} [106]. The transport is therefore electrogenic, and besides numerous other less dynamic mitochondrial parameters, depends on $\Delta\Psi m$ [107]. The transporter can work in both directions, the exchange of cytosolic ADP for matrix ATP is the forward mode. The reversal potential (the membrane potential at which net transport is zero) is approximately -100 mV [107]. It is the most abundant protein in the IMM, responsible for 10% of its protein content [108].

The ANT was first sequenced in 1982, isolated from beef heart, which consists of 297 amino-acids [109]. It has six trans-membrane domains, and both terminals face towards the cytosol [110]. Whether the ANT functions as homodimers [111, 112], or monomers [113, 114] is debated. The bovine ANT has been solved at a resolution of 2.2 Å [115].

It was also first shown in bovine, that ANT has different organ specific isoforms [116, 117]. There are four human isoforms known. ANT1 is primarily expressed in skeletal and heart muscle [118], ANT2 is found in proliferating cells [119], ANT3 is ubiquitously present in all tissues [120], and ANT4 is expressed the testis [121]. The ANT isoforms show a fair overall homology with the phosphate carrier and the uncoupling proteins, suggesting a common origin of solute carriers in mitochondria [122].

There are two known groups of inhibitors of the ANT, atractylosides and bongkrekate derivatives. Atractyloside is found in the toxic thistle *Atractylis gummifera*. It was originally discovered to cause inhibition of the respiration of mitochondria [106], and it was not long until it was realized, that it mediates its action through blocking the transport of ATP [123]. It binds on the outer surface of the ANT to the translocator site, competitively to ADP [115, 124, 125]. Atratylosides are specific and the ANT has a high affinity towards them. Other than inhibition of the ANT, they also predispose mitochondria to pore opening.

Bongkrekic acid (BKA) is produced by the bacterium *Pseudomonas cocovenenans*, which infects coconut [126, 127]. It is known to act on the mitochondrial side, but its exact binding site on the ANT is unknown. Only the fully protonated $BKAH_3$ is lipophilic enough to pass through membranes, therefore acidic pH augments the effect of BKA [128, 129]. Low temperature slows diffusion and causes a long offset in the effect of BKA [130, 131]. In contrast with atractyloside, BKA is an inhibitor of PTP opening.

To date the ANT has been the most promising candidate as structural element of the PTP [132]. Numerous effectors of the translocator have been described, and without an exception all having an impact on pore open probability. Three endogenous ligands – ADP, ATP (both inhibiting the PTP) [89, 133], and acyl-CoA and its esters (opening the PTP) [134, 135] – plus four poisons – atractyloside, carboxyatractyloside (cATR) (both favoring pore opening), bongkrekic acid (BKA) and isobongkrekic acid (both promoting pore closure) [136-138] – have been identified. Other, less well-characterized, inhibitors of ANT have also been reported [139]. Therefore the ANT has been under thorough investigation.

The patch-clamping of reconstituted purified bovine heart ANT containing lipid bilayers yielded characteristics similar to that of the PTP [140, 141] described earlier. Ca^{2+}, pH and voltage dependence were all measured [142]. Heterologously expressed ANT of *Neurospora crassa* in E. coli showed pore opening dependence on cypD [143].

However it was later rejected, as transgenic mice, expressing no ANT1 nor ANT2 isoforms in their liver were shown to exhibit CsA sensitive permeability transition [144]. Based on

the mentioned results, the consensus regarding the role of the ANT in PTP is that it is regulatory and nonessential.

3.3.3.2. Cyclophilin D

Cyclophillin D (CypD) gained interest when it was discovered to bind CsA [145, 146]. It is a peptidyl-prolyl cis-trans isomerase located in the matrix of mitochondria, however its substrate is unknown. Cyclophillin D is encoded by the Ppif gene, for which knock-out mice have been successfully generated [62-65]. Surprisingly phenotypic changes in Ppif -/- mice manifest in high levels of anxiety/emotionality in open field and elevated plus maze tests; facilitation of the learning in tasks of active and passive avoidance; increased incidence of adult-onset obesity [147]; prosperity to heart failure, lung edema and reduced survival in response to sustained exercise stimulation [148].

Mitochondria harvested from various tissues of Ppif -/- mice however show a delay in pore opening, and also increased Ca^{2+} uptake capacity. CsA had no effect on the Ppif knockouts, furthermore wild type mitochondria treated with CsA show similar Ca^{2+} kinetics to Ppif -/- mice [62]. Ischemia/reperfusion damage is greatly reduced in Ppif -/- mice [63].

A binding site for CypD was recently identified. It was found that CypD associates to the oligomeric forms of the ATP synthase and specifically interacts with OSCP, subunit d, and subunit b of the lateral stalk, decreasing its enzymatic activity, binding being favored by P_i, and that CsA displaces CypD from the ATP synthase complex, resulting in stimulation of the enzyme [149]. This does not translate to changes in mitochondrial ATP output upon treatment of CsA, due to the ~2.2 fold lower flux control coefficient of the F_oF_1-ATP synthase compared to that of the ANT [150, 151]. This implies that the inhibition of the F_oF_1-ATP synthase by CypD is rather serves a function of an in-house control for regulating the matrix ATP/ADP ratio. The mechanism by which CypD regulates the PTP could therefore be indirect, through effecting ATP/ADP ratio, and therefore changing the extent of inhibition.

The above findings indicate that CypD is a dispensable regulator, but not a component, of the PTP, the structure of which is unlikely to be altered by the absence of CypD.

3.3.3.3. Voltage-dependant anion channel

The voltage-dependant anion channel (VDAC) is a highly expressed OMM protein. It has 3 highly redundant isoforms in mammals. Several lines of evidence suggested the VDAC could be structural element of the PTP. Purified VDAC incorporated into planar phospholipid bilayers forms channels with properties comparable to those of the PTP [152, 153]; furthermore VDAC channel activity is affected by known modulators of the PTP. Furthermore chromatography of mitochondrial extracts on a CypD affinity matrix allowed purification of VDAC and the ANT, leading to the conclusion of these proteins being structural elements of the PTP [154].

Though the above findings gave a firm base to conclude, further experiments elaborated below invalidated the concept of the VDAC being an indispensible structural element of the pore. Genetic ablation of VDAC isoforms had been attempted. Mice missing VDAC1, VDAC3 or both were viable showing isoform-specific phenotypes, but were susceptible to permeability transition [155-157], while the unconditional elimination of VDAC2 resulted in embryonic lethality [158]. VDAC was irrevocably rejected to be a structural candidate after mouse embryonic fibroblasts null for Vdac1/Vdac3 were treated with a siRNA against VDAC2, resulting in an *in vitro* model essentially lacking all three VDAC isoforms. These cells showed no defect in PTP [159].

3.3.3.4. 18 kDa translocator protein

The 18 kDa translocator protein (TSPO), formally called peripheral benzodiazepine receptor is a hydrophobic OMM protein. As the former name implies, it binds benzodiazepine with high affinity and it is thought to be responsible for the adverse effects of benzodiazepines on the immune system, however the structure, localization and function is different [160]. TSPO plays a role in importing cholesterol, protoporphyrins and porphyrins into mitochondria [161-164]. Selective ligands exhibiting PTP inducing activity

have been described [165, 166], furthermore porphyrin-induced phototoxicity was shown on isolated mitochondria to be mediated through the TSPO [167], but had no effect on mitoplasts, devoid of the OMM, where TSPO is found [168]. This suggests TSPO is an important regulator, but not structural element of the PTP.

3.3.3.5. F_oF_1-ATP synthase

The finding of a CypD binding site on the F_oF_1-ATP synthase had raised suspicion that it could be involved in pore formation. An earlier study demonstrated that purified subunit c of the F_oF_1-ATP synthase has pore activity when reconstituted in lipids [169]. It was recently demonstrated that susceptibility to permeability transition correlates with the expression level (altered by overexpression or silencing) of the ring-forming subunit c of the membrane spanning F_o unit of the F_oF_1-ATP synthase [170].

Another recent paper also identifies the F_oF_1-ATP synthase as the PTP. In the study CypD binding to OSCP is reconfirmed. OSCP was knocked down by siRNA, which resulted in premature pore opening. Finally purified F_oF_1-ATP synthase was reconstituted in lipid bilayers examined by electrophysiology. Pore formation similar to PTP was observed exclusively when dimers of the F_oF_1-ATP synthase were used [171, 172].

Though these conclusions are based on well-designed experiments and are nevertheless intriguing; many questions regarding the actual mechanism, components and regulation remain open. Furthermore these findings are yet to be proven by direct evidence, such as transgenic *in vivo* models to support them. The F_oF_1-ATP synthase being responsible for ~90% of the ATP produced in the cell will hardly be an easy target for genetic manipulation [173, 174].

3.3.4. Possible physiological role

Despite the PTP being a highly conserved evolutionary trait [175], there is no well-established physiological function, other than cell death. One hypothesis is that the short transients ("flickering") of permeability transition may serve as rapid Ca^{2+} release pathway [75, 176]. The phenomenon was demonstrated on isolated mitochondria [177] and intact

cells [178]. This notion is supported by the finding that both CsA treatment [179] and genetic ablation of CypD [63, 64] inhibits mitochondrial Ca^{2+} release.

It is also worth noting, that the PTP was described to be involved in transport of DNA in plants [180].

3.3.5. Pathological aspects of the PTP

A large body of evidence implies the relevance of permeability transition in a variety of untreatable diseases. Here a short overview is given on the subject.

The involvement of PTP in neurodegenerative diseases such as Alzheimer's, Parkinson's Huntington's disease and amyotropic lateral sclerosis is widely accepted. The increase in PTP opening probability is primarily attributed to mitochondrial mutations, bioenergetic impairment, oxidative stress, deficient mitochondrial quality control or errors in mitochondrial dynamics, which as a consequence lead to permeability transition, and cell death [181, 182].

Abnormalities in **Huntington`s disease** is attributed to the mutated form of the huntingtin protein (mHTT) exhibiting polyglutamine repeats. The exact mechanism by which mHTT expression leads to the clinical phenotype is unknown, but there is evidence of its interaction with mitochondria. mHTT was found to be localized to the outer surface of mitochondria and also to form aggregates inside the matrix [183], leading to decreased membrane potential, Ca^{2+} handling capacity, mitochondrial trafficking and increased pore opening probability [184-186]. These findings were also confirmed on transgenic mouse models of the disease [187-189]. It was suggested that mHTT affects the peroxisome proliferator-activated receptor gamma co-activator 1α (PGC-1α), a key regulator of mitochondrial biogenesis, energy homeostasis and adaptive thermogenesis [190]. CsA was shown to improve cognitive functions in rodents in the 3-nitropropionic acid induced model of the disease.

The proteins shown on Table 3 [191] have been linked to the familiar form of **Parkinson`s disease**. Many of these proteins play an important role in mitochondrial physiology. PINK1 and Parkin are involved in mitophagy and are therefore essential in the maintenance of mitochondrial quality. Genetic knock down of either of these proteins leads to impaired bioenergetics parameters, which increase PTP opening probability [192-194]. α-synuclein was shown to be localized to the mitochondria causing oxidative stress and increase autophagy [191, 195-197].

Table 3: Gene loci identified for Parkinson's disease. AD, autosomal dominant; AR, autosomal recessive. Reprinted from [193], no permission required.

Locus	Gene	Chromosome	Inheritance	Probable function
PARK1 and PARK4	α-Synuclein	4q21	AD	Presynaptic protein, Lewy body
PARK2	Parkin	6q25.2-27	AR	Ubiquitin E3 ligase
PARK3	Unknown	2p13	AD	Unknown
PARK4	Unknown	4p14	AD	Unknown
PARK5	UCH-L1	4p14	AD	Ubiquitin C-terminal hydrolase
PARK6	PINK1	1p35-36	AR	Mitochondrial kinase
PARK7	DJ-1	1p36	AR	Chaperone, Antioxidant
PARK8	LRRK2	12p11.2	AD	Mixed lineage kinase
PARK9	ATP13A2	1p36	AR	Unknown
PARK10	Unknown	1p32	AD	Unknown
PARK11	Unknown	2q36-37	AD	Unknown
PARK12	Unknown	Xq21-q25	Unknown	Unknown
PARK13	HTRA2	2p12	Unknown	Mitochondrial serine protease

Alzheimer's disease (AD) is the most common cause of dementia. The most conspicuous and well known trait in AD is excessive neuronal death and the presence of amyloid beta aggregates in the affected cells. More recent results however indicate that decreased synaptic mitochondrial motility, synaptic dysfunction and the loss of synapses are prior pathological hallmarks to cell death and brain tissue atrophy in AD [198]. Synapses are sites of high energy demand and extensive calcium fluctuations; accordingly, synaptic transmission requires high levels of ATP and causes constant calcium fluctuation [199]. There is a growing number of evidence associating decreased mitochondrial function and increased production of ROS with the disease [200-204]. If axonal mitochondria become less competent in providing energy for Ca^{2+} handling, the overload will result in permeability transition. The genetic ablation of CypD was shown to rescue axonal

mitochondrial transport in affected neurons [205], which put an emphasis on the relevance of PTP in the pathology of AD.

Amyothropic lateral sclerosis (ALS) is the most prevalent adult onset motoneuron disease, characterized by selective loss of upper and lower motor neurons [206]. Mitochondria from the spinal cord and muscle of ALS patients revealed decreased activity of the respiratory chain complexes, which fact [207-210]. Studies on familiar types of the disease (accounting for approximately 5% [211] of the cases) provide some insight into the role of mitochondria in the pathology of ALS. There have been 12 genes identified that can cause the disease phenotype, of which the most relevant ones are SOD1, TDP-43 and FUS [212, 213]. Mutated Cu-Zu superoxide dismutase (SOD1) is responsible for 10% of familiar ALS [214]. The disease mechanism by which SOD1 causes ALS is unknown, but genetic ablation of SOD1 does not lead to disease phenotypes in cells [215] or mouse [216], suggesting that mutations cause ALS by a toxic "gain of function" rather than by loss. Mutant SOD1 proteins were shown to be associated to mitochondria in higher quantities than the wild type form, mostly on the outer membrane and intermembrane space, but also in the matrix [217-226]. The localization of mutant SOD1 is thought to interfere with mitochondrial functions. Mutant SOD1 overexpressing mouse show large, membrane-bound vacuoles derived from degenerating mitochondria in motor neurons [227-229]. These vacuoles show increased immunoreactivity for mutant SOD1, suggesting that accumulation of mutant SOD1 by mitochondria is responsible for their degradation [221]. Another sign of decreased mitochondrial function is the increased cytoplasmatic concentration of Ca^{2+} in in neuroblastoma cells transfected with mutant SOD1 [230]. In summary the findings above describe conditions in the disease models of ALS in which mutant SOD1 is expressed that favor PTP opening. The crossing of mutant SOD1 expressing mice with CypD knockouts, in which pore opening probability is reduced, results in increased lifespan and later onset of the disease, which findings put an emphasis on the relevance of the PTP in the pathology of ALS .

Ischaemia is caused by insufficient or completely lost blood perfusion, which can affect any tissue and leads to necrosis and inflammation. Damage is most devastating and rapid when affecting highly aerobic and energy dependent organs like the brain or the heart. Furthermore the capacity of the tissues of these organs to regenerate are nearly zero.

The inevitable bioenergetic failure during ischaemia leads to the unavailability of cytosolic ATP, which causes an insufficient activity of plasma membrane pumping mechanisms, resulting in elevated cytosolic Na^+ and Ca^{2+} and consequently, also matrix Ca^{2+} levels due to mitochondrial Ca^{2+} uptake. A popular notion was that because both the ANT and the F_oF_1-ATP synthase can reverse, during ischemia mitochondria could become cytosolic ATP consumers, further contributing to cytosolic ATP depletion, however due to the inhibition of the F_oF_1-ATP synthase by IF1, this is not likely to occur [231]. The opening of the PTP and the conseqential swelling of mitochondria are well described events that manifest primarily when the ichaemic region is reperfused [232-237]. Reperfusion is accompanied by high oxidative stress, elevation of the pH (therefore the loss of the inhibitory effect of acidic pH on PT [238, 239]) and further mitochondrial overload of Ca^{2+}. Cell death in the brain by necrosis expands to a greater region than primarily affected by ischaemia-reperfusion due to the phenomenon of glutamate excitotoxicity. Glutamatergic neurons depleated of ATP are incapable of polarizing their plasma membrane and therefore release glutamate at synapses from their axons, which by overexciting glutamate receptors like the N-methyl-D-aspartate receptor (NMDA) causes Ca^{2+} overload and necrosis on postsynaptic neurons [234].

There are two treatments offering some level of protection in ischemia/reperfusion injury, ischemic preconditioning is a process where short episodes of ischemia are applied, while in ischemic postconditioning reperfusion is interrupted by periods of ischemia. PTP is involved in the mechanism these phenomena [240, 241]. Attempts to inhibit PT by CsA or knocking down CypD were shown to reduce infarct size in cerebral ichaemia [63, 242-245]. Interestingly, CypD KO mice could not be further protected by preconditioning, suggesting CypD is the mediator of protection [246].

Additionally, based on the protective effects of CsA, the PTP has been implied in brain damage as a result of **hyperglycemia** [247, 248], **hypoglycemia** [249, 250], **trauma** [251-255] and in cell death following **facial motoneuron axotomy** in neonatal rodents [256] and in photoreceptor apoptosis [257] [93].

Several anti-**cancer** agents induce cell death by triggering PT [258, 259], which is also responsible for their adverse effects [260-264]. The inhibition of the PTP has been shown to reduce the cardiotoxicity of anthracyclines [265, 266].

3.3.6. Species lacking the PTP

Mitochondria from various species have been described to exhibit pore forming properties [175]. This includes vertebrates, such as mammals (vast majority of the literature), fish [267-269], amphibians [269, 270]; invertebrates, like drosophila [271]; fungi (yeast species) [272] and a number of plants, primarily of agricultural importance [180, 273-284]. However, PTP characteristics in non-mammalian species show significant deviations from the mammalian consensus. For example, mitochondria from the yeast species *Saccharomyces cerevisiae* have a PTP that is inhibited by ADP and has comparable size exclusion properties to the homologous structure in mammalian mitochondria, but these mitochondria are CsA-insensitive [175, 285, 286]. Mitochondria isolated from pea stems (*Pisum sativum L.*) and potatoes (*Solanum tuberosum L.*) require dithioerythritol for the CsA to inhibit the PTP [273, 276]. In contrast, CsA failed to afford protection from the PTP in wheat (*Triticum aestivum L.*) mitochondria, even in the presence of dithioerythritol [277].

The PTP seems to be a widely spread and highly conserved trait of eucaryotes. There are only a few species described in which permeability transition cannot be elicited; no Ca^{2+}-induced PTP could be found in mitochondria from the yeast *Endomyces magnusii* [287-289], ghost shrimp (*Lepidophthalmus louisianensis*) [290] and embryos of brine shrimp (*Artemia franciscana*) [291]. The embryonic cysts of *Artemia* remain viable after exposure to extremes such as high or low temperature, radiation, anoxia and desiccation for decades.

In most of these conditions PTP is triggered in mammalian cells, therefore it was a reasonable idea to examine PTP opening in these animals. The ghost shrimp is another extremophile, which was investigated by the same group as the *Artemia*.

Furthermore, mitochondria isolated from the blue crab (*Callinectes sapidus*) [292], shore crab, (also known as European green crab, *Carcinus maenas*) [293], and Caribbean spiny lobster (*Panulirus argus*) [294], also belonging to the exhibited impressive calcium uptake capacities. While lack of PTP has not been explicitly sought, mitochondria from the latter organisms did not display spontaneous losses of sequestered calcium. On the other hand, cadmium, which is known to induce permeability transition [295], causes in situ mitochondrial swelling in freshwater crab (*Sinopotamon yangtsekiense*) [296], and the crustacean isopod *Jaera nordmanni* [297]. Excluding the yeast, the mentioned species all belong to the crustacean subphylum.

4. Objectives

The mitochondrial permeability transition pore is a molecular machinery implicated in various presently untreatable conditions. Despite the attention it has been appreciating since its description over 34 years ago the structure of the PTP remains elusive. The primary objective of the ongoing study described in this thesis is the identification of the proteins comprising the PTP. This goal is highly ambitious and is well beyond the scope of a single PhD project. The work I participated in aims at laying down the fundamentals to achieve this goal. Because during this period our hypothesizes were frequently changing in light of our newest findings, our specific aims cannot be discussed without describing some of our results.

Initially we were focused on the thorough biochemical characterization of the only animal species known at the time proven directly not to exhibit classical PTP, the brine shrimp, *Artemia franciscana* [291], in order to find hints about the molecular basis of their unique trait. This animal is a primitive and ancient arthropod, belonging to the crustacean subphylum, inhabiting salt-water lakes. *Artemia*, especially in their embryonic forms are remarkably resilient to a variety of physical and chemical stress, and the lack of PTP was believed to be a key adaptation in this species for its survival in the harsh environment of salt-water lakes. Based on our findings in *Artemia* we hypothesized that the unique ANT isoform expressed in *Artemia* could be connected to the absence of PT in this species.

To expand on the subject we sought for a model animal exhibiting PTP and phylogenetically close to *Artemia*. The PTP was barely studied in phyla other than chordates, with the vast majority of the literature describing it in only one class of vertebrates, mammals. Therefore we analyzed species that like *Artemia* belong to the crustacean subphylum. Surprisingly, our results (which have been published: [298, 299]) suggest that crustaceans generally lack the specific machinery for orchestrating the Ca^{2+}-induced permeability transition pore, regardless of their natural environment. We became interested if the loss of the PTP was a unique trait of crustaceans, and at what point in their evolution did it happen.

Because the analysis of crustaceans instead of identifying good models for comparison, yielded further examples that lack the PTP, we started studying species belonging to a number of different phyla in which the presence of the PTP was unknown. Our goal at this point was not only to find proper models for comparison, but to possibly identify other phyla lacking the PTP.

We found that the ANT in mitochondria isolated from the embryos of *Artemia* was refractory to BKA. A parallel goal to investigating the PTP was to find the BKA binding site of the ANT and to evaluate if resistance to BKA is connected to the absence of the PTP.

We believe that there is a chance to identify key proteins of the PTP, by data from state of the art techniques of proteomics and genome sequencing subjected to bioinformatics methods. The aim of the project now is identify the structural components of the permeability transition pore by gene mapping and phylogenetic analysis of organisms that do not exhibit the Ca^{2+} inducible permeability transition versus those that do.

5. Materials and methods

5.1. Mitochondrial isolation

5.1.1. Artemia franciscana

Mitochondria from embryos of *A. franciscana* were prepared as described elsewhere, with minor modifications [300]. Dehydrated, encysted gastrulae of *A. franciscana* were obtained from Salt Lake, Utah, through Global Aquafeeds (Salt Lake City, UT, USA) or Artemia International LLC (Fairview, TX, USA) and stored at 4 °C until use. Embryos (15 g) were hydrated in 0.25 M NaCl at room temperature for at least 24 h. After this developmental incubation, the embryos were dechorionated in modified antiformin solution (1% hypochlorite from bleach, 60 mM $NaCO_3$, 0.4 m NaOH) for 30 min, and this was followed by a rinse in 1% sodum thiosulfate (5 min) and multiple washings in ice-cold 0.25 M NaCl as previously described [301]. After the embryos had been filtered through filter paper, ~ 10 g was homogenized in ice-cold isolation buffer consisting of 0.5 M sucrose, 150 mM KCl, 1 mM EGTA, 0.5% (w/v) fatty acid-free BSA, and 20 mM K^+-Hepes (pH 7.5) with a glass–Teflon homogenizer at 850 r.p.m. for 10 passages. The homogenate was centrifuged for 10 min at 300 g and 4 °C, the upper fatty layer of the supernatant was aspirated, and the remaining supernatant was centrifuged at 11 300 g for 10 min. The resulting pellet was gently resuspended in the same buffer, but without resuspending the green core. This green core was discarded, and the resuspended pellet was centrifuged again at 11 300 g for 10 min. The final pellet was resuspended in 0.4 ml of ice-cold isolation buffer consisting of 0.5 M sucrose, 150 mM KCl, 0.025 mM EGTA, 0.5% (w/v) fatty acid-free BSA, and 20 mM K^+-Hepes (pH 7.5), and contained ~ 80 mg protein·ml−1 (wet weight). The mitochondrial protein concentration was determined using the bicinchoninic acid assay [302]. For *Artemia* the incubation medium used in the experiments contained 500 mM sucrose, 150 mM KCl, 20 mM Hepes (acid), 10 mM potassium phosphate, 5 mM potassium glutamate, 5 mM potassium malate, 5 mM potassium succinate, 1 mM $MgCl_2$ (where indicated), 5 mg/ml· BSA (fatty-acid free), pH 7.5. Experiments were performed at 27 °C.

5.1.2. Vertebrates (*Xenopus laevis,* mouse and rat)

Mitochondria from the livers of *Xenopus* were isolated in a similar manner as for rat and C57Bl/6N mouse liver mitochondria, as described elsewhere [303]. Male Sprague-Dawley rats weighing 300–350 g were used. All animal procedures were performed according to the local animal care and use committee (Egyetemi Allatkiserleti Bizottsag) guidelines. The *X. laevis* liver is a melanin-containing organ, owing to the presence of melanomacrophage centers [304]; the presence of melanin in the mitochondrial pellet precluded the reliable calibration of the Calcium Green 5N hexapotassium salt (CaGr-5N) fluorescence signals (see below). Protein was measured by the bicinchonic assay. The incubation media used for experimentation contained 8 mM KC, 110 mM K-gluconate, 10 mM NaCl, 10mM Hepes, 10 mM KH_2PO_4 (where indicated), 0.005 mM EGTA, 10 mM mannitol, 0.5 mM $MgCl_2$ (or 1, where indicated), glutamate 1, succinate 5 (substrates where indicated), 0.5 mg/ml bovine serum albumin (fatty acid-free), pH 7.25. Experiments were performed at 30 °C for *Xenopus* and 37 °C for the rodents.

5.1.3. *Drosophila melanogaster* and *Caenorhabditis elegans*

Wild type *D melanogaster* were supplied by Viktor András Billes from the Department of Genetics, Eötvös Loránd University. 500-600 animals were pooled together and mitochondria was isolated in a similar manner as in [305], with minor modifications: the media used for isolation was identical to that described in [303].

C. elegans was provided by Csaba Sőti from the Department of Medical Chemistry, Molecular Biology and Pathobiochemistry, Semmelweis University.

Experimental buffer for these species was identical with what was used for the vertebrate species. Experiments were performed at 28 °C.

5.1.4. Freshwater crustaceans (*Cyclops vicinus vicinus* and *Daphnia pulex*)

Daphnia and *Cyclops* can be harvested at local ponds and rivers in high quantities by filtering. The abundance of plankton species differs throughout the year: the ratio of Cyclops mass in the filtrate is highest in the winter, while Daphnia concentrates at summer. The plankton samples of both *C. vicinus vicinus* and *D. pulex* harvested were 90-95% pure. Isolation was done in a similar manner as in [305], but with modified isolation buffers. The plankton was homogenized in ice-cold buffer containing, in mM: mannitol 225, sucrose 125, Hepes 5, EGTA 1, and 1 mg ml−1 bovine serum albumin (BSA, fatty acid-free), with the pH adjusted to 7.4 using Trizma. The homogenates were passed through one layer of muslin and centrifuged at 1,250 g for 10 min; the pellets were discarded, and the supernatants were centrifuged at 10,000 g for 10 min; this step was repeated once. At the end of the second centrifugation, the supernatants were discarded, and the pellets were suspended in 0.15 ml of the same buffer with 0.1 mM EGTA. Protein was measured by the bicinchonic assay. The experimental medium contained 225 mM mannitol, 125 mM sucrose, 5mM Hepes, 0.1 mM EGTA, 10 mM KH_2PO_4, 1 mM $MgCl_2$, 5 mM glutamate, 5 mM malate, 5 mM succinate, 0.5 mg/ml bovine serum albumin (fatty acid-free), pH = 7.25. Experiments were performed at 27 °C.

5.1.5. Marine species

The marine species used in this study (*Crangon crangon, Palaemon serratus, Carcinus maenas, Pagurus bernhardus, Asterias rubens, Paracentrotus lividus, Nephtys hombergii, Mytilus edule, Cerastoderma edule, Patella vulgata, Branchiostoma lanceolatum*) were obtained from Service d'Expédition de Modèles Biologiques - CNRS/FR2424 - Station Biologique de Roscoff, France. Animals were kept in aquariums filled with artificial sea water and algae at 6–8°C on 12 hours light/dark illumination cycles, until use. No ethical permissions are required for handling invertebrates for our research purposes. The harvesting of tissue for mitochondrial preparation differed for the species: For *C. crangon and P. serratus* 10-15 animals were pooled for each preparation. The cephalothorax of each

animal was removed and then the abdominal muscle was de-shelled. For *C. maenas* the hepatopancreas of 4-5 animals was pooled. For *P. bernhardus* the cephalothorax of each animal was removed and then the abdomen was used. For *A. rubens and P. lividus* the gastrointestinal tracts of 3-4 animals were pooled. For *N. hombergii and B. lanceolatum* 10-15 of animals were used. For *M. edule, C. edule and P. vulgata* 9-12 animals were de-shelled and pooled. The tissue harvested was chopped and homogenized in ice-cold buffer and processed in the same manner as *C. vicinus vicinus and D. pulex*. Protein was measured by the bicinchonic assay. Experimental buffer used for the investigation of these species was identical to that described for freshwater crustaceans. Experiments were performed at 27 °C.

5.2. ΔΨm determination

ΔΨm was estimated by fluorescence quenching of the cationic dye Safranin O owing to its accumulation inside energized mitochondria [306]. Mitochondria (amounts can be found in the figure legends) were added to 2 ml of the incubation medium (described for the specific species under mitochondrial isolation) plus 5 μM Safranin O. Fluorescence was recorded in a Hitachi F-4500 spectrofluorimeter (Hitachi High Technologies, Maidenhead, UK) at a 2-Hz acquisition rate, with 495- and 585-nm excitation and emission wavelengths, respectively. To convert Safranin O fluorescence into millivolts, a voltage–fluorescence calibration curve was constructed. To this end, Safranin O fluorescence was recorded in the presence of 5 nm valinomycin and stepwise increasing [K^+] (in the 0.2–120 mm range), which allowed calculation of ΔΨm from the Nernst equation, assuming a matrix [K^+] of 120 mm [306]. Pilot experiments with various substrates showed that the combination of glutamate, malate and succinate (all at 5 mM) yielded the most reproducible and most negative ΔΨm values of these mitochondria (not shown).

5.3. Extramitochondrial [Ca^{2+}] determination by Ca-Gr 5N fluorescence

Mitochondria (amounts can be found in the figure legends) were added to 2 ml of incubation medium (described for the specific species under mitochondrial isolation) plus 1 μM CaGr-5N. Fluorescence was recorded in a Hitachi F-4500 spectrofluorimeter at a 2-Hz acquisition rate, with 506- and 530-nm excitation and emission wavelengths, respectively. Where Mitochondria were not used for TEM, calibration of CaGr-5N fluorescence signal with free [Ca^{2+}] was performed as recently described [307], but because mitochondria used in these experiments was in most cases processed for TEM, calibration was not possible.

5.4. Mitochondrial swelling

Swelling of isolated mitochondria was assessed by measuring light scatter at 660 nm in a Hitachi F-4500 fluorescence spectrophotometer. Mitochondria (amounts described in the figure legends) were added to 2 ml of experimental medium. At the end of each experiment, the nonselective pore-forming peptide alamethicin was added as a calibration standard to cause maximal swelling.

5.5. Determination of free mitochondrial [Mg^{2+}] ([$Mg^{2+}]_f$) by Magnesium Green fluorescence in the extramitochondrial volume of isolated mitochondria and conversion of [$Mg^{2+}]_f$ to ADP–ATP exchange rate mediated by ANT

The ADP–ATP exchange rate was estimated with the method recently described by our team [303], exploiting the differential affinity of ADP and ATP for Mg^{2+}. The rate of ATP appearing in the medium following addition of ADP to energized mitochondria (or vice versa in the case of de-energized mitochondria) is calculated from the measured rate of change in $[Mg^{2+}]_f$ with the use of standard binding equations. The assay is designed for ANT to be the sole mediator of changes in [Mg^{2+}] in the extramitochondrial volume, as a result of ADP–ATP exchange. Mitochondria (amounts described in the figure legends)

were added to 2 ml of an incubation medium plus 2 μM Magnesium Green pentapotassium salt and 50 μM A_p5A. Fluorescence was recorded in a Hitachi F-4500 spectrofluorimeter at a 2-Hz acquisition rate, with 506- and 530-nm excitation and emission wavelengths, respectively. For the calculation of [ATP] or [ADP] from free [Mg^{2+}], the constants for K_{ADP}, and K_{ATP} were estimated for the respective buffer and temperature conditions (not shown).

5.6. Transmission electron microscopy (TEM)

Isolated mitochondria were pelleted by centrifugation (10 000 g for 10 min) and fixed overnight in 4% gluteraldehyde and 175 mM sodium cacodylate buffer (pH 7.5) at 4 °C. Subsequently, pellets were postfixed with 1% osmium tetroxide for 100 min, dehydrated with alcohol and propylene oxide, and embedded in Durcupan. Series of ultrathin sections (76 nm) were prepared with an ultramicrotome, mounted on single-slot copper grids, contrasted with 6% uranyl acetate (20 min) and lead citrate (5 min), and observed with a JEOL 1200 EMX (Peabody, MA, USA) electron microscope. The volume fraction of intramitochondrial Ca^{2+}–P_i precipitates was determined by adaptive thresholding performed in image analyst MKII (Image Analyst Software, Novato, CA, USA). To this end, the electronmicrographs, digitized at 8 bits, were inverted, background subtracted, nonlinearly scaled with a gamma value of 0.25, and smoothed by Wiener filtering. The inverted images were then binarized by adaptive thresholding with local maximum search. The fraction of positive pixels within the area bound by the inner boundary membrane was calculated, yielding the volume fraction of precipitates. No stereological correction was applied for projection, so both conditions were systematically biased towards overestimation of volume fractions.

5.7. Energy-filtered transmission electron microscopy (EFTEM)

Single-slot copper grids carrying 40-nm sections of the fixed pellets of *Artemia* mitochondria were produced as above, contrasted only by lead citrate for 5 min, and coated with carbon. Grids were imaged with a JEOL 3010 transmission electron microscope

equipped with a Tridiem-type Gatan Imaging Filter (Gatan GmbH, München, Germany), and elemental maps were recorded at 300 keV. In contrast to the alternative spectrometer mode of operation, the Gatan Imaging Filter was used in energy filter mode. Electrons with a preselected energy are only used to form an image in EFTEM mode. A spatial map of one selected element (calcium or phosphorus) was obtained by computer processing of three images, recorded at three, slightly different, energies. The first two energy windows were positioned below the absorption edge, characteristic of the excitation of an inner electron shell of the preselected element, and the third energy window was positioned just above the maximum intensity of the edge. Net intensity, indicative of the presence of the given element, was calculated on a pixel-by-pixel basis by extrapolating background from the first two windows under the third one, as described by Egerton [308]. The images were smoothed by anisotropic diffusion filtering, and contrasted for improved visualization with image analyst MKII.

5.8. Mitochondrial respiration

Oxygen consumption was performed polarographically using an Oxygraph-2k (Oroboros Instruments, Innsbruck, Austria). 0.5 mg of mitochondria were suspended in 2 ml incubation medium. Oxygen concentration and oxygen flux (pmol/(s*mg); negative time derivative of oxygen concentration, divided by mitochondrial mass per volume) were recorded using DatLab software (Oroboros Instruments).

5.9. Mitochondrial matrix pH (pH_i) determination of mouse liver and Artemia cyst mitochondria

The pH_{in} of mouse liver and *Artemia* cyst mitochondria mice was estimated as described previously [309], with minor modifications. Briefly, mouse liver mitochondria (20 mg) were suspended in 2 ml of medium containing (in mM): 225 mannitol, 75 sucrose, 5 Hepes, and 0.1 EGTA [pH 7.4 using Trizma, Sigma (St Louis, MO, USA)] and incubated with 50 µM BCECF-AM (Invitrogen, Carlsbad, CA, USA) at 30°C. After 20 min, mitochondria were centrifuged at 10,600 g for 3 min (at 4°C), washed once and re-centrifuged. The final

pellet was suspended in 0.2 ml of the same medium and kept on ice until further manipulation. A similar procedure was used for *Artemia* cysts with the exception that the medium consisted of 500 mM sucrose, 150 mM KCl, 1 mM EGTA, 0.5% (w/v) fatty acid-free BSA, and 20 mM K^+-Hepes (pH 7.5), and the temperature was 27°C. Fluorescence of hydrolyzed BCECF trapped in the matrix was measured in a Hitachi F-4500 spectrofluorimeter in a ratiometric mode at a 2 Hz acquisition rate, using excitation and emission wavelengths of 450/490 nm and 531 nm, respectively. Buffer composition for mouse liver mitochondria was, in mM: KCl 8, K-gluconate 110, NaCl 10, Hepes 10, KH_2PO_4 10, EGTA 0.005, mannitol 10, $MgCl_2$ 1, glutamate 5, malate 5, 0.5 mg/ml BSA (fatty acid-free), pH 7.25, and 50 µM Ap5A. For *Artemia* cysts, buffer composition was: 500 mM sucrose, 150 mM KCl, 20 mM Hepes (acid), 10 mM KH_2PO_4, 5 mm glutamate, 5 mM malate, 5 mM succinate, 1 mM $MgCl_2$, 5 mg·mL−1 BSA (fatty-acid free), pH 7.5. The BCECF signal was calibrated using a range of buffers of known pH in the range 6.6–7.6, and by equilibrating matrix pH to that of the experimental volume by 250 nM SF 6847 plus 1 µM nigericin. For converting BCECF fluorescence ratio to pH, we fitted the function: $f = a \times \exp[b/(x + c)]$ to BCECF fluorescence ratio values, where x is the BCECF fluorescence ratio, a, b and c are constants and f represents the calculated pH. The fitting of the above function to BCECF fluorescence ratio values obtained by subjecting mitochondria to buffers of known pH returned $r^2>0.99$ and the SE of the estimates of a and c constants were in the range 0.07–0.01, and <0.1 for b.

5.10. Cloning of ANT expressed in Artemia franciscana

Approximately 1 g of dechorionated Artemia cysts was homogenized in ice-cold TRIzol Reagent (Invitrogen, Carlsbad, CA, USA) with a glass-Teflon homogenizer. Total RNA was isolated according to the manufacturer’s instructions. RNA was subjected to 5′-RACE and 3′-RACE with the GeneRacer kit (Invitrogen), following the manufacturer’s protocol. Briefly, total RNA was treated with calf intestinal alkaline phosphatase to remove 5′-phosphates, a step that eliminates truncated mRNA and non-mRNA from subsequent ligation with the GeneRacer RNA oligonucleotide. Subsequently, tobacco acid

pyrophosphatase removed the cap structure from the 5′ -ends of full-length mRNAs and left a 5′ -phosphate required for ligation to the GeneRacer RNA oligonucleotide. The ligated mRNA was reverse transcribed to cDNA with the GeneRacer Oligo dT Primer, using SuperScript III RT. To obtain 5′ -ends, the cDNA template was amplified with a reverse gene-specific primer (AAGACCACTGAATTCACGCTCAGCAG) and the GeneRacer 5′ -primer. To obtain 3′ -ends, cDNA template was amplified with a forward gene-specific primer (TGCTGCTGGTGCAACCTCTCTGTGCTT) and the GeneRacer 3′ -primer. PCR fragments were subcloned into pCR 4-TOPO vector. (TOPO TA Cloning Kits for Sequencing; Invitrogen). Sequencing was performed by AGOWA GmbH, Berlin, Germany. The author of the thesis did not contribute to this work.

5.11. Partial sequencing of mRNA from Crangon crangon and Palaemon serratus transcribing the ANT

~1 gr of de-shelled abdominal muscle (devoid of the cephalothorax) of *Crangon crangon* and *Palaemon serratus* were each homogenized in ice-cold TRIzol Reagent (Invitrogen, Carlsbad, CA, USA) using a glass-Teflon homogenizer. Total RNA isolated by TRIzol, was reverse transcribed using Superscript II (Invitrogen) according to the manufacturer's instructions. The cDNA obtained was used as a template for amplification by PCR reaction. Primers used were: For *Crangon crangon*, forward: GTTGACAAGAAGACCCAATTCTGG; reverse: CCAGACTGCATCATCATTCG. For *Palaemon serratus*, forward: AGTGGACAAGAAGACCCAGTTCTGG; reverse: CCAGACTGCATCATCATGCG. PCR products were cloned into the pCR®2.1-TOPO® vector and transformed into E. coli TOP10 (TOPO TA Cloning Kit, Invitrogen). Sequencing of the colonies was performed by AGOWA GmbH, Berlin, Germany. The author of the thesis did not contribute to this work.

5.12. Multiple sequence alignment of protein sequences isoforms of ANT expressed in different species

Multiple sequence alignment was performed by Clustal Omega [310], and the output was generated by ESPript [311].

5.13. Reagents

Standard laboratory chemicals, cyclosporin A, Durcupan, gluteraldehyde, uranyl acetate, lead citrate, P1,P5-Di(adenosine-5′) pentaphosphate (Ap5A), and Safranin O were from Sigma (St. Louis, MO, USA). SF 6847 was from Biomol (BIOMOL GmbH, Hamburg, Germany). Magnesium Green $5K^+$ salt and Calcium Green 5N $6K^+$ salt were from Invitrogen (Carlsbad, CA, USA). Bongkrekic acid was from Merck (Merck KGaA, Darmstadt, Germany). All mitochondrial substrate stock solutions were dissolved in bi-distilled water and titrated to pH = 7.0 with KOH. ADP was purchased as a K^+ salt of the highest purity available (Merck) and titrated to pH = 6.9 with KOH. Bongkrekic acid was dissolved in 1 M ultrapure NH4OH in 10 mM stocks and kept at −20°C.

6. Results

6.1. Artemia franciscana

6.1.1. *Artemia* mitochondria lack the PTP

In order to confirm that mitochondria obtained from the embryos of this crustacean lack the PTP as originally shown by Menze et al. [291], we adapted our scheme [29] demonstrating a cyclosporin A-refractory PTP. In this scheme, addition of an uncoupler in the presence of phosphate carrier blockers (NEM and nBM) to Ca^{2+}-loaded rat liver mitochondria previously treated with oligomycin causes an immediate and precipitous opening of the PTP. As shown in Fig. 3A, this was not observed in mitochondria isolated from embryos of *A. franciscana*. It is of note that, in the presence of oligomycin and ADP, addition of Ca^{2+} failed to induce an increase in light scattering (Fig. 3A), consistent with the notion that ADP entering mitochondria is required for Ca^{2+}–P_i complexation [25]. Addition of the pore-forming peptide alamethicin induced mitochondrial swelling, manifested as an abrupt decrease in light scattering (Fig. 3A,B). However, in accordance with the mammalian consensus, addition of ADP in the absence of oligomycin to the suspension caused *Artemia* mitochondria to show 'shrinkage' upon addition of $CaCl_2$ (Fig. 3B), which is known to occur because of complexation of matrix Ca^{2+} with P_i affecting light scattering [25, 88]. From Fig. 3B, it is notable that addition of Ca^{2+} even in the absence of ADP caused a considerable increase in light scattering, although to a lesser extent than in the presence of the nucleotide. This is at odds with the finding that mitochondrial Ca^{2+} capacity is decreased in the presence of adenine nucleotides, and even the volume fraction of the calcium-rich and phosphorus-rich electron-dense material is smaller in the latter case (see Fig. 6B); however, the effect of alamethicin in mitochondria treated with ADP was not as great as the effect of the peptide in the absence of the nucleotide, and therefore a reliable comparison cannot be made.

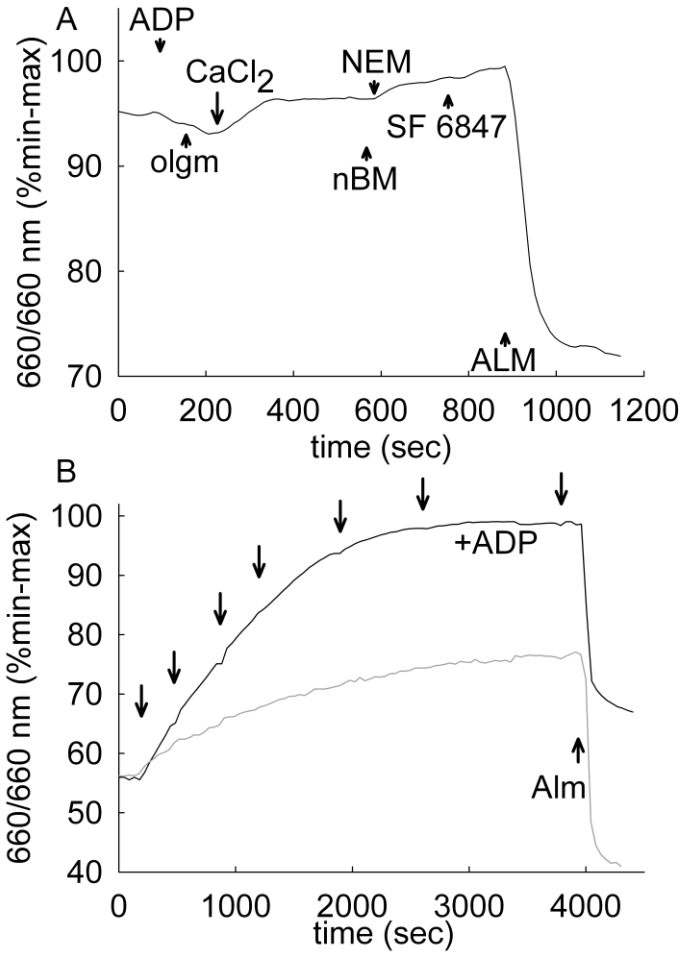

Figure 3: Absence of the PTP evaluated by 660/660-nm excitation/emission in Artemia mitochondria. (A) ADP (1 mM), oligomycin (olgm, 10 μM), CaCl2 (0.1 mM, free), n-butyl-malonate (nBM, 50 μM), N-ethylmaleimide (NEM, 0.5 mM), SF 6847 (250 nm) and alamethicin (ALM, 80 μg) were added where indicated. (B) $CaCl_2$ (0.2 mM) was added as indicated by the arrows (both traces). In the upper trace (black), 1 mM ADP was added prior to addition of mitochondria. Alamethicin (80 μg) was added where indicated as a calibration standard of maximum swelling. Results shown in both panels are representative of at least four independent experiments.

6.1.2. Effect of adenine nucleotides on Ca^{2+} sequestration of *Artemia* mitochondria

It has been well established that in mammalian mitochondria, adenine nucleotides increase Ca^{2+} uptake capacity [25, 88, 89]. In order to investigate whether this also applies to *Artemia* mitochondria, we tested the effect of ADP and ATP in the presence and absence of the ANT inhibitory ligand cATR, and of the F_oF_1-ATP synthase inhibitor oligomycin. The results are shown in Fig. 4. In Fig. 4A, ADP was present prior to the addition of mitochondria in all traces. In the presence of ADP (Fig. 4A, trace a) when neither cATR nor oligomycin was present, a clamped [Ca^{2+}] is difficult to achieve, owing to the interconversions of ADP to ATP by mitochondria, as these two nucleotides show different

K_d values for Ca^{2+}. When cATR or oligomycin was present, the amount of ADP was assumed to be static (see below), and therefore the estimations of free extramitochondrial Ca^{2+} were reliable. In the presence of ATP (Fig. 4B), as the mitochondrial membrane potential ($\Delta\Psi m$) did not exceed the reversal potential of ANT (see Fig. 4A), the amount of ATP added was assumed to be static, assisting the reliable calculations of the total amount of $CaCl_2$ added. What is apparent from Fig. 4A,B is that both ADP and ATP significantly decreased Ca^{2+} uptake rates as compared with the condition in which adenine nucleotides were absent (Fig. 4C), and thereby Ca^{2+} uptake capacity. The effect of ADP was considerably mitigated by cATR and oligomycin (Fig. 4A), implying that ADP mediated its effect after being taken up by mitochondria, most likely through ANT. Inhibition of F_oF_1-ATP synthase by oligomycin also lead to cessation of the function of ANT [303]. It is apparent from Fig. 4C that even cATR alone slightly accelerated mitochondrial Ca^{2+} uptake, in the absence of nucleotides. We conservatively attributed this to the inhibition of mitochondrial ADP or ATP uptake (depending on the prevalent $\Delta\Psi m$) by cATR, thereby eliminating any effect of nucleotides released from broken mitochondria in the suspension. The effect of oligomycin alone is hard to predict, because this inhibitor blocks both ATP formation by polarized mitochondria and ATP hydrolysis by depolarized mitochondria found in the same suspension. It is of note that BKA had no effect as compared with its vehicle (5 mM ammonium hydroxide; not shown), but it also failed to inhibit the ADP–ATP exchange rate of *Artemia* mitochondria (see below).

In summary, Fig. 4 shows that exogenously added adenine nucleotides decrease Ca^{2+} uptake rate and capacity in mitochondria isolated from embryos of *A. franciscana*, a phenomenon that is apparently at odds with the mammalian consensus.

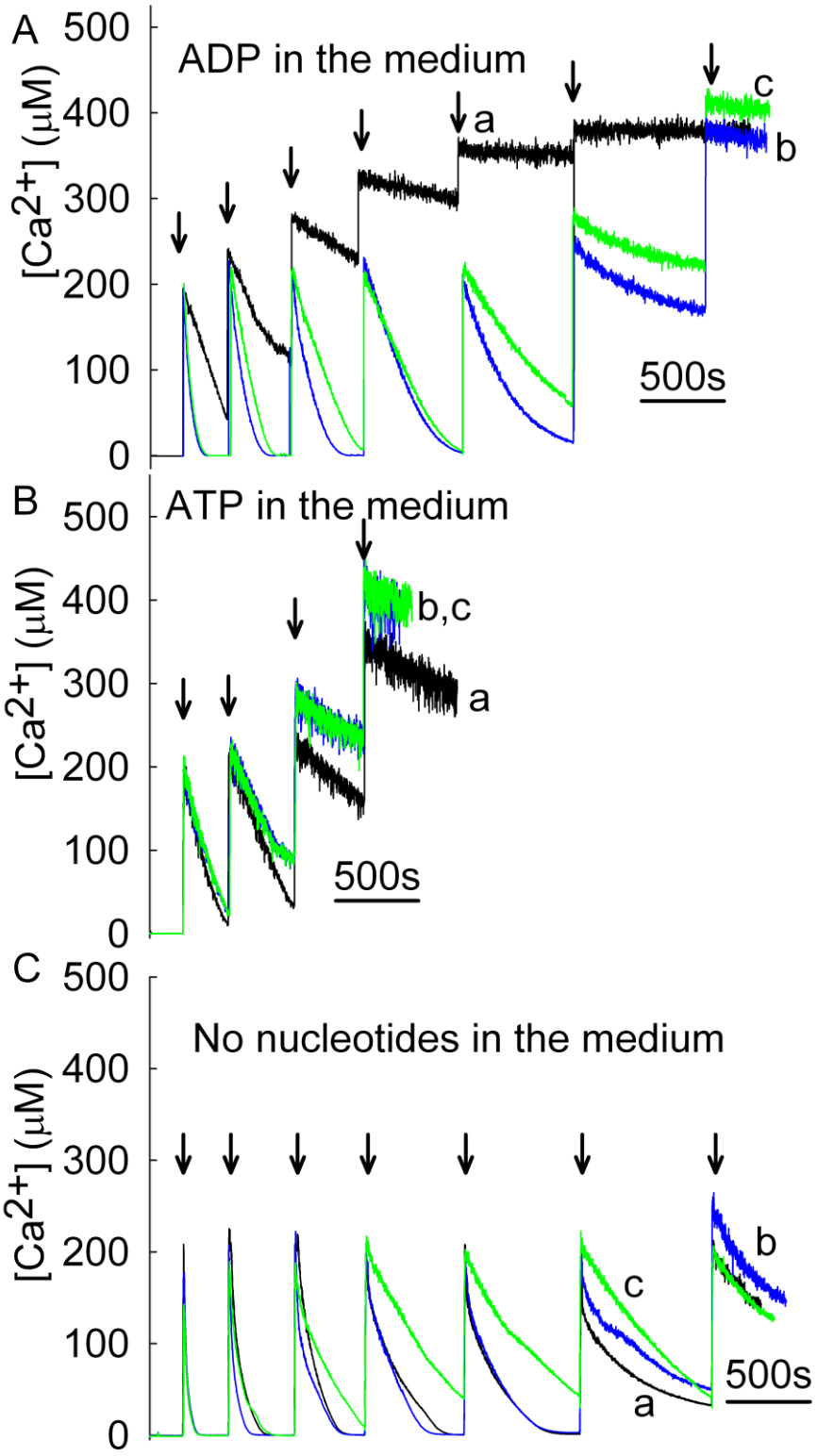

Figure 4: Effect of ANT ligands on Ca^{2+} uptake capacity in *Artemia* mitochondria. (A) Reconstructed time courses of extramitochondrial $[Ca^{2+}]$ calculated from CaGr-5N fluorescence. Mitochondria were added at 50 s, and this was followed by the addition of 2 mM ADP; 200 μM $CaCl_2$ (total) was added where indicated by the arrows. For trace b (blue), 4 μM cATR was added, and for trace c (green), 10 μM oligomycin was added, followed by 2 mM ADP prior to addition of mitochondria. In trace a, no inhibitors were present. (B) As for (A), but ATP was added instead of ADP. (C) As for (A) and (B), but no nucleotides were present. Results shown in all panels are representative of at least four independent experiments.

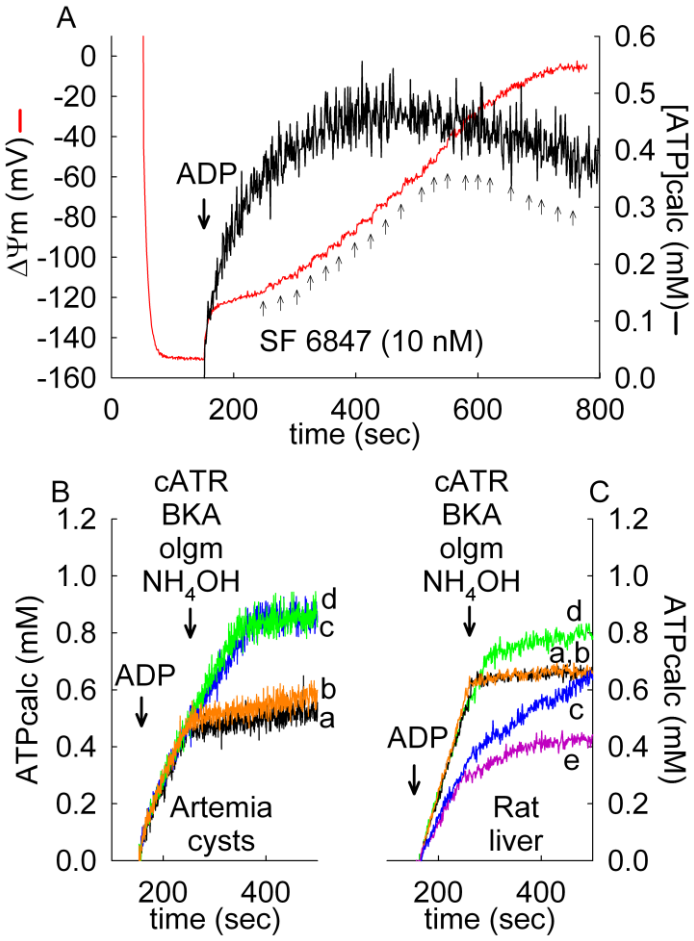

Figure 5: ADP–ATP exchange rate and ΔΨm profile of Artemia mitochondria. The effect of ANT ligands on the ADP–ATP exchange rate. (A) Reconstructed time courses of ΔΨm, calculated from Safranin O fluorescence, and extramitochondrial [ATP] appearing in the medium upon addition of ADP (at 150 s) calculated from Magnesium Green fluorescence as described in the Methods chapter. For both traces, small arrows indicate the addition of 10 nM SF 6847. (B) Reconstructed time courses of extramitochondrial [ATP] appearing in the medium upon addition of ADP (where indicated) in Artemia mitochondria, and effect of mitochondrial inhibitors. cATR (trace a), oligomycin (olgm, trace b), vehicle (5 mM NH_4OH, trace c) or BKA (50 µM, trace d) was added where indicated. (C) Reconstructed time courses of extramitochondrial [ATP] appearing in the medium upon addition of ADP (where indicated) in rat liver mitochondria, and effect of mitochondrial inhibitors. cATR (trace a), oligomycin (olgm, trace b), vehicle (5 mM NH_4OH, trace c), BKA (50 µM, in buffer at pH 7.25, trace d), or BKA (50 µM, in buffer at pH 7.5, trace e) was added where indicated. Results shown in all three panels are representative of at least four independent experiments.

6.1.3. Demonstration of the function of ANT in *Artemia franciscana* by the ADP–ATP exchange rate–ΔΨm profile

As adenine nucleotides produced unusual effects on the Ca^{2+} uptake characteristics in *Artemia* mitochondria, it was important to evaluate the functional status of ANT in these mitochondria. For this, a recently described method was used [303], in which the ADP–ATP exchange rate mediated by ANT is measured as a function of ΔΨm. Such an experiment is shown in Fig. 5A. The ADP–ATP exchange rate mediated by ANT (in the

presence of diadenosine pentaphosphate, a blocker of adenylate kinase) was measured by exploiting the differential affinity of ADP and ATP for Mg^{2+}. The rate of ATP appearance in the medium following addition of ADP to energized mitochondria was calculated from the measured rate of change in free extramitochondrial [Mg^{2+}] by the use of standard binding equations [303]. During the course of this experiment, ADP–ATP exchange rates were gradually altered by stepwise additions of an uncoupler (10 nM SF 6847) until complete collapse of ΔΨm. In parallel experiments, ΔΨm was measured by Safranin O fluorescence, and calibrated to millivolts as detailed in the Methods chapter. As shown in Fig. 5A, ATP appeared in the medium after ADP addition, and at the same time there was a depolarization by ~25 mV. Subsequent stepwise additions of the uncoupler SF 6847 led to a stepwise decrease in ΔΨm accompanied by a decrease in the ADP–ATP exchange rate. This culminated at approximately -90 to -100 mV, and thereafter ANT was gradually reversed. The ATP influx rate (reverse mode of ANT) was much slower than the ADP influx rate, *i.e.* the forward mode of ANT. From these experiments, we concluded that the ANT of our mitochondrial preparations of *A. franciscana* embryos is fully functional.

6.1.4. ANT of *Artemia franciscana* is refractory to BKA

As mentioned above, BKA was without an effect on Ca^{2+} uptake rate and capacity in *Artemia* mitochondria. Here, we tested whether BKA (three different LOT stocks were tested) was able to act on the fully functional ANT. As shown in Fig. 5B, addition of either cATR (trace a) or oligomycin (trace b) immediately stopped further ATP appearance in the medium, implying a cessation of ANT operation. In contrast, addition of BKA (50 μM, trace d) failed to inhibit ANT operation as compared with the control (5 mM NH_4OH, which is the vehicle of BKA, trace c). With the same BKA stocks, this poison fully inhibited ANT operation in rat liver mitochondria (Fig. 5C) and also induced state 4 from state 3 respiration (not shown). BKA was also tested at pH 7.5, the pH of the buffer used for experiments with *Artemia* mitochondria; this is important, because BKA needs to be protonated in order to exert its action [128], and at pH 7.5 it will be less efficient. Still, as shown in Fig. 5C, 50 μM BKA inhibited the ADP-ATP exchange rate in rat liver

mitochondria (trace e), although with a delay, as explained in [127, 130, 131], as compared with its vehicle (trace c). NH_4OH at 5 mM reduced the ADP-ATP exchange rate, probably because of matrix alkalinization, in accordance with our findings reported earlier [303], however, this was not observed in *Artemia* mitochondria. It is also notable that at pH 7.5 (traces c and e of Fig. 5C), ADP-ATP exchange rates are smaller than those obtained in buffer at pH 7.25, in line with the results obtained in [303]. Furthermore, as shown below, the same BKA inhibited Ca^{2+}-induced swelling in Xenopus liver mitochondria. From the results shown in Fig. 5B,C, we postulated that the ANT isoform(s) of *A. franciscana* may lack a BKA-binding site.

6.1.5. Ca^{2+}-P_i matrix complexation in *Artemia* mitochondria shows a unique morphology

As shown above, mitochondria from the embryos of *A. franciscana* sequester Ca^{2+}, although adenine nucleotides decrease uptake rates and capacity. The effect of ADP probably took place at the matrix side, as cATR mitigated its action. However, the effect of ATP also seems to be mediated by a cATR/oligomycin-insensitive mechanism. Adenine nucleotide-sensitive site(s) that alter maximum Ca^{2+} uptake capacity other than ANT have been reported in a variety of mitochondria [2], although their identity is still unknown. The complexation/precipitation of Ca^{2+} with P_i in the mitochondrial matrix and the involvement of matrix adenine nucleotides as phosphate donors have been firmly established in mammalian mitochondria [25, 29, 88]. We were therefore interested in the nature of this phenomenon in *Artemia* mitochondria, as the functional data deviated so significantly from the mammalian consensus. As shown in Fig. 7A, mitochondria from the crustacean incubated in the absence of adenine nucleotides and $MgCl_2$ showed needle-like electron-dense structures. If ADP (Fig. 7B) or $MgCl_2$ (Fig. 7C) was present during Ca^{2+} loading, dot-like electron-dense structures were observed instead. In order to confirm that the electron-dense structures were indeed Ca^{2+}-P_i precipitates, we performed energy-filtered transmission electron microscopy (EFTEM) of Ca^{2+}-loaded mitochondria in the absence of adenine nucleotides and $MgCl_2$, as detailed under the Methods chapter. Spatial maps of

calcium and phosphorus were recorded (Fig. 7D,E), and confirmed a high degree of colocalization (Fig. 7F,G). Image stability was insufficient (owing to very long exposure times – 10 min each – under high magnification, bar 50 nm) to allow the same experiments to be performed in mitochondria loaded with Ca^{2+} in the presence of adenine nucleotides or $MgCl_2$, during which dot-like electron dense structures are observed. Quantification by adaptive thresholding (Fig. 6) revealed that the volume fraction of the electron-dense material in the volume bounded by the inner boundary membrane was significantly higher in mitochondria untreated with ADP than in those treated with the nucleotide. This is in line with the experimental findings on Ca^{2+} uptake capacity in the presence and absence of adenine nucleotides.

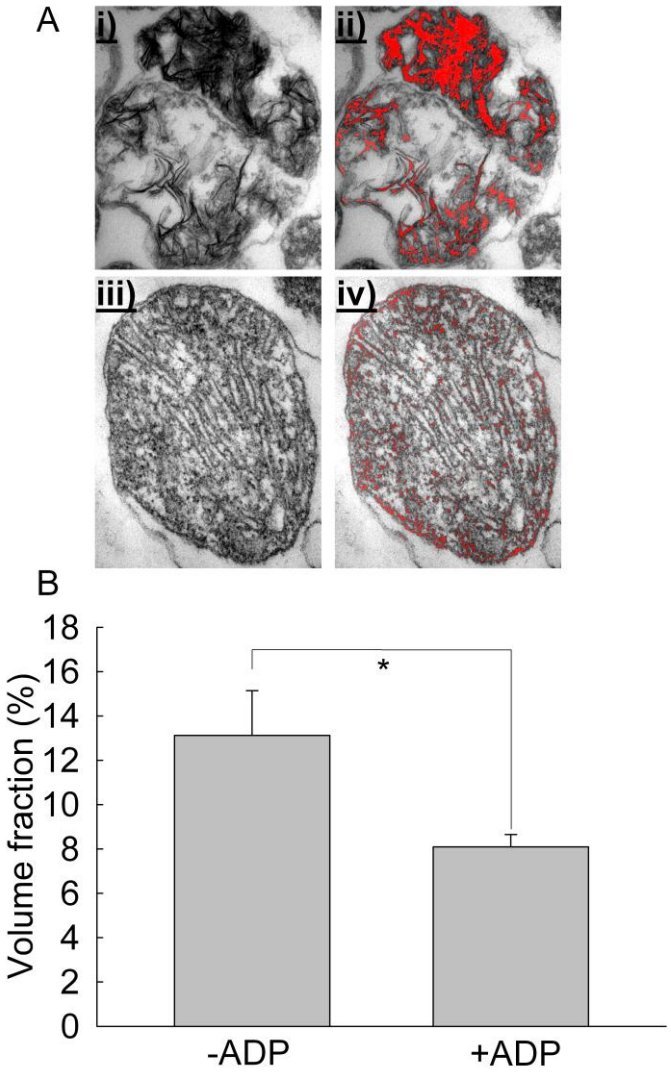

Figure 6: Quantification of the Ca^{2+}–P_i-rich areas of Ca^{2+}-loaded Artemia mitochondria by adaptive thresholding. (A) Images of Artemia mitochondria loaded with Ca^{2+}: (i) incubated in the absence of $MgCl_2$ or adenine nucleotides; (ii) same image with adaptive thresholding (red); (iii) incubated in the presence of ADP; (iv) same image as in (iii), with adaptive thresholding (red). (B) Volume fractions of the electron-dense material in the mitochondria loaded with Ca^{2+} with or without ADP, in the absence of $MgCl_2$, as calculated by the fractional area of positive pixels [red in (A)] of the mitochondrion ($P = 0.031$ by Mann–Whitney rank-sum test; 29 TEM images in total).

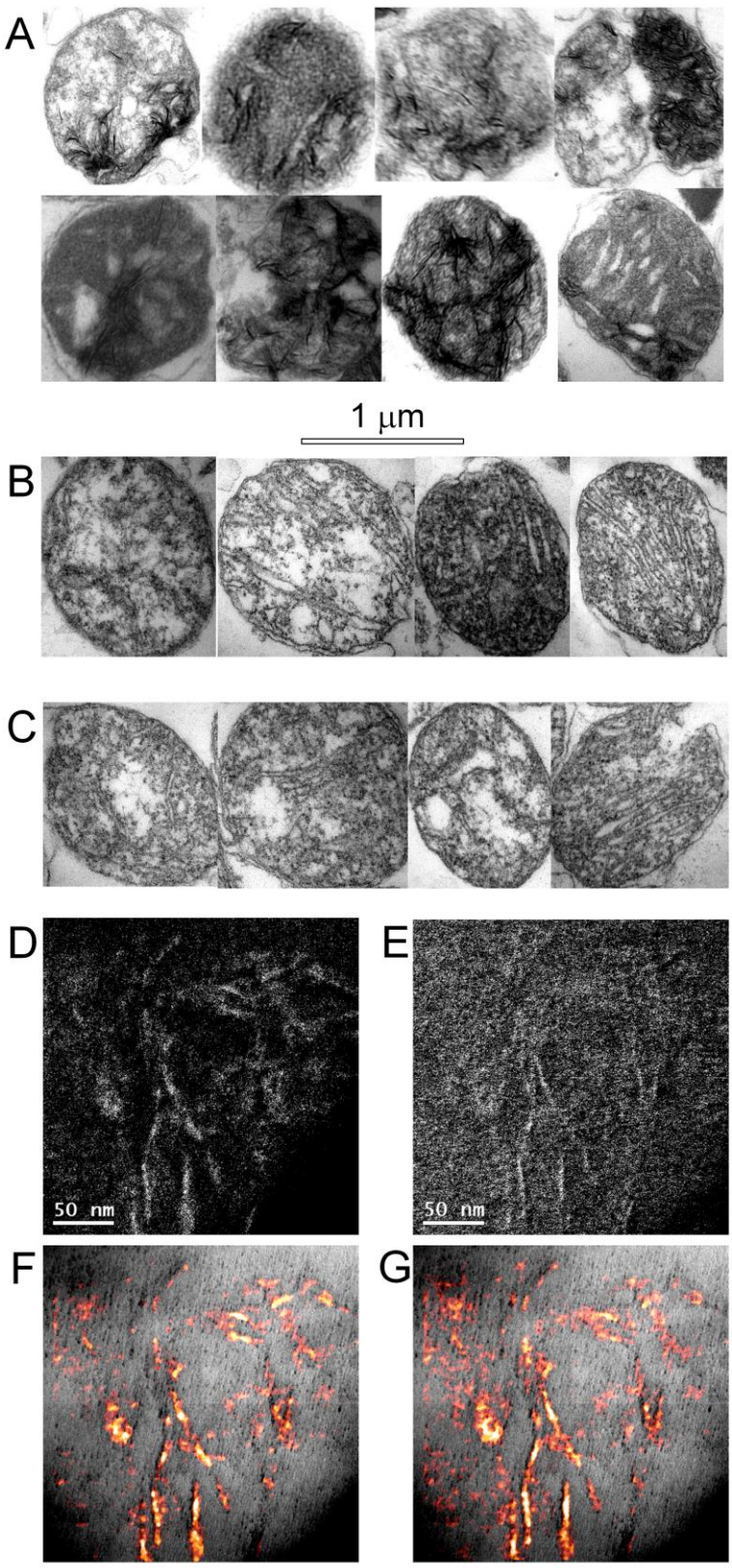

Figure 7: TEM and EFTEM images of Ca^{2+}-loaded Artemia mitochondria. (A, B) TEM images of Artemia mitochondria loaded with Ca^{2+}, incubated in the absence (A) or presence (B) of ADP. (C) TEM images of Artemia mitochondria loaded with Ca^{2+} in the presence of 2 mM $MgCl_2$ incubated in the absence of ADP. The 1-μm bar applies to all images in (A–C). (D) Calcium map obtained from EFTEM imaging. (E) Phosphorus map obtained from EFTEM imaging. (F) Pseudocolor image of (D). (G) Pseudocolor image of (E). The scale bars of (D) and (E) also apply to (F) and (G), respectively.

6.1.6. Mitochondria isolated from *Xenopus* liver reveal a classical Ca^{2+}-induced PTP that is sensitive to cyclosporin A and BKA

By alignment of the ANT sequences from various organisms, we deduced that the two closest homologs of *A. franciscana* ANT, readily sequenced at the time were those expressed in *Drosophila melanogaster* and *Xenopus laevis*, both of which are similar to each other but not to A. *franciscana* ANT regarding the 221-229 amino acid region (see in the "Comparison of the primary sequence of *Artemia* ANT with that of other species"

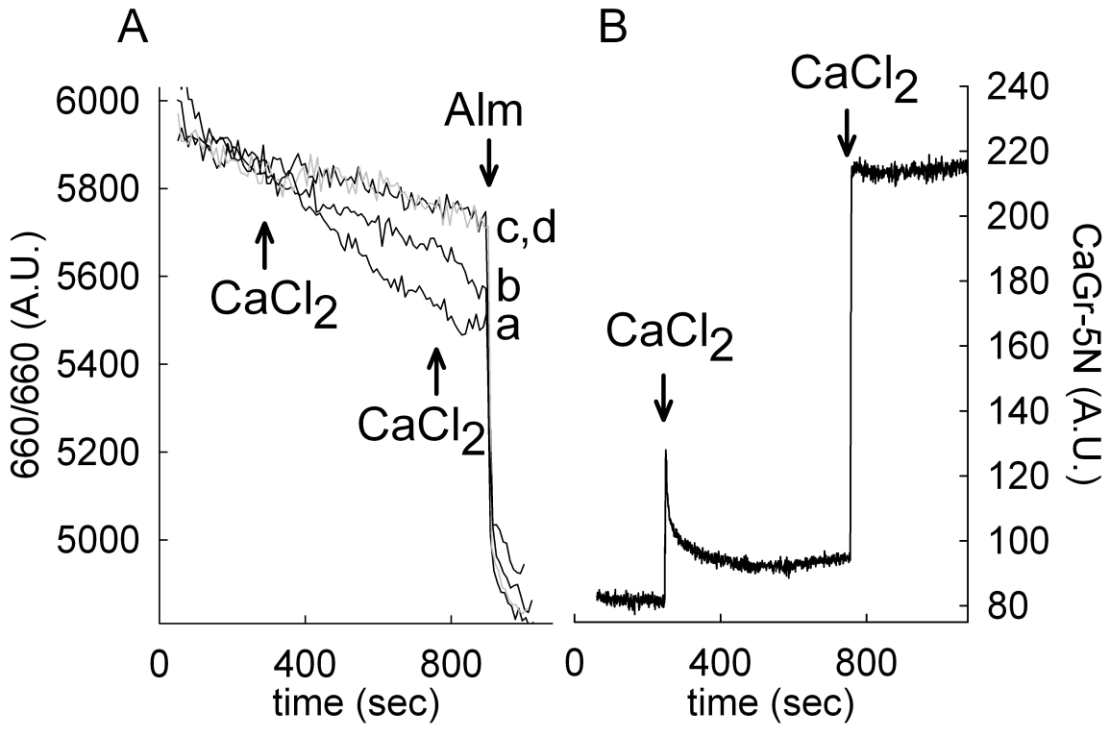

Figure 8: Effect of Ca^{2+} uptake on light scattering in mitochondria isolated from the liver of *X. laevis*. (A) Time courses of light scattering of *X. laevis* liver mitochondria followed by 660/660-nm excitation/emission. $CaCl_2$ (20 μM) was added where indicated by the arrows. Trace a, only Ca^{2+} addition; trace b, Ca^{2+} addition plus BKA (50 μM); trace c, no Ca^{2+} addition; trace d, Ca^{2+} addition plus 1 μM cyclosporin A. Cyclosporin A or BKA was present in the medium prior to the addition of mitochondria. (B) Reconstructed time course of extramitochondrial [Ca^{2+}] obtained from CaGr-5N fluorescence. Mitochondria were added at 50 s, and this was followed by addition of 20 μM CaCl2, where indicated by the arrows. Results shown in both panels are representative of at least four independent experiments.

chapter). *D. melanogaster* shows a Ca^{2+}-regulated permeability pathway with features intermediate between the PTP of yeast and that of vertebrates [271]. Amphibians were

reported to have PTP [269, 270], but the *X. laevis* itself had not been tested. We were therefore interested in whether mitochondria isolated from tissues from *X. laevis* show the Ca^{2+}-induced PTP. As shown in Fig. 8A, when 20 μM $CaCl_2$ was added to *Xenopus* liver mitochondria, a decrease in light scatter was observed (trace a) as compared with no addition of $CaCl_2$ (trace d) that was completely sensitive to cyclosporin A (trace c) and partially sensitive to BKA (trace b). From this experiment, we concluded that *Xenopus* liver mitochondria have a classical PTP that is induced by Ca^{2+} and is sensitive to cyclosporin A and BKA.

We sequenced the ANT expressed in *Artemia* and performed multiple sequence alignment in order to identify the BKA binding site. These results will be discussed in a later chapter.

6.2. PTP and BKA sensitivity in species related to Artemia: the crustacean subphylum

Xenopus and *Drosophila* are distinctly related to Artemia, furthermore mindful of the studies carried out on other crustacean species demonstrating remarkable calcium uptake capacities [292-294], we hoped to find further species without PTP but BKA insensitivity. The two crustacean species that were easily accessible are the locally native zooplanktons: the water flea (*Daphnia pulex*) and the cyclops (*Cyclops vicinus vicinus*).

6.2.1. Cyclops vicinus vicinus

The characterization of mitochondria from the *Cyclops vicinus vicinus* was addressed by similar methods but in some cases different protocols from those used to investigate *Artemia* mitochondria. Like *Artemia*, Cyclops mitochondria also show a remarkable Ca^{2+} uptake capacity with no abrupt release of Ca^{2+}. In the experiment shown by Fig. 9A, extramitochondrial Ca^{2+} is measured by Calcium Green 5N. 50 µM steps of $CaCl_2$ are added until no further sequestration is seen. Similar protocols were used to measure uptake capacity in other species, which will be discussed in the next chapters. Ca^{2+} uptake is similar to that of *Artemia*, showing no signs of PTP. Note that electron microscopic images of the preparation show high amount of impurities (see below), therefore quantification of mitochondria by measuring protein was not reliable.

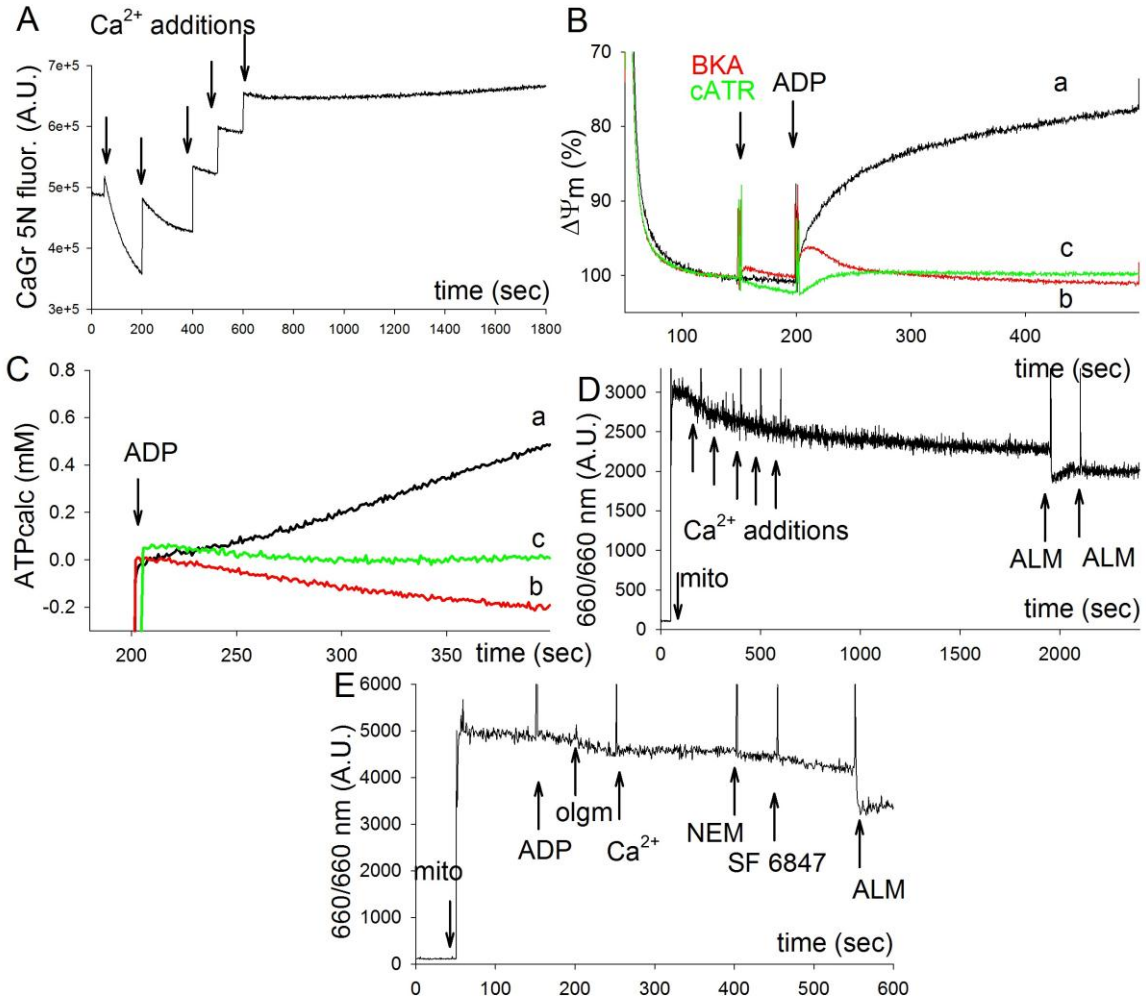

Figure 9: BKA sensitivity and presence of PTP in *Cyclops vicinus vicinus*. (A) Reconstructed time courses of CaGr-5N fluorescence.1 mg/ml mitochondria was added at the start of the experiment and consequently challenged with 50 µM $CaCl_2$ pulses when indicated by the arrows. (B) Reconstructed time courses of Safranin O fluorescence expressed in percentage of polarization. 20 µM BKA (trace b, red) or 10 µM cATR (trace c, green) was added at 150 s, followed by 2 mM ADP. (C) Reconstructed time courses of ATP appearing in the medium calculated from MgGr-5N fluorescence. Experimental scheme and markings are identical to B. (D) Reconstructed time courses of 90° light scattering measured at 660 nm. 1 mg/ml mitochondrial preparation was added at 50 s followed by 50 µM $CaCl_2$ pulses when indicated by the arrows, and finally by 20 µg Alamethicin. (E) Light scattering measured as in D. ADP (1 mM), oligomycin (olgm, 10 µM), CaCl2 (0.1 mM, free), n-butyl-malonate (nBM, 50 µM), N-ethylmaleimide (NEM, 0.5 mM), SF 6847 (250 nm) and alamethicin (ALM, 80 µg) were added where indicated.

Fig. 9B shows time courses of Safranin O fluorescence reflecting ΔΨm (% scale). Maximum (100%) polarization is the value of Safranin O fluorescence prior to the addition of ADP; minimum (0%) polarization is the value of Safranin O fluorescence after the addition of 1 µM SF6947 (omitted from the graph). We use this scale, because the limited amount of sample in the case of the majority of species investigated did not allow precise calibration of Safranin O signals. Membrane potential (Fig. 9B) and ATP production (Fig. 9C) is measured to address ANT sensitivity to BKA and cATR. In these experiments the inhibitors were added prior to ADP in order to avoid artifacts caused by slow penetration of BKA through the membrane. As seen on both panels B and C, both BKA (b traces, red) and cATR (c traces, green) are effective blockers of the ANT of *Cyclops vicinus vicinus*. A stable Mg^{2+} signal could not be acquired in the ATP measurements with these species, which caused the slopes of traces b and c on Fig.9C to be negative when inhibited.

Light scattering of mitochondria from *Cyclops* were monitored at 660/660 nm while challenged to swell by two different protocols; i) by addition of $CaCl_2$ exceeding uptake capacity, according to Fig. 9A (Fig. 9D) or ii) by the same scheme described previously [29] (Fig. 9E). No decrease in light scattering that would indicate permeability transition was observed. The relatively small effect of alamethicin is probably due to the high quantity of impurities of the sample as mentioned earlier.

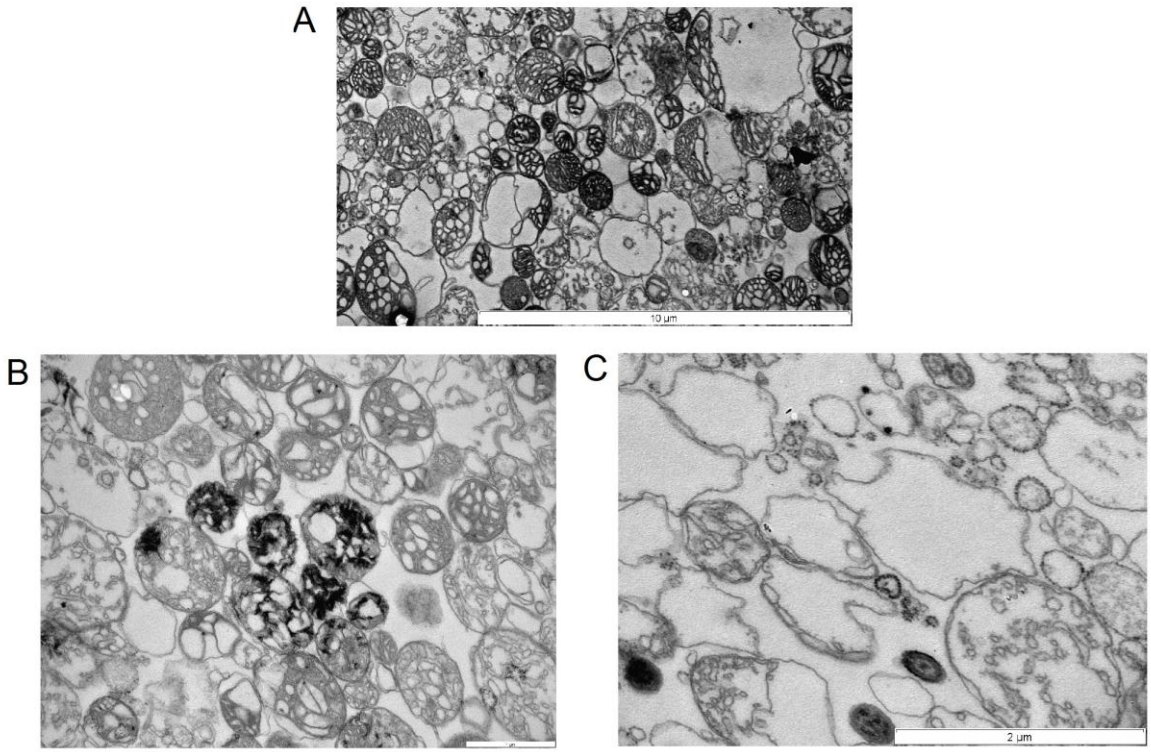

Figure 10: TEM images of *Cyclops* mitochondria. Panel A shows control, panel B sows mitochondria loaded with Ca^{2+} in the experiment shown on Fig. 9 panel A, panel C shows mitochondria treated with 20 µg Alamethicin. Bars shown in the lower right corners of each panel are as follows: A: 10 µm, B: 1 µm, C: 5 µm.

Finally, TEM images further confirm Cyclops mitochondria to lack Ca^{2+} inducible permeability transition. Mitochondria show normal morphology when untreated (Fig. 10A), needle like structures, but normal size after prolonged exposure to $CaCl_2$ above uptake capacity (Fig. 10B), and swelling upon treatment with alamethicin (Fig. 10C). In light of the above results it is unambiguous that *Cyclops vicinus vicinus*, similarly to *Artemia franciscana*, lacks the classical PTP, however it is sensitive to inhibition by BKA.

6.2.2. Daphnia pulex

Daphnia species are taxonomically the closest relatives to *Artemia* investigated to date in this study (Fig. 28). Ca^{2+} uptake capacity is high and there is no evidence of PTP after saturation by Ca^{2+} (Fig. 11A). In our experimental media, these species did not show stable polarization, however ΔΨm was sufficiently high to drive the ANT forward, and the repolarization upon both cATR and BKA conferred sensitivity to these agents (Fig 11B). Sensitivity to BKA is also demonstrated on ATP production rate (Fig. 11C). Subsequent

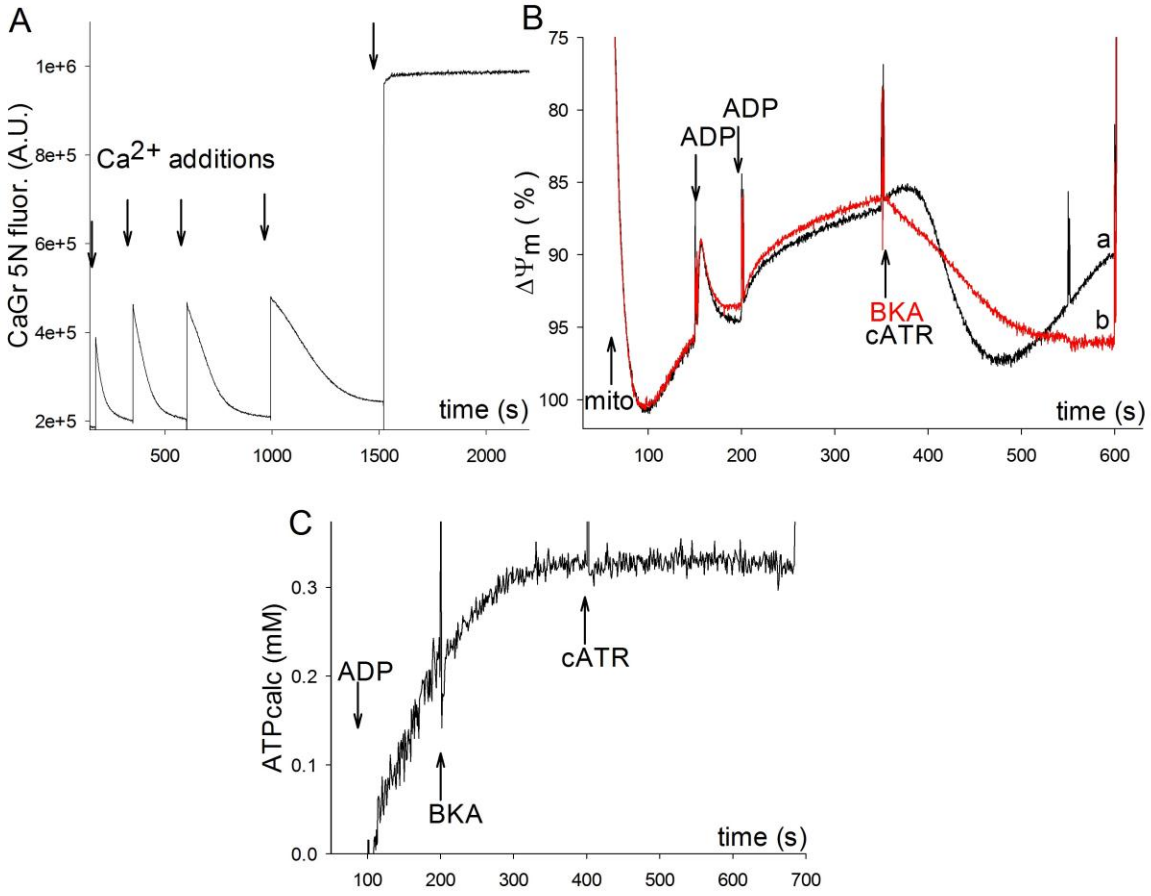

Figure 11: BKA sensitivity and Ca^{2+} uptake in *Daphnia pulex*. (A) Reconstructed time courses of CaGr-5N fluorescence.1 mg/ml mitochondria was added at the start of the experiment and consequently challenged with 100 µM $CaCl_2$ pulses when indicated by the arrows. (B) Reconstructed time courses of Safranin O fluorescence expressed in percentage of polarization. 1 mg/ml mitochondria was injected at 50 s, at 150 and 200 s 2 mM ADP was added followed by 20 µM BKA (trace b, red) or 10 µM cATR (trace a, black) at 350 s. (C) Reconstructed time courses of ATP appearing in the medium calculated from MgGr-5N fluorescence. 1 mg/ml mitochondria was added at 50 s, followed by 2 mM ADP at 100s and 20 µM BKA at 200 s. Subsequent addition of cATR (400 s) caused no further inhibition.

addition of cATR did not cause further inhibition, the effect of BKA was complete. No profound decrease of light scattering can be observed under the previously described experimental protocols (Fig. 12). Though TEM images have not yet been produced, the above findings suggest sensitivity to BKA and the lack of PTP in *Daphnia pulex*.

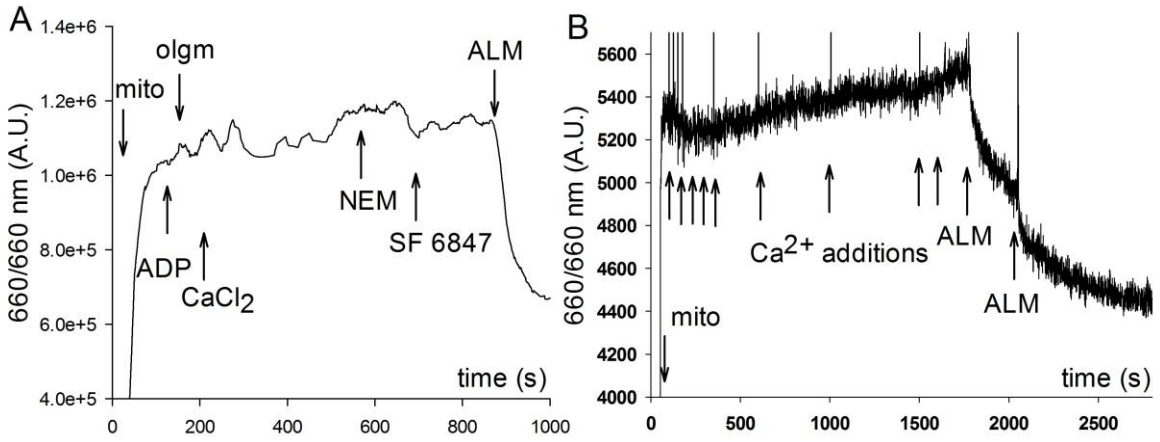

Figure 12: Light scattering in *Daphnia pulex*. (A) Reconstructed time courses of 90° light scattering measured at 660 nm. 1 mg/ml mitochondrial preparation was added at 50 s followed by 100 µM $CaCl_2$ pulses when indicated by the arrows, and finally by 20 µg Alamethicin. (B) Light scattering measured as in A. ADP (1 mM), oligomycin (olgm, 10 µM), $CaCl_2$ (0.1 mM, free), n-butyl-malonate (nBM, 50 µM), N-ethylmaleimide (NEM, 0.5 mM), SF 6847 (250 nM) and alamethicin (ALM, 80 µg) were added where indicated.

6.2.3. Crangon crangon

Artemia are extremophiles that tolerate complete desiccation for decades and anoxia for years, allowing them to survive in salt water lakes. The lack of permeability transition in *Artemia* was ascribed to be a trait necessary to survive the biochemical consequences of such events. The lack of PTP in freshwater crustaceans was unexpected, and directed us towards investigating further species from the subphylum. The brown shrimp (*Crangon*

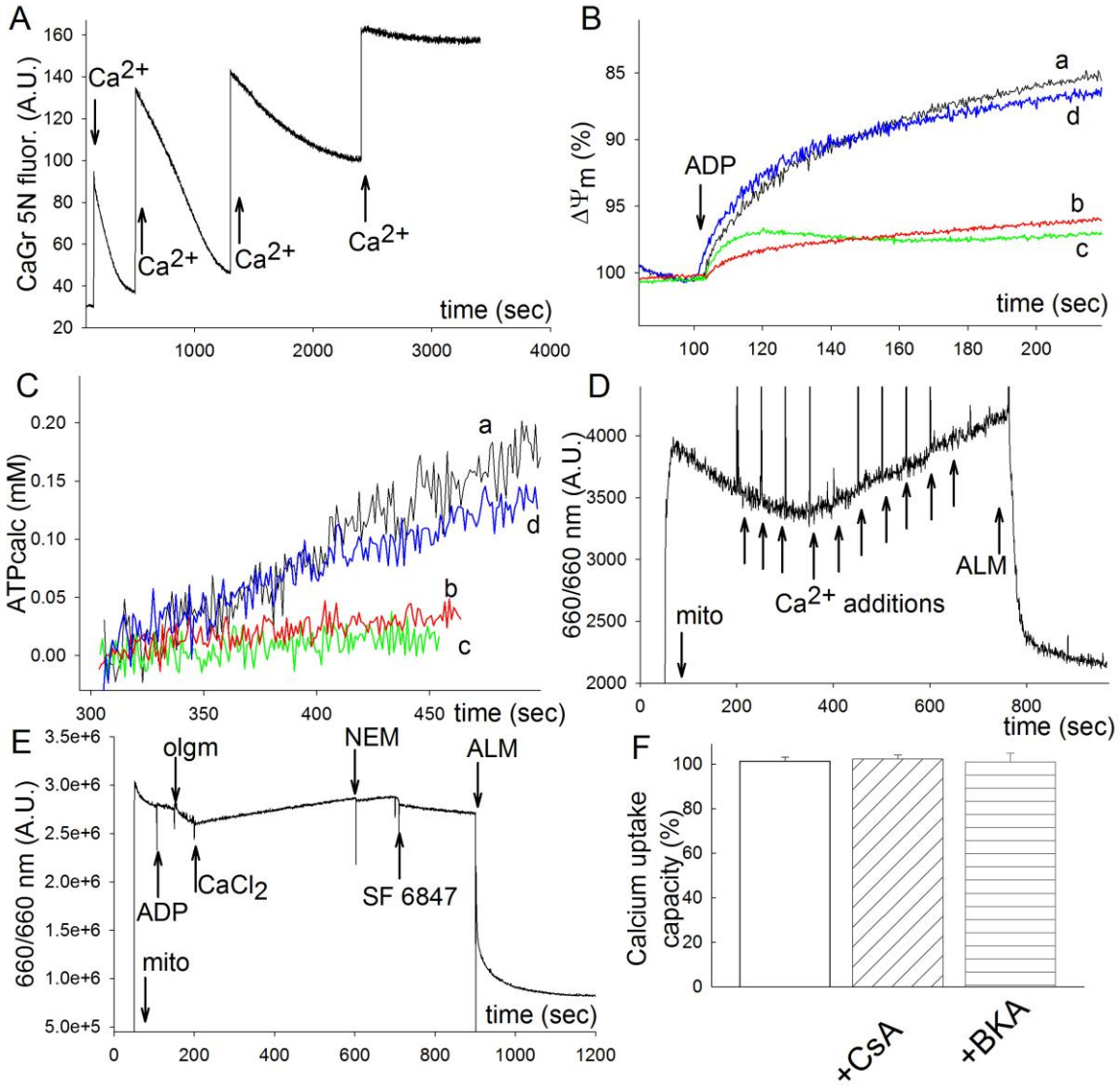

Figure 13: BKA sensitivity and presence of PTP in *Crangon crangon*. (A) Reconstructed time courses of CaGr-5N fluorescence.1 mg/ml mitochondria was added at the start of the experiment and consequently challenged with 200 µM $CaCl_2$ pulses when indicated by the arrows. (B) Reconstructed time courses of Safranin O fluorescence expressed in percentage of polarization. Trace a (black) is control, trace b (red) contained 20 µM BKA, trace c (green) contained 1 µM cATR, trace d (blue) contained vehicle of BKA (2 mM NH_4OH) in the medium prior to the experiment. 1 mg/ml mitochondria was injected at 50 s and at 100 s 2 mM ADP was added. (C) Reconstructed time courses of ATP appearing in the medium calculated from MgGr-5N fluorescence. Experimental procedure is identical to that in panel B. (D) Reconstructed time courses of 90° light scattering measured at 660 nm. 1 mg/ml mitochondrial preparation was added at 50 s followed by 200 µM $CaCl_2$ pulses when indicated by the arrows, and finally by 40 µg Alamethicin. (E) Light scattering measured as in D. ADP (1 mM), oligomycin (olgm, 10 µM), $CaCl_2$ (0.1 mM, free), n-butyl-malonate (nBM, 50 µM), N-ethylmaleimide (NEM, 0.5 mM), SF 6847 (250 nm) and alamethicin (ALM, 40 µg) were added where indicated. (F) Bar graphs of maximum Ca^{2+} uptake capacity (% scale) calculated from the number of 100 µM $CaCl_2$ additions given to mitochondria until no further decrease in CaGr-5N fluorescence (implying maximum mitochondrial calcium uptake) was observed, in the presence of 1 µM cyclosporin A or 20 µM BKA, (n = 3). The rates of Ca^{2+} uptake of the last addition were compared among treatment groups, where it exhibited a small variability, but no statistical significance (p = 0.933, ANOVA on Ranks). The rates of Ca^{2+} uptake of all previous $CaCl_2$ additions were virtually identical among all treatment groups.

crangon) is a marine crustacean species common in the Baltic, Atlantic coast of Europe from the White Sea to Portugal, Mediterranean, Black Sea and Atlantic coast of Morocco.

Applying our experimental schemes to mitochondria isolated from *Crangon crangon* revealed it to be similar to *Cyclops* and *Daphnia*. Measuring Ca^{2+} uptake, we found high uptake capacity and no sign of PTP (Fig. 13A). Mitochondria obtained from *Crangon crangon* were able to accumulate approximately 1.2 µmol of Ca^{2+} per mg protein, however the extent of contamination (as deduced from electron microscopy images) from non-mitochondrial material in these preparations amounted to more than 40%, which suggests an even greater capacity. Uptake capacity was unaffected by PTP inhibitors CsA and BKA (Fig. 13F). Mitochondria produced stable membrane potential in the presence of substrates, and depolarized upon ADP (Fig. 13B/a). No depolarization by ADP was observed when BKA (Fig. 13B/b) or cATR (Fig. 13B/c) was present in the experimental medium prior to ADP. The ADP response was unaffected when vehicle of BKA (2 mM NH_4OH) was added prior to ADP (Fig. 13B/d). Fig. 13C shows ATP production in the same experimental protocol as Fig. 13B. BKA (trace b) and cATR (trace c) cause complete inhibition of ATP production, while NH_4OH (trace d) has no effect compared to the control (trace a). No sign of PTP is detected on light scattering experiments when mitochondria from *Crangon crangon* are challenged by the previously described protocols (Fig 13D,E) until alamethicin

is added. TEM shows no PTP triggered by Ca^{2+} (Fig. 14B). Needle like electron dense formations can be observed at higher magnifications (Fig. 14C), similar to what we found in *Artemia* and *Cyclops*. Alamethicin effectively causes swelling (Fig. 14D). Our conclusion is that mitochondria isolated from *Crangon crangon* also lacks the Ca^{2+} inducible CsA sensitive PTP and that the ANT expressed in *Crangon* is sensitive to BKA.

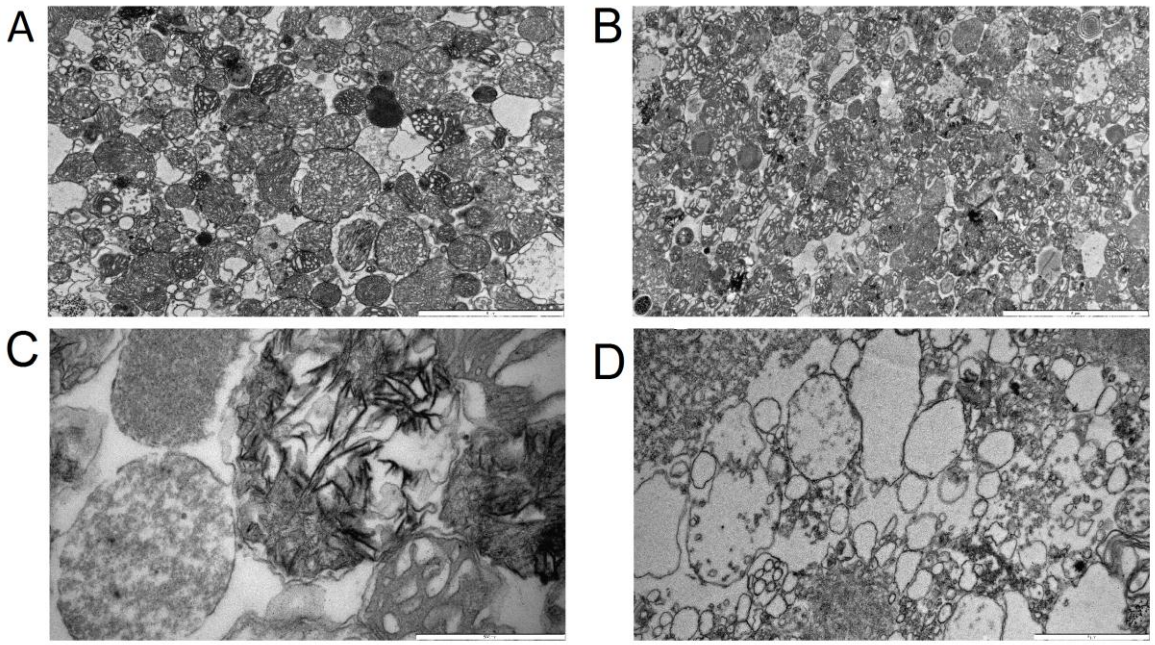

Figure 14: Transmission electron microscopy of *Crangon crangon* mitochondria. (A) Mitochondria were fixed after incubating in the absence of Ca^{2+} for 1 hour. (B) Mitochondria were treated as in the experiment shown in Fig. 12A and fixed 2 hours after the last addition of 200 µM $CaCl_2$. (C) as in panel B, but viewed at a higher magnification, demonstrating the needle-like appearance of calcium phosphate mitochondrial precipitates. (D) Mitochondria treated with 40 µg of alamethicin. Bars shown in the lower right corners of each panel are as follows: A, B: 5 µm, C: 500 nm, D: 2 µm.

6.2.4. Palaemon serratus

Palaemon serratus is another species of marine shrimp found in the Atlantic Ocean from Denmark to Mauritania, and in the Mediterranean Sea and Black Sea. Mitochondria obtained from *Palaemon serratus* were able to accumulate approximately 0.6 µmol of Ca^{2+} per mg protein, without showing sign of permeability transition (Fig. 15A). Similarly to *Crangon*, uptake capacity could not be influenced by CsA or BKA (Fig. 15D). Sensitivity to BKA was confirmed by the same protocol used to investigate *Crangon* ΔΨm and ATP production on *Palaemon* (Fig. 15B,C). Swelling could not be induced by repeated additions of Ca^{2+} (Fig. 15E). The effect of BKA on mitochondrial respiration could not be reliably tested because of a very high rate of oxygen consumption in the absence of exogenously added adenine nucleotides, see panel 3E. This was not due to a high fraction of damaged mitochondria, because Safranin O fluorescence measurements reflecting ΔΨm prompt ADP-induced depolarization (Fig. 15B/a,d) implying the presence of sufficiently polarized, thus intact mitochondria. Respiratory control ratio for *Palaemon serratus* (panel F) was ~2.

Oxygen consumption was cyanide-sensitive. The addition of dithionite after cyanide showing the disappearance of the remaining oxygen in the buffer implied that the effect of cyanide was genuine, and did not coincide with the depletion of oxygen from the medium. Uncoupled respiration (induced by SF 6847) was significantly higher than state 3 (a respiratory state in which ADP, substrates or oxygen is not limiting) respiration. This is in line with the above claim that these mitochondrial preparations did not have a high fraction of damaged mitochondria. TEM images shown in Fig. 16 were acquired after the same treatment as described under *Crangon*. Like the other crustacean species swelling can only be triggered by alamethicin and Ca^{2+} loaded mitochondria show needle-like electron dense formations.

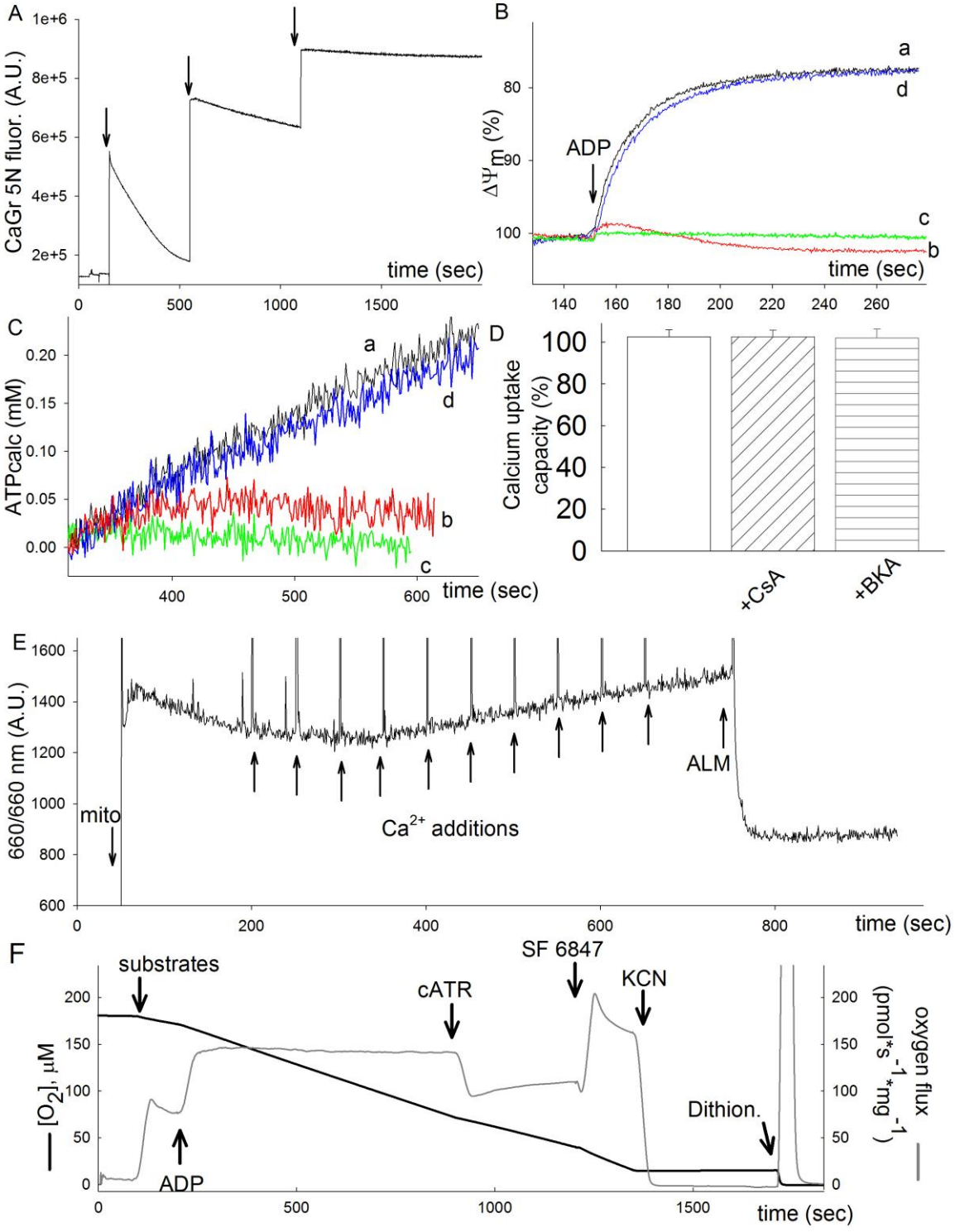
A
CaGr 5N fluor. (A.U.)
time (sec)
B
ΔΨm (%)
ADP
a
d
c
b
time (sec)
C
ATPcalc (mM)
a
d
b
c
time (sec)
D
Calcium uptake capacity (%)
+CsA
+BKA
E
660/660 nm (A.U.)
mito
Ca2+ additions
ALM
time (sec)
F
substrates
cATR
SF 6847
KCN
Dithion.
ADP
[O2], μM
oxygen flux (pmol*s-1*mg-1)
time (sec)

Figure 16: BKA sensitivity and presence of PTP in *Palaemon Serratus*. (A) Reconstructed time courses of CaGr-5N fluorescence.1 mg/ml mitochondria was added at the start of the experiment and consequently challenged with 200 µM $CaCl_2$ pulses when indicated by the arrows. (B) Reconstructed time courses of Safranin O fluorescence expressed in percentage of polarization. Trace a (black) is control, trace b (red) contained 20 µM BKA, trace c (green) contained 1 µM cATR, trace d (blue) contained vehicle of BKA (2 mM NH_4OH) in the medium prior to the experiment. 1 mg/ml mitochondria was injected at 50 s and at 100 s 2 mM ADP was added. (C) Reconstructed time courses of ATP appearing in the medium calculated from MgGr-5N fluorescence. Experimental procedure is identical to that in panel B. (D) Bar graphs of maximum Ca^{2+} uptake capacity (% scale) calculated from the number of 100 µM $CaCl_2$ additions given to mitochondria until no further decrease in CaGr-5N fluorescence (implying maximum mitochondrial calcium uptake) was observed, in the presence of 1 µM cyclosporin A or 20 µM BKA, (n = 3). The rates of Ca^{2+} uptake of the last addition were compared among treatment groups, where it exhibited a small variability, but no statistical significance (p = 0.989, ANOVA on Ranks). The rates of Ca^{2+} uptake of all previous $CaCl_2$ additions were virtually identical among all treatment groups. (E) Reconstructed time courses of 90° light scattering measured at 660 nm. 1 mg/ml mitochondrial preparation was added at 50 s followed by 100 µM $CaCl_2$ pulses when indicated by the arrows, and finally by 40 µg Alamethicin. (F) Black trace represents a time course of oxygen consumption, by 0.5 mg *Palaemon serratus* mitochondria suspended in a 2 ml volume. Grey trace represents the negative time derivative of oxygen concentration, divided by mitochondrial mass per volume. Additions of substances are indicated by arrows. ADP: 0.2 mM. cATR: 2 µM. SF 6847: 1 µM. KCN: 1 mM. Dithion.: Dithionite (added in excess).

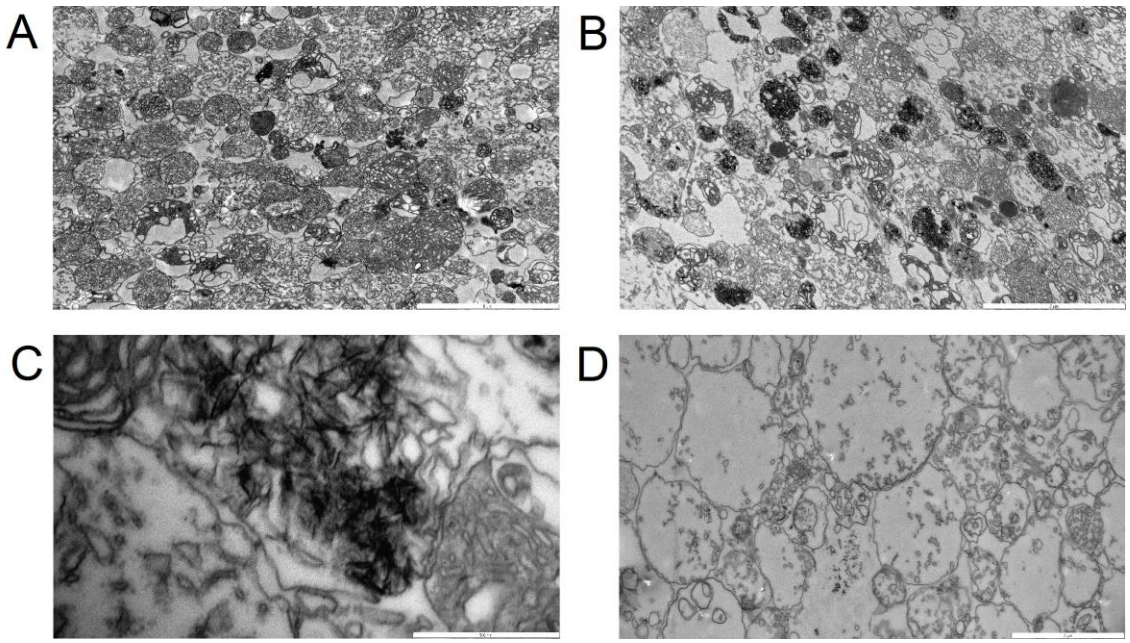

Figure 15: Transmission electron microscopy of *Palaemon serratus* mitochondria. (A) Mitochondria were fixed after incubating in the absence of Ca^{2+} for 1 hour. (B) Mitochondria were treated as in the experiment shown in Fig. 14A and fixed 2 hours after the last addition of 200 µM $CaCl_2$. (C) as in panel B, but viewed at a higher magnification, demonstrating the needle-like appearance of calcium phosphate mitochondrial precipitates. (D) Mitochondria treated with 40 µg of alamethicin. Bars shown in the lower right corners of each panel are as follows: A, B: 5 µm, C: 500 nm, D: 2 µm.

6.2.5. Carcinus maenas

The closely related blue (*Callinectes sapidus*) and green (*Carcinus maenas*) crabs have been demonstrated to maintain mitochondrial functions after sequestering high quantities of Ca^{2+}, however presence of the PTP was not investigated directly [292, 293]. Similarly to the rest of the crustacean species mitochondria from *Carcinus maenas* demonstrated robust Ca^{2+} uptake (Fig. 17A). Swelling could not be induced by Ca^{2+} (Fig. 17B). In our experimental conditions the membrane potential was not stable and not sufficiently high to drive ATP production, therefore BKA and cATR sensitivity could not be demonstrated (not shown). The transmission electron microscopic images show, that mitochondria from *Carcinus maenas* do not undergo permeability transition upon prolonged incubation with high Ca^{2+} (Fig. 18C), but are sensitive to alamethicin (Fig. 18B).

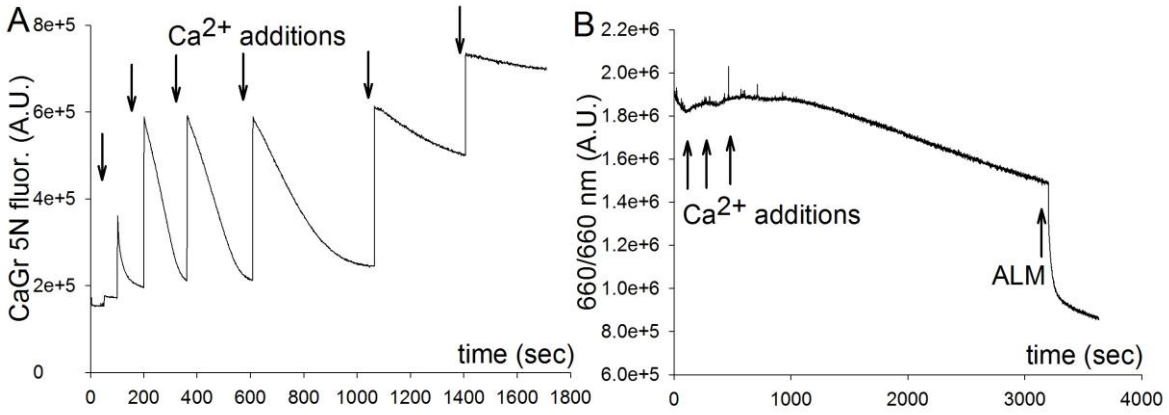

Figure 17: Ca^{2+} uptake and swelling of mitochondria from *Carcinus maenas*. (A) Reconstructed time courses of CaGr-5N fluorescence.20 µl (approx. 1 mg/ml) mitochondria was added at the start of the experiment and consequently challenged with 100 µM $CaCl_2$ pulses when indicated by the arrows. (B) Reconstructed time courses of 90° light scattering measured at 660 nm. 30 µl (approx. 1 mg/ml) mitochondrial preparation was added at 50 s followed by 100 µM $CaCl_2$ pulses when indicated by the arrows, and finally by 20 µg alamethicin.

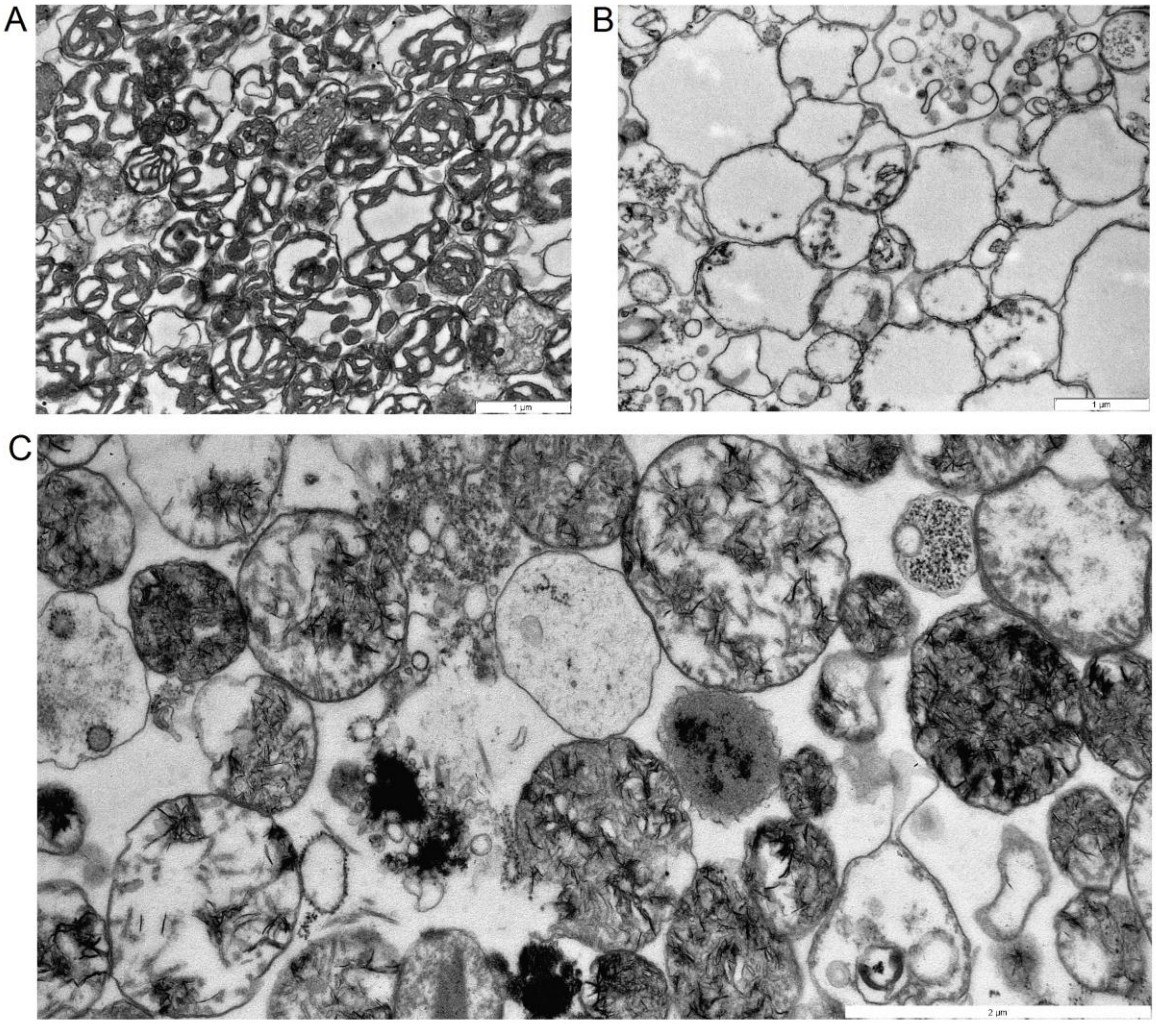

Figure 18: TEM images of mitochondria from *Carcinus maenas*. Mitochondria were treated as in the experiment shown on Fig 17 panel A and fixed 2 hours after the last addition of 100 µM $CaCl_2$. Bars shown in the lower right corners of each panel are as follows: A, B: 5 µm, C: 2 µm.

6.2.6. Pagurus bernhardus

The last crustacean we tested so far was the hermit crab (*Pagurus bernhardus*). Our results on this species are similar to our findings on the other members of the subphylum. Signs of Ca^{2+} induced PTP could not be seen on measurements of Ca^{2+} uptake (Fig. 20A), swelling (Fig. 20D) or TEM (Fig. 19). Membrane potential was unstable, however mitochondria were polarized sufficiently to drive the ANT in the forward mode, and sensitivity to BKA and cATR could be demonstrated by measuring $\Delta\Psi m$ or ATP production (Fig. 20 B,C).

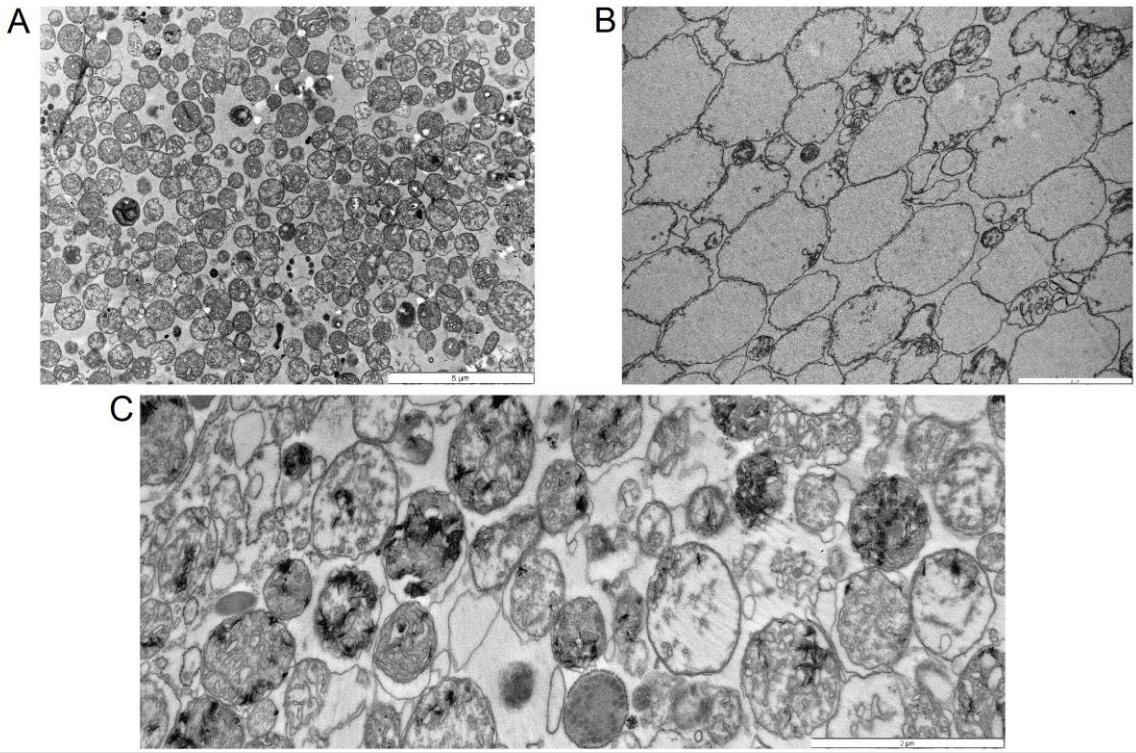

Figure 19: TEM images of mitochondria from *Pagurus bernhardus*. (A) Mitochondria were fixed after incubating in *t*he absence of Ca^{2+} for 1 hour. (B) Mitochondria treated with 20 µg of alamethicin. (C) Mitochondria were treated as in the experiment shown on Fig 20 panel A and fixed 2 hours after the last addition of 100 µM $CaCl_2$. Bars shown in the lower right corners of each panel are as follows: A: 5 µm, B, C: 2 µm.

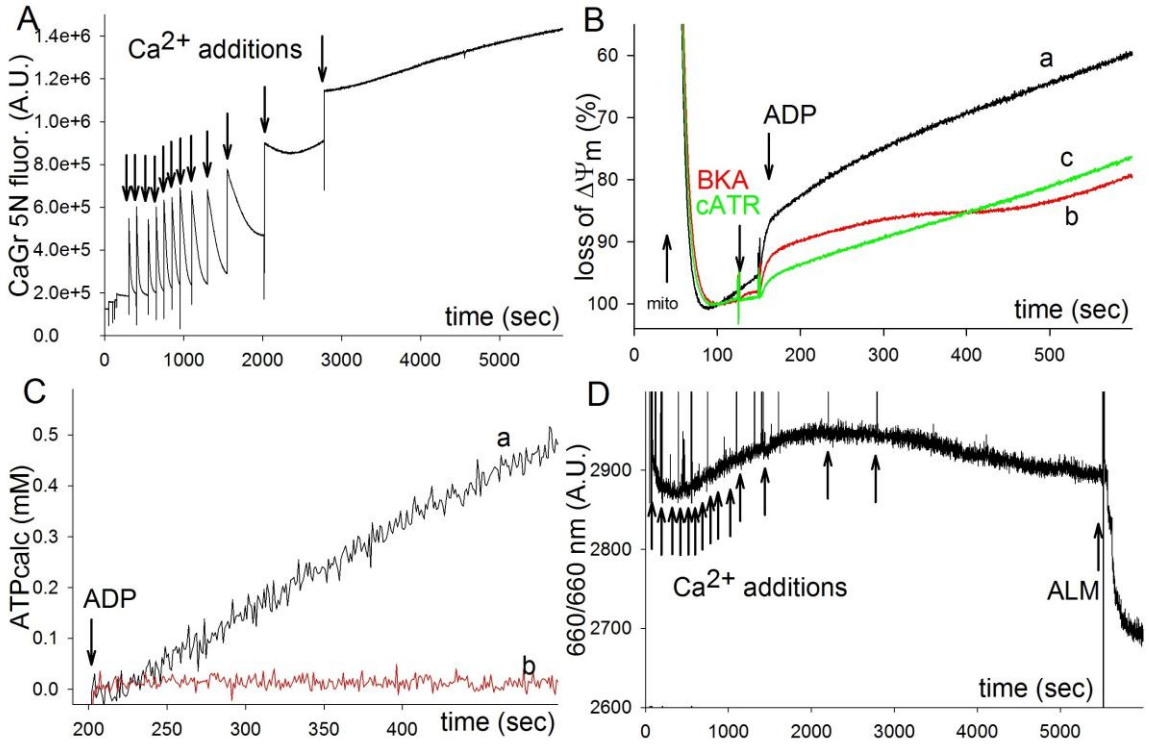

Figure 20: Ca^{2+} uptake, BKA sensitivity and swelling of mitochondria from *Pagurus bernhardus*. (A) Reconstructed time courses of CaGr-5N fluorescence. 30 µl (approx. 1 mg/ml) of mitochondria was added at the start of the experiment and consequently challenged with 100 µM $CaCl_2$ pulses when indicated by the arrows. (B) Reconstructed time courses of Safranin O fluorescence expressed in percentage of polarization. Trace a (black) is control, in trace b (red) 20 µM BKA, in trace c (green) 1 µM cATR was added at 125 s, followed by 2 mM of ADP at 150 s. (C) Reconstructed time courses of ATP appearing in the medium calculated from MgGr-5N fluorescence. Experimental procedure is identical to that in panel B: trace a (black) is control, in trace b (red) 20 µM BKA was added at 125 s. (D) Reconstructed time courses of 90° light scattering measured at 660 nm. 30 µl (approx. 1 mg/ml) mitochondrial preparation was added at 50 s followed by 100 µM $CaCl_2$ pulses when indicated by the arrows, and finally by 20 µg Alamethicin.

6.2.7. The lack of Ca^{2+} induced PTP and insensitivity to BKA are unrelated characteristics of mitochondria isolated from *Artemia*

None of the newly characterized crustaceans were refractory to BKA, but they all lacked the PTP. This had proven our hypothesis regarding a possible connection between BKA sensitivity and presence of the PTP to be false. Also, this finding prompted us to scrutinize further our previous report on *Artemia franciscana*, The effect of BKA is dependent on pH; BKA requires to become protonated in order to exert its action [128], and as such it becomes less effective at increasing pH. It is therefore possible, that the matrix of *Artemia* mitochondria is sufficiently alkaline in order to prevent the sufficient protonation of BKA and thus its mode of action inhibiting the ANT. To test this we performed a series of experiments recording the extent of ADP-induced depolarization (measured by Safranin O) in a range of BKA concentrations (0, 1.25, 2.5, 5, 10 and 20 μM) for a range of buffers with pH_o varying from 6.67 to 7.46 for both *Artemia* cyst and mouse liver mitochondria. Mouse liver was used as a tissue known to exhibit sensitivity to BKA where we could therefore establish the pH range at which BKA becomes ineffective. A complete series of such an experiment is shown in Fig. 21. ADP-induced depolarization (% value) as a function of BKA concentration for various pH_o indicated in the insets on the right is shown for mouse liver mitochondria (panel A) and *Artemia* mitochondria (panel B). In these settings, the more effective BKA is, the smaller the ADP-induced depolarization. It is evident that at pH_o = 7.3, (i.e. pH_{in} = 7.33, orange bar panel A), 10 μM BKA was sufficient to almost completely block ADP-induced depolarization, i.e. inhibit the ANT in mouse liver mitochondria. At almost the same pH_{in}, in *Artemia* mitochondria not even double the amount of BKA could affect ADP-induced depolarization (green bar, panel B). In *Artemia* mitochondria only at pH_o = 6.7 (i.e. pH_{in} = 7.05) was 20 μM BKA effective, a pH value at which there must be very substantial BKA protonation. At pH_o 7.25 in the other crustaceans examined mitochondria pH_{in} should be no less than 7.35; however, they were still BKA-sensitive. From these experiments we reaffirm the refractoriness of *Artemia* mitochondria to BKA.

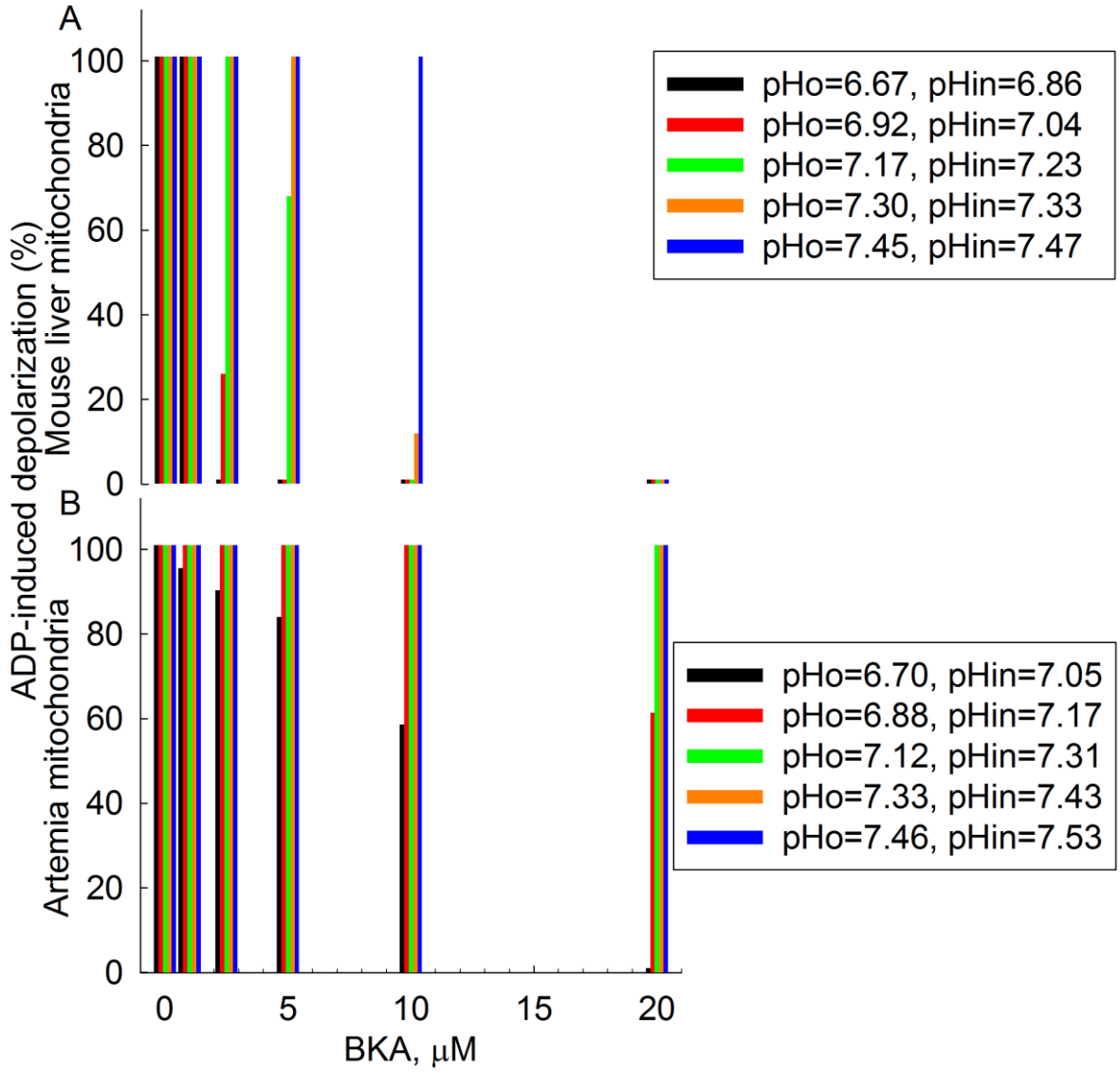

Figure 21: ADP-induced depolarization (% values) in mouse liver (A) and Artemia cyst (B) mitochondria subjected to various pH_o, as a function of BKA concentration (0, 1.25, 2.5, 5, 10 and 20 μM). In the insets to the right the values of pH_{in} as a function of pH_o is shown. Data represent a representative experiment (from three independent experiments) performed in a single run. Experimental data were not pooled in order to be presented as a bar graph with SE bars because pH_o showed a slight variation among different experiments.

6.3. PTP and BKA sensitivity in non-crustacean species

We identified six new species in which Ca^{2+} induced permeability transition is absent, which increased the total number of species without classical PTP to eight: *Lepidophthalmus louisianensis* [290], *Artemia franciscana* [291], *Cyclops vicinus vicinus*, *Daphnia pulex*, *Crangon crangon*, *Palaemon serratus*, *Carcinus maenas* and *Pagurus bernhardus*. All of these species are crustaceans.

Knowing numerous species with a common feature increases the effectiveness of bioinformatics methods such as comparison of proteome or transcriptome of identifying the molecular entity responsible for the particular phenotype. We saw an opportunity to identify the molecular structure of the long elusive PTP by generating and comparing the proteome and transctiptome of species without PTP.

The genome of several species susceptible to permeability transition was available, which could be used for comparison. The majority of these species are vertebrate chordates, and there are several other phyla in which presence of the PTP was unknown. Therefore to get a more diverse set of organisms exhibiting PTP for comparison, and to possibly find organisms outside the crustacean subphylum lacking PTP, we selected species to investigate the presence of PTP from phyla different from chordates. We tested species from echinoderms, nematodes (round worms), mollusks, annelids (segmented worms). Furthermore we were interested in invertebrate chordates.

Finding other species showing Bongkrekate insensitivity than *Artemia* would have great value for the identification of the binding site, therefore we continued to test BKA sensitivity.

6.3.1. Asterias rubens

The common starfish (*Asterias rubens*) is an echinoderm. Ca^{2+} induced PTP in this species is evident from the spontaneous Ca^{2+} release on Fig. 18A and the decrease in light scattering on Fig. 18C upon addition of Ca^{2+}. TEM images show profound swelling in the Ca^{2+} treated sample (Fig. 18E), compared to the control (Fig. 18D). Repolarization of the membrane potential can be observed upon treatment with BKA or cATR after ADP induced depolarization indicating sensitivity to these agents. ATP production rates were too low to show a statistical difference between control and BKA/cATR treatment (not shown).

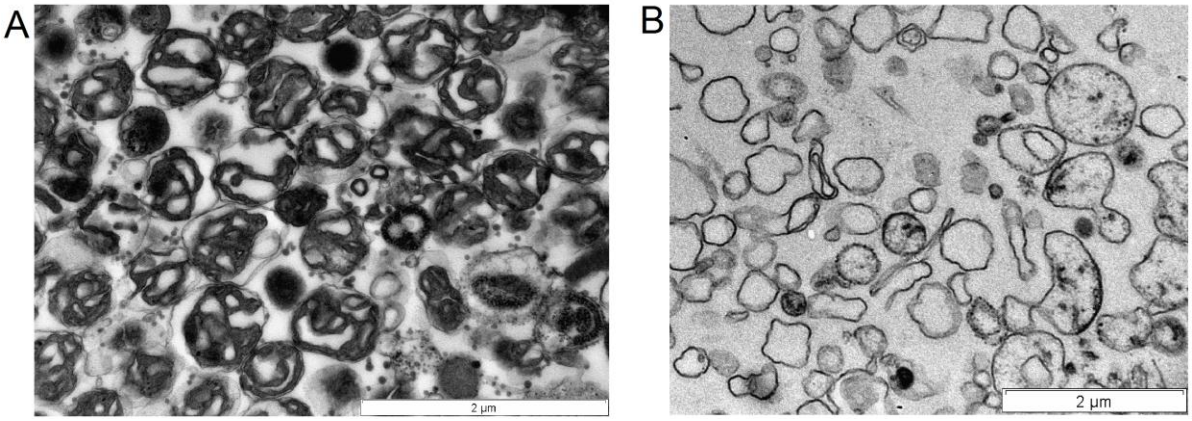

Figure 22: TEM images of isolated mitochondria from *Asterias rubens*. (A) Mitochondria were fixed after incubating in the absence of Ca^{2+} for 1 hour. (B) TEM. Mitochondria were treated as in the experiment shown on Fig. 23 panel C and fixed 2 hours after the last addition of 100 µM $CaCl_2$. Bars shown in the lower right corners of both panels are 2 µm.

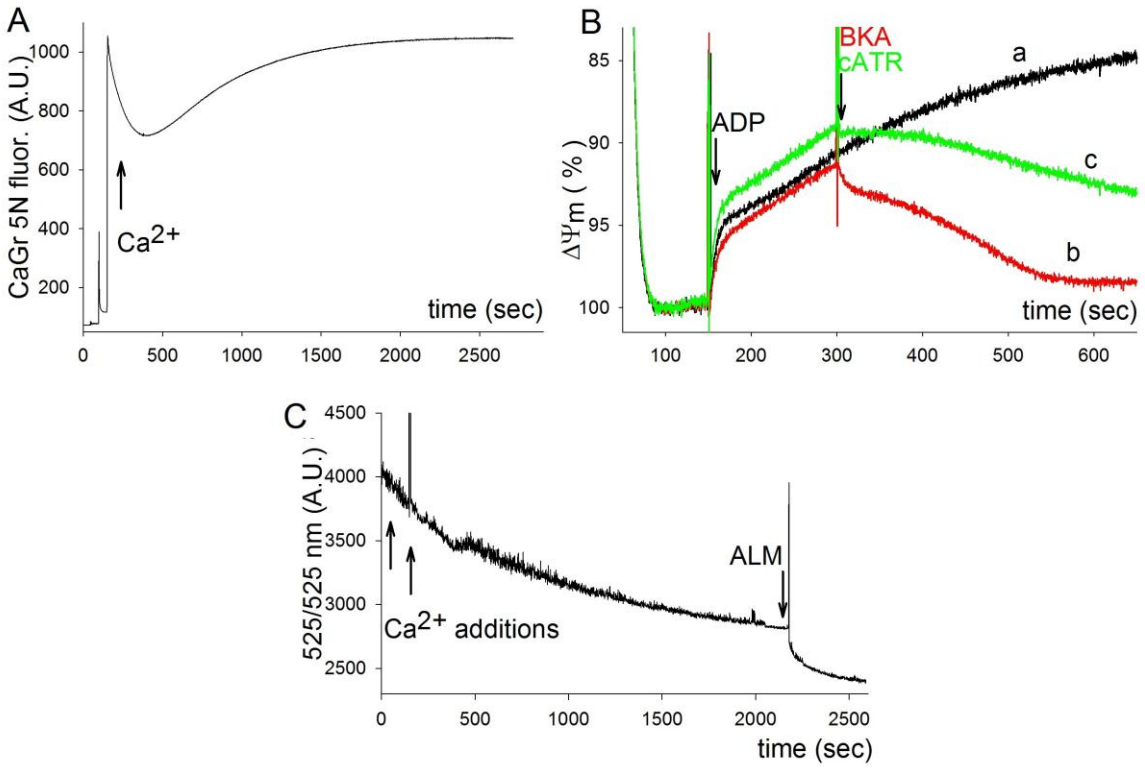

Figure 23: BKA sensitivity and presence of PTP in *Asterias rubens*. (A) Reconstructed time courses of CaGr-5N fluorescence.80 µl (approx. 1 mg/ml) of mitochondria was added at the start of the experiment and consequently challenged with a 100 µM $CaCl_2$ pulse when indicated by the arrow. (B) Reconstructed time courses of Safranin O fluorescence expressed in percentage of polarization. 1 mg/ml mitochondria was injected at 50 s, at 150 s 2 mM ADP was added followed by 20 µM BKA (trace b, red) or 4 µM cATR (trace c, green) at 300 s. (C) Reconstructed time courses of 90° light scattering measured at 660 nm. 80 µl (approx. 1 mg/ml) mitochondrial preparation was added at 50 s followed by 100 µM $CaCl_2$ pulses when indicated by the arrows, and finally by 20 µg Alamethicin.

6.3.2. Paracentrotus lividus

The sea urchin (*Paracentrotus lividus*) is another echinoderm. Our results addressing PTP in this animal are controversial, as no sign of permeability transition is evident from Ca^{2+} uptake (Fig. 24A) or swelling (Fig. 24B) experiments, however the TEM images clearly show the morphological changes accompanied by PTP upon Ca^{2+} treatment (Fig. 24C: control, Fig. 24D: alamethicin treatment, Fig. 24E: Ca^{2+} treatment). The fact that Ca^{2+} uptake and light scattering did not indicate permeability transition supports that these methods may be unreliable, and TEM images are necessary to evaluate the presence of PTP. *Paracentrotus* mitochondria did not depolarize upon addition of ADP but depolarized significantly after the addition of ATP, as seen on Fig. 24B, indicating that these mitochondria cannot support their membrane potential by oxidative phosphorylation in our experiments. Due to our limited access to the sample, we could not optimize our conditions for this species, and BKA sensitivity was demonstrated in the reverse mode. BKA induces depolarization on Fig. 24B, as it blocks mitochondrial import of ATP which would be hydrolyzed by the F_oF_1-ATP synthase to maintain $\Delta\Psi m$.

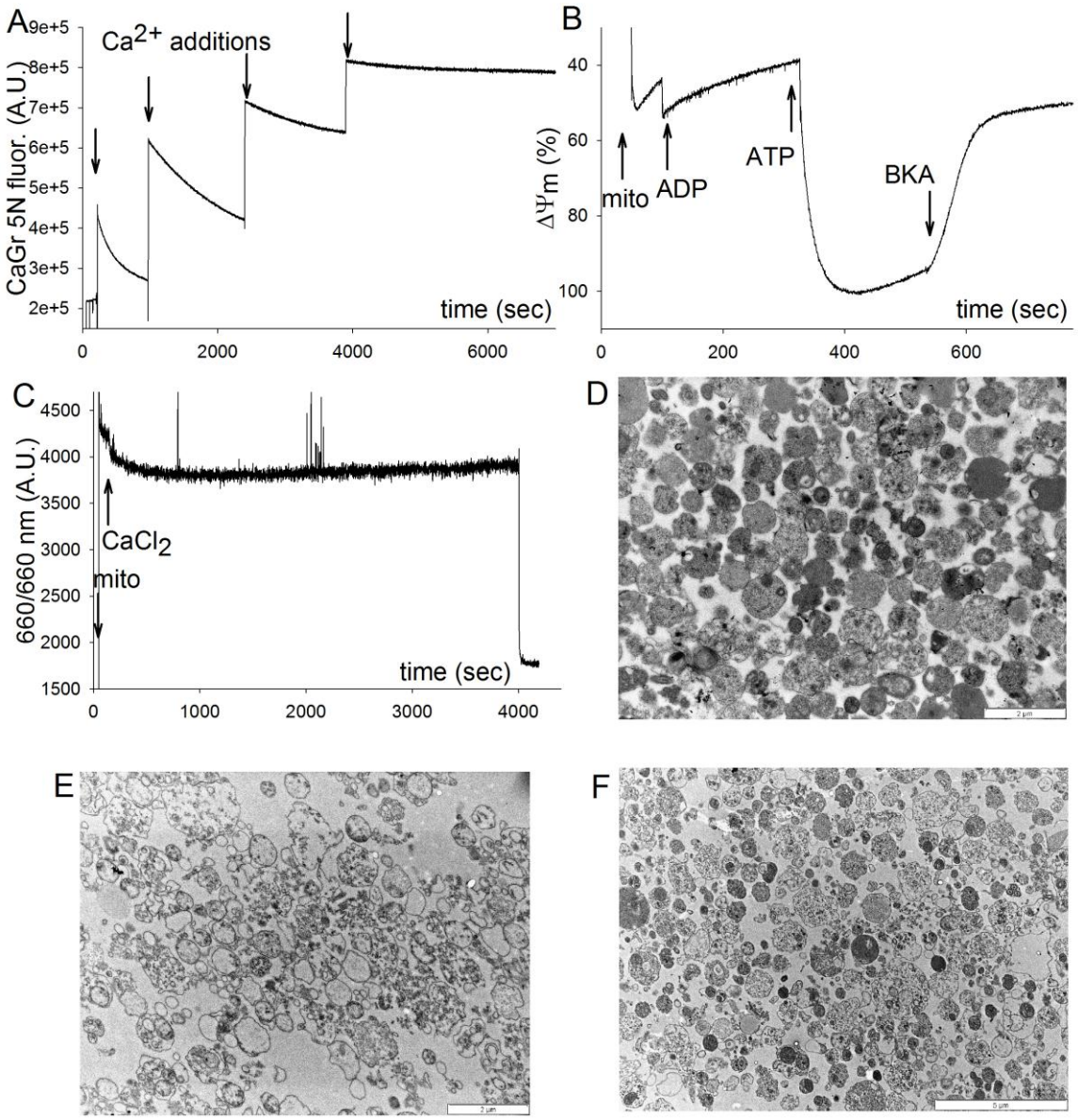

Figure 24: BKA sensitivity and presence of PTP in *Paracentrotus lividus*. (A) Reconstructed time courses of CaGr-5N fluorescence.50 µl (approx. 1 mg/ml) of mitochondria was added at the start of the experiment and consequently challenged with a 100 µM $CaCl_2$ pulses when indicated by the arrows. (B) Reconstructed time courses of Safranin O fluorescence expressed in percentage of polarization. 50 µl (approx. 1 mg/ml) mitochondria was injected at 50 s, at 150 s 2 mM ADP was added followed by 2 mM ATP at 300 s, finally ATP consumption was inhibited by 20 µM BKA at 550 s. (C) Reconstructed time courses of 90° light scattering measured at 660 nm. 50 µl (approx. 1 mg/ml) mitochondrial preparation was added at 50 s followed by 100 µM $CaCl_2$ pulses when indicated by the arrows, and finally by 20 µg Alamethicin. (D) TEM. Mitochondria were fixed after incubating in the absence of Ca^{2+} for 1 hour. (E) TEM. Mitochondria treated with 20 µg of alamethicin. (F) TEM. Mitochondria were treated as in the experiment shown on panel A and fixed 2 hours after the last addition of 100 µM $CaCl_2$. Bars shown in the lower right corners of each panel are as follows: D,E: 2 µm, F: 5 µm.

6.3.3. Caenorhabditis elegans

The nematode Caenorhabditis elegans is a popular experimental model in a number of fields, primarily in genetics and developmental biology. Its full genome is available and PTP was documented in these species [312, 313]. Our experiments were limited only to demonstrate BKA sensitivity, which was evident from the measurement of both ΔΨm (Fig. 25A) and ATP production (Fig. 25B).

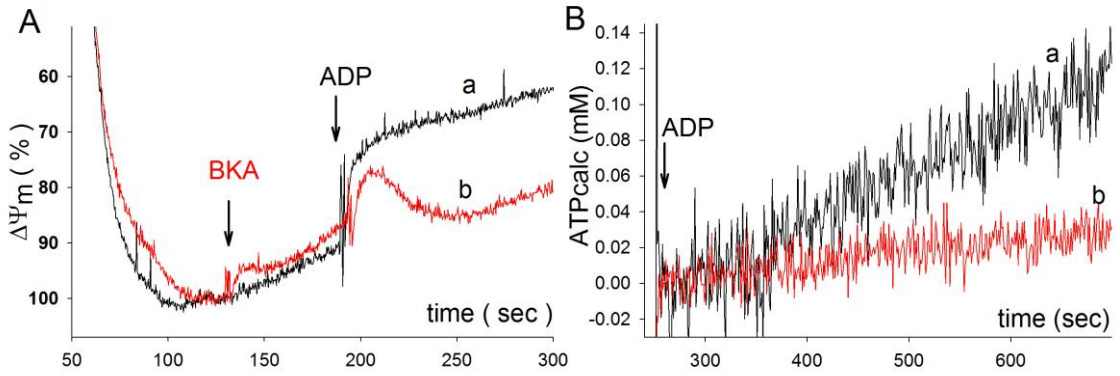

Figure 25: BKA sensitivity in *Caenorhabditis elegans*. (A) Reconstructed time courses of Safranin O fluorescence expressed in percentage of polarization. 50 µl (approx. 1 mg/ml) mitochondria was injected at 50 s, at 200 s 2 mM ADP was added in both experiments, 20 µM BKA was added at 125 s in trace b (red). (B) Reconstructed time courses of ATP appearing in the medium calculated from MgGr-5N fluorescence. Experimental procedure is identical to that in panel A: trace a (black) is control, in trace b (red) 20 µM BKA was added at 125 s.

6.3.4. Nephtys hombergii

The annelid *Nephtys hombergii* shows signs of PTP on Ca^{2+} uptake (Fig. 26A) and light scattering, following substantial shrinkage (Fig.26C), TEM images provide clear evidence of permeability transition in these species (Fig. 26D:control, Fig. 26E: alamethicin treatment, Fig. 26F: Ca^{2+} treatment). $\Delta\Psi m$ measurements (Fig. 26B) prove sensitivity to BKA (trace c: control, trace a: control with ADP, trace b: BKA treatment)

We attempted to isolate mitochondria from another annelid, the honeycomb worm, *Sabellaria alveolata*, however the yield of isolated mitochondria was so low from this species, that further investigation was not feasible.

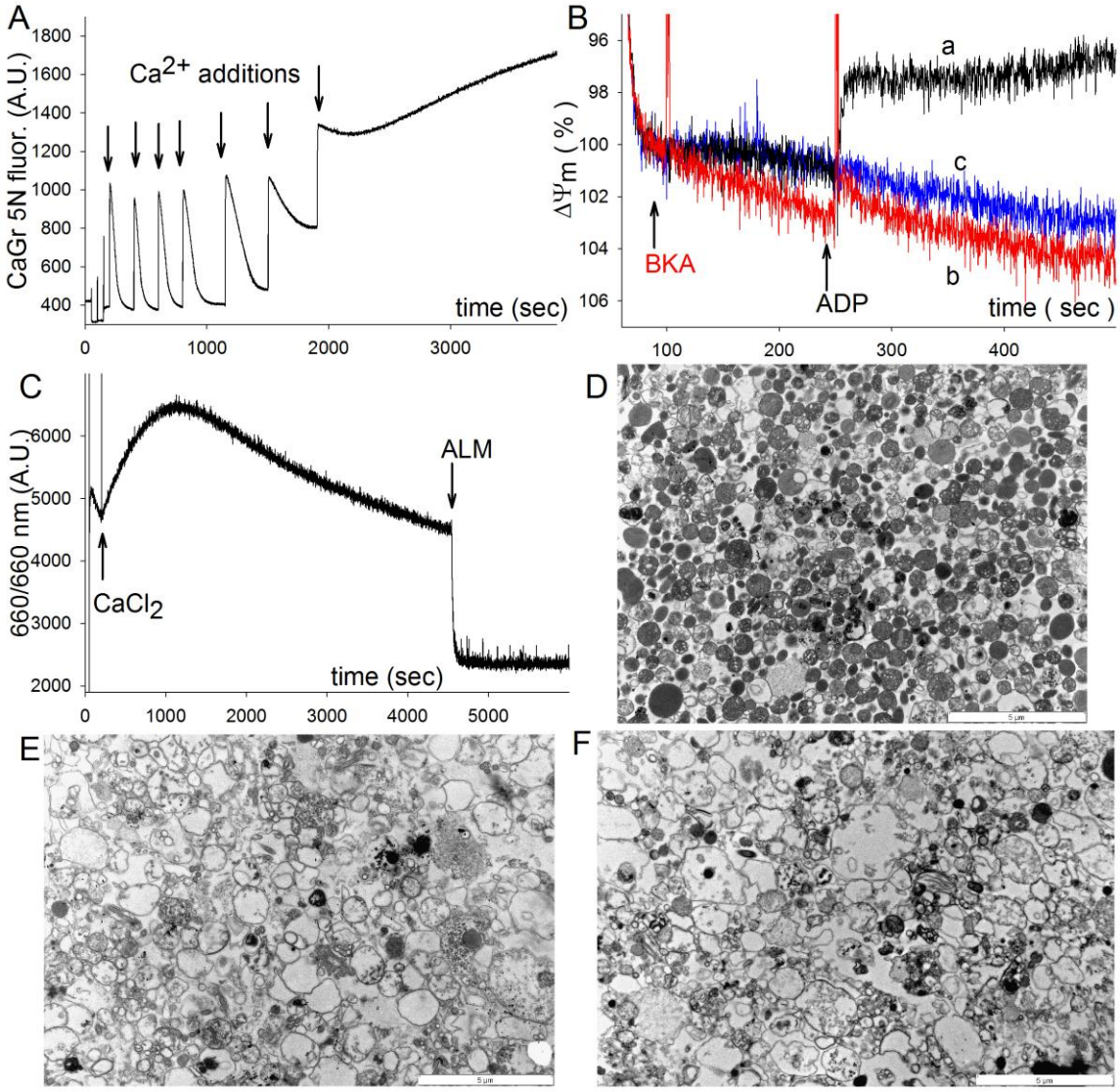

Figure 26: BKA sensitivity and presence of PTP in *Nephtys hombergii*. (A) Reconstructed time courses of CaGr-5N fluorescence.20 µl (approx. 1 mg/ml) of mitochondria was added at the start of the experiment and consequently challenged with a 100 µM $CaCl_2$ pulses when indicated by the arrows. (B) Reconstructed time courses of Safranin O fluorescence expressed in percentage of polarization. 20 µl (approx. 1 mg/ml) mitochondria was injected at 50 s, trace c: no treatment, trace a: ADP at 250 s, trace b: BKA at 100 s and ADP at 250 s. (C) Reconstructed time courses of 90° light scattering measured at 660 nm. 20 µl (approx. 1 mg/ml) mitochondrial preparation was added at 50 s followed by a single 900 µM $CaCl_2$ pulse when indicated by the arrow, and finally by 20 µg Alamethicin. (D) TEM. Mitochondria were fixed after incubating in the absence of Ca^{2+} for 1 hour. (E) TEM. Mitochondria treated with 20 µg of alamethicin. (F) TEM. Mitochondria were treated as in the experiment shown on panel A and fixed 2 hours after the last addition of 100 µM $CaCl_2$. Bars shown in the lower right corners of all panels are 5 µm.

6.3.5. Mytilus edule

The blue mussel (*Mytilus edule*) is one of the three species from the phylum of mollusks we tested. Results on Ca^{2+} uptake (Fig. 27A), light scattering (Fig. 27B) and TEM (Fig. 27C: control, D: Ca^{2+} treatment) agree on the presence of PTP in this species. We have not yet measured sensitivity to BKA.

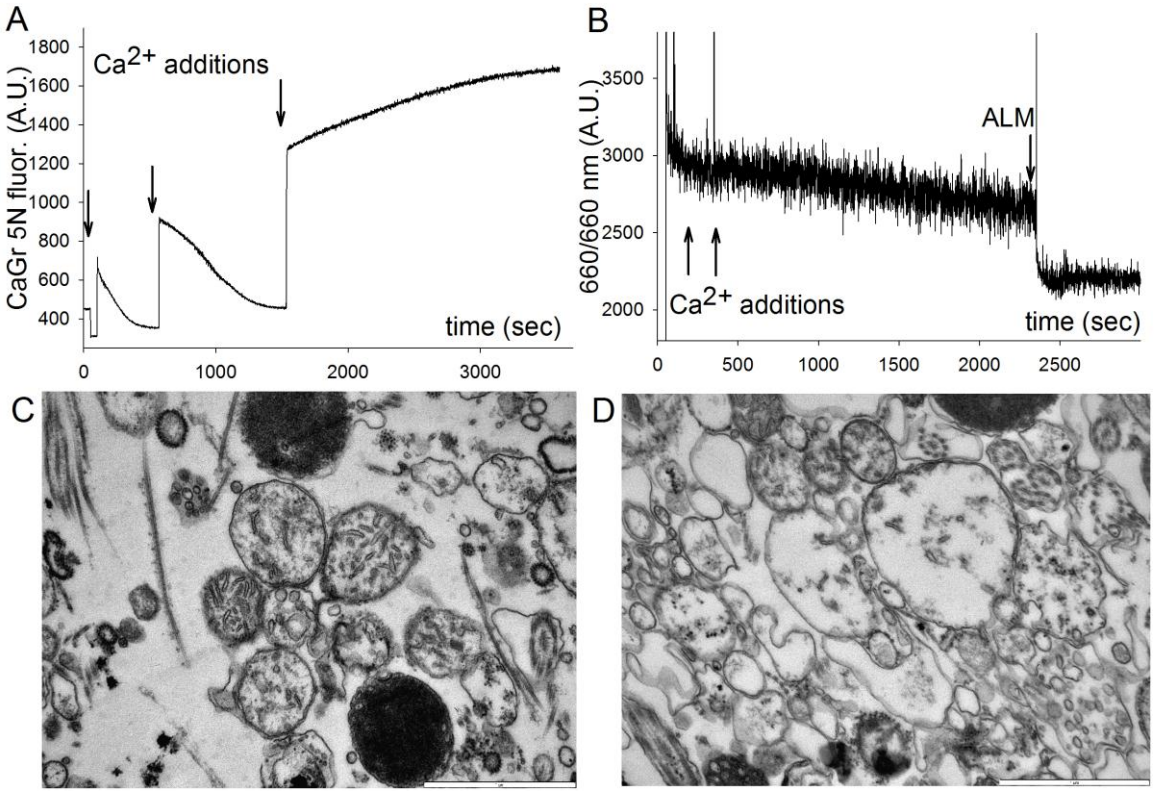

Figure 27: Presence of PTP in *Mytilus edule*. (A) Reconstructed time courses of CaGr-5N fluorescence.30 µl (approx. 1 mg/ml) of mitochondria was added at the start of the experiment and consequently challenged with a 100 µM $CaCl_2$ pulses when indicated by the arrows.(B) Reconstructed time courses of 90° light scattering measured at 660 nm. 30 µl (approx. 1 mg/ml) mitochondrial preparation was added at 50 s followed by 100 µM $CaCl_2$ pulses when indicated by the arrows, and finally by 20 µg Alamethicin. (C) TEM. Mitochondria were fixed after incubating in the absence of Ca^{2+} for 1 hour (D) TEM. Mitochondria were treated as in the experiment shown on panel A and fixed 2 hours after the last addition of 100 µM $CaCl_2$. Bars shown in the lower right corners of all panels are 1 µm.

6.3.6. Cerastoderma edule

From measurements of Ca^{2+} (Fig. 28A) uptake and light scattering (Fig. 28D) we deduce the PTP is present in the common cockle (*Cerastoderma edule*). TEM images of untreated mitochondria show normal morphology (Fig. 29), images of Ca^{2+} loaded mitochondria are yet to be collected. BKA and cATR added prior to ADP cause inhibition of the ANT, which is visible on both ΔΨm (Fig. 28B) and ATP production measurements (Fig. 28C).

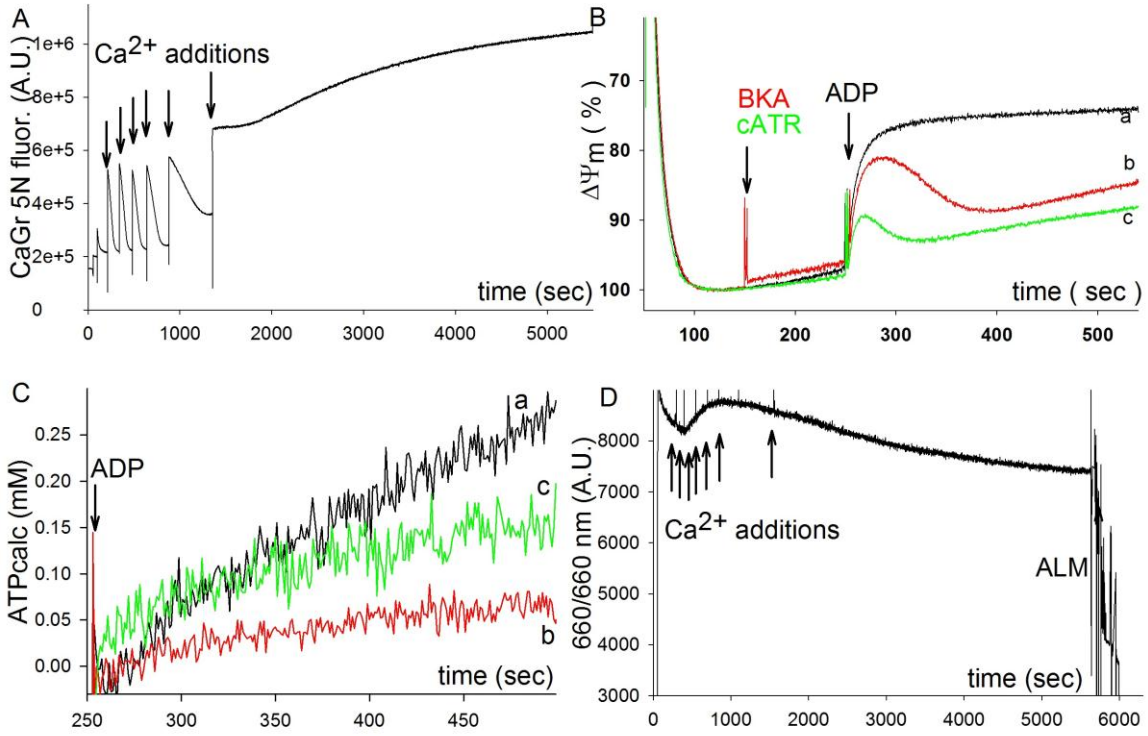

Figure 28: Ca^{2+} uptake, BKA sensitivity and swelling in mitochondria from *Cerastoderma edule*. (A) Reconstructed time courses of CaGr-5N fluorescence.50 µl (approx. 1 mg/ml) of mitochondria was added at the start of the experiment and consequently challenged with a 100 µM $CaCl_2$ pulses when indicated by the arrows. (B) Reconstructed time courses of Safranin O fluorescence expressed in percentage of polarization. 30 µl (approx. 1 mg/ml) mitochondria was injected at 50 s, 2 mM ADP (all experiments), 20 µM BKA (trace b only) and 2 µM cATR (trace c only) were added when indicated by the arrows. (C) Reconstructed time courses of ATP appearing in the medium calculated from MgGr-5N fluorescence. Experimental procedure is identical to that in panel B. (D) Reconstructed time courses of 90° light scattering measured at 660 nm. 50 µl mitochondrial preparation was added at 50 s followed by 100 µM $CaCl_2$ pulses when indicated by the arrows, and finally by 20 µg Alamethicin.

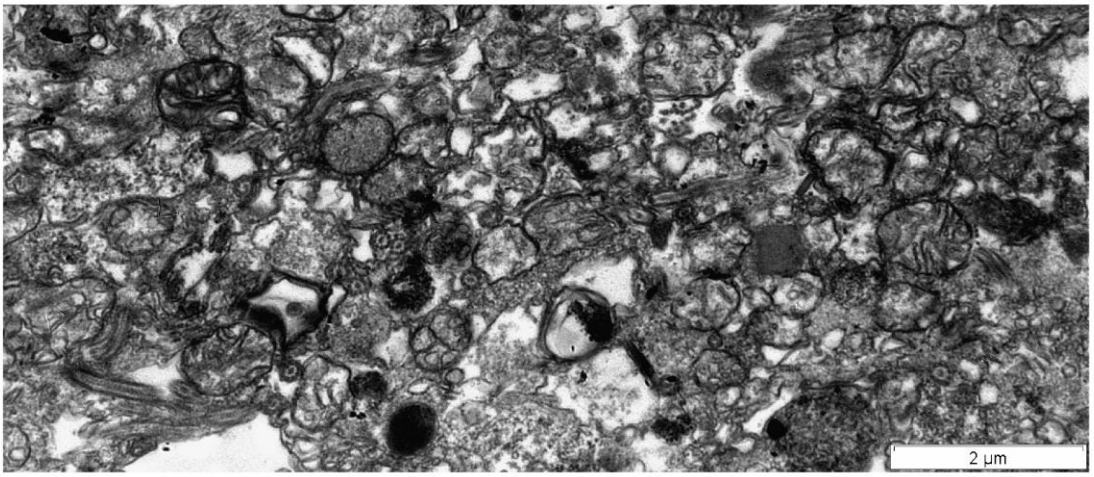

Figure 29: TEM image of mitochondria from *Cerastoderma edule*. Mitochondria were fixed after incubating in the absence of Ca^{2+} for 1 hour. The bar shown in the lower right corner is 2µm.

6.3.7. Patella vulgata

Ca^{2+} uptake (Fig. 31A) and light scattering (Fig. 31D) of mitochondria from the common limpet (*Patella vulgata*) does not convincingly support the presence of PTP in this species upon Ca^{2+} loading, however TEM images clearly show the morphological features (Fig. 30A: control, B: alamethicin treatment, C: Ca^{2+} treatment). Sensitivity to BKA is evident from ATP production (Fig 30C). ΔΨm measurements were hard to evaluate due to instable polarization of mitochondria in our experimental conditions (not shown), therefore we tested BKA sensitivity in the reversed assay, in which mitochondria are polarized by extramitochondrial ATP, and depolarize when the ANT is inhibited.

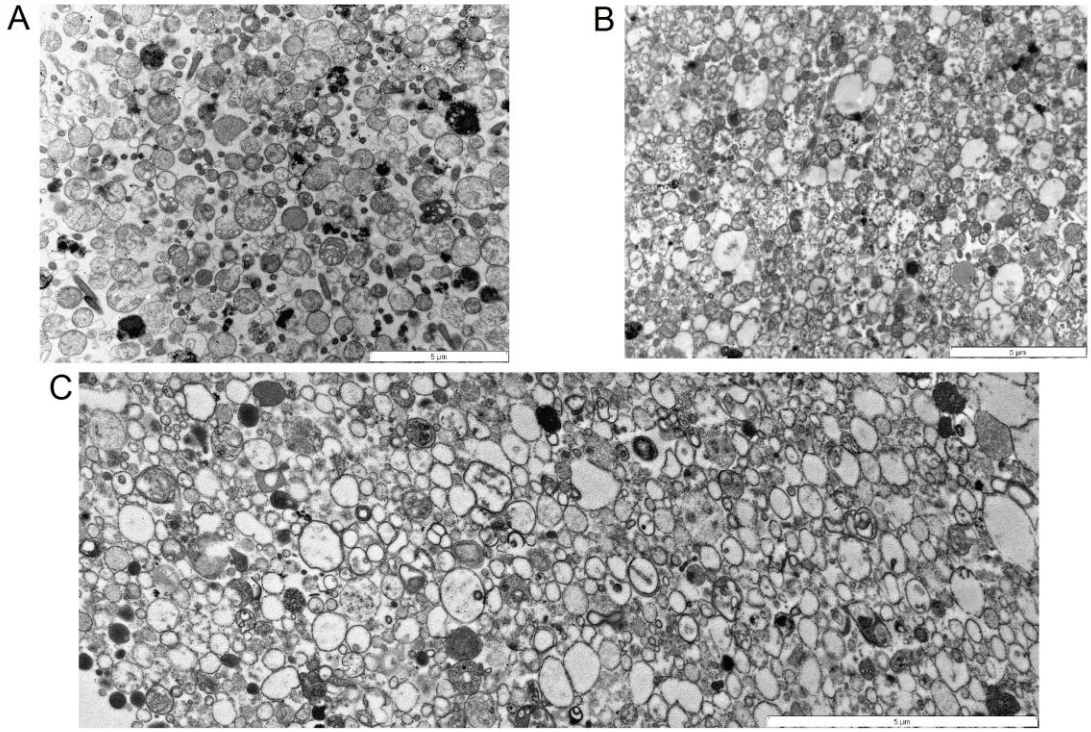

Figure 30: BKA sensitivity and presence of PTP in *Patella vulgata*. (A) Mitochondria were fixed after incubating in the absence of Ca^{2+} for 1 hour. (B) Mitochondria treated with 20 µg of alamethicin. (C) Mitochondria were treated as in the experiment shown on Fig. 31 panel A and fixed 2 hours after the last addition of 100 µM $CaCl_2$. Bars shown in the lower right corners of all panels are 5 µm.

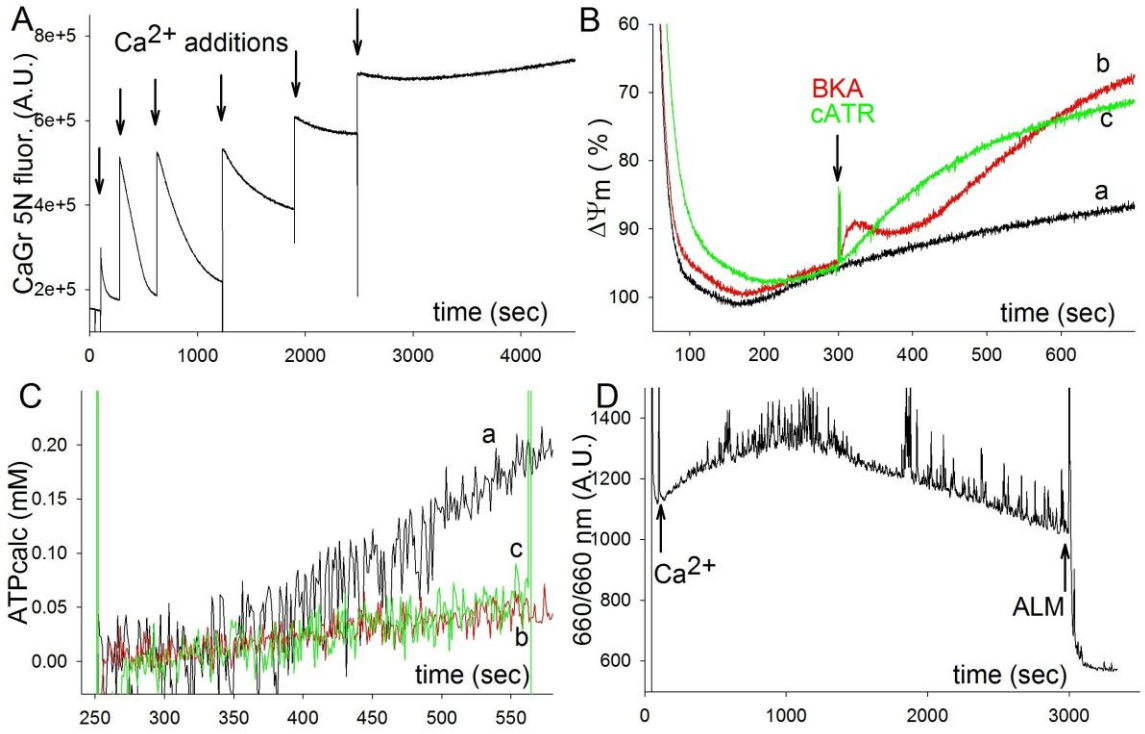

Figure 31: Ca2+ uptake, BKA sensitivity and swelling in mitochondria from *Patella vulgata*. (A) Reconstructed time courses of CaGr-5N fluorescence.20 µl (approx. 1 mg/ml) of mitochondria was added at the start of the experiment and consequently challenged with a 100 µM $CaCl_2$ pulses when indicated by the arrows. (B) Reconstructed time courses of Safranin O fluorescence expressed in percentage of polarization. 30 µl (approx. 1 mg/ml) mitochondria was injected at 50 s to experimental media containing no substrates (glutamate, malate and succynate) but 2 mM ATP. 20 µM BKA (trace b, red) or 2 µM cATR (trace c, green) were added when indicated by the arrows. (C) Reconstructed time courses of ATP appearing in the medium calculated from MgGr-5N fluorescence. 20 µl (approx. 1 mg/ml) mitochondrial preparation was added at 50s, inhibitors (BKA: b, red; cATR: c, green) were added at 100s and 2 mM of ADP at 250s. (D) Reconstructed time courses of 90° light scattering measured at 660 nm. 30 µl mitochondrial preparation was added at 50 s followed by the addition of 600 µM $CaCl_2$ at 100 s, and finally by 20 µg Alamethicin at 3000 s.

6.3.8. Drosophila melanogaster

The common fruit fly (*Drosophila melanogaster*) is well documented to have permeability transition [271], its full genome has been sequenced and like crustaceans it is an arthropod, which makes this species valuable for comparison. BKA sensitivity is hard to evaluate on the basis of ΔΨm experiments (Fig. 32), because ΔΨm was unstable and was affected by BKA. As the membrane potential is slightly hyperpolarized when BKA was present (trace b, red) compared to the control (trace a, black), we conclude that the ANT present in *D. melanogaster* is sensitive to BKA.

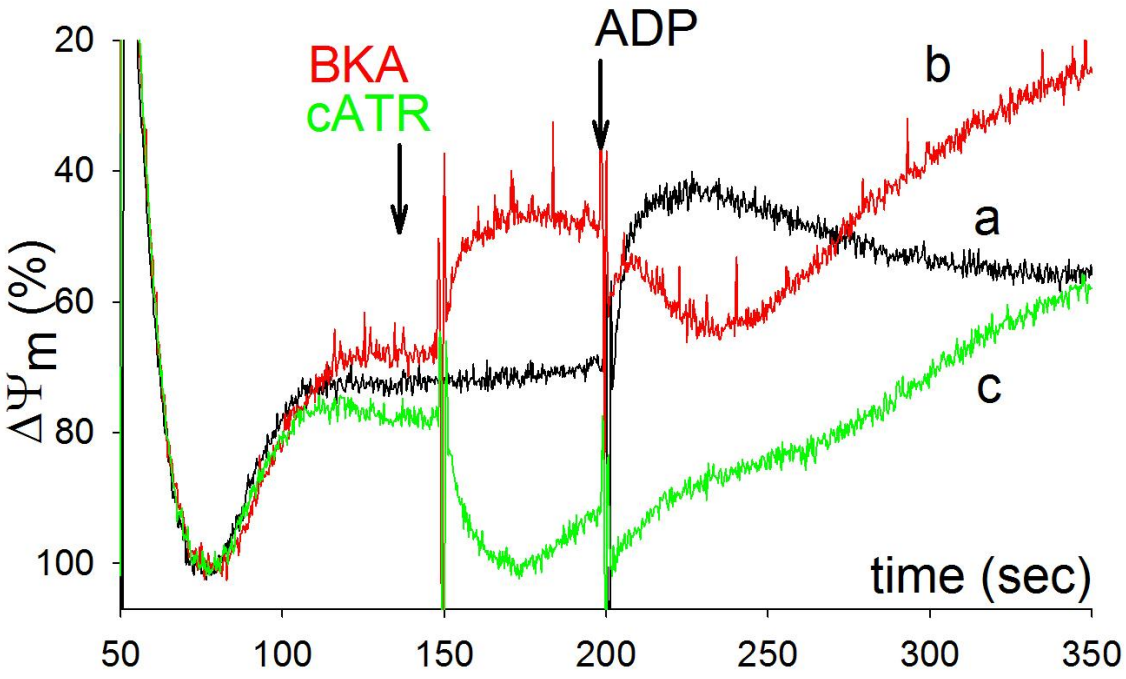

Figure 32: Safranin O fluorescence expressed in percentage of polarization of *Drosophila melanogaster* mitochondria. 0.25 mg/ml mitochondria was injected at 50 s to the experimental media. 20 µM BKA (trace b, red) or 2 µM cATR (trace c, green) were added when indicated by the arrows. 2 mM ADP was added at 200 s.

6.3.9. Branchiostoma lanceolatum

Both quality and quantity of mitochondria yielding from the invertebrate chordate, *Branchiostoma lanceolatum* were low, and only the demonstration of BKA sensitivity could be achieved using this species (Fig. 33). We attempted but failed to isolate mitochondria from another invertebrate chordate: *Ciona intestinalis*.

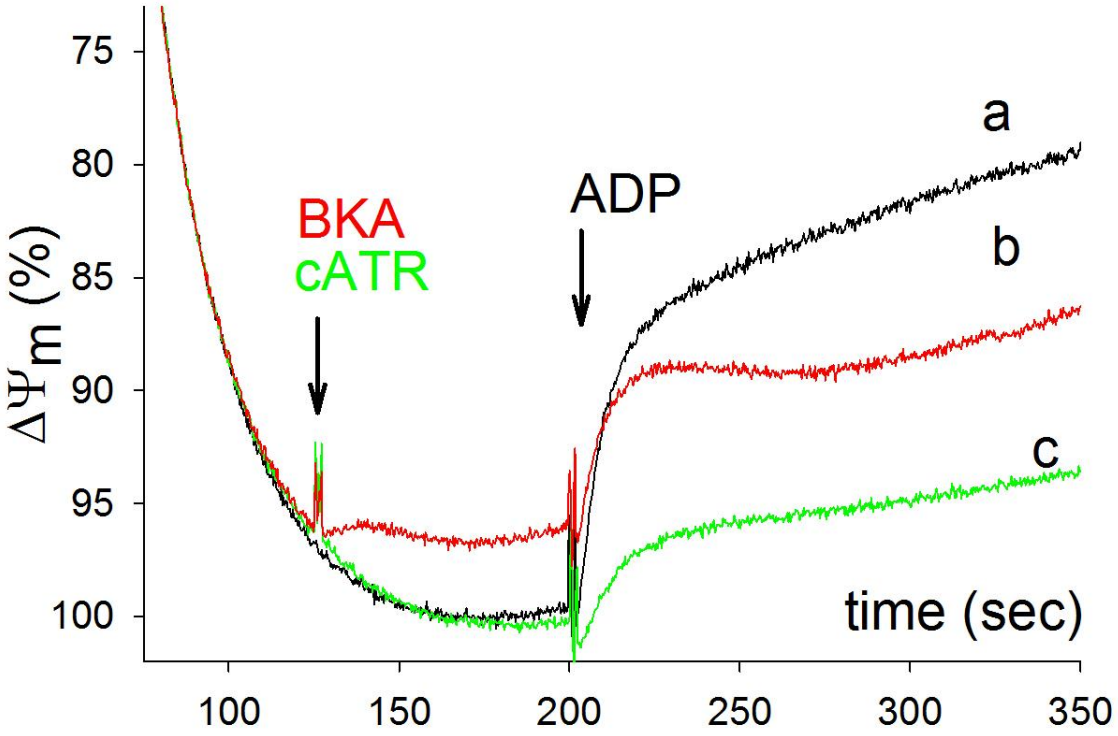

Figure 33: Safranin O fluorescence expressed in percentage of polarization of *Branchiostom lanceolatum* mitochondria. 0.25 mg/ml mitochondria was injected at 50 s to the experimental media. 20 µM BKA (trace b, red) or 2 µM cATR (trace c, green) were added when indicated by the arrows. 2 mM ADP was added at 200 s.

The BKA binding site remains elusive

BKA is an inhibitor of both the ANT and the PTP in mammals. The identification of the BKA binding site could lead to the design of novel PTP inhibitors that do not effect nucleotide translocation of mitochondria. We have shown that mitochondria from *Artemia* are refractory to inhibition by BKA, and identified taxonomically close species from the crustacean subphylum that are sensitive to it.

6.4.1. Sequencing the ANT of *Artemia franciscana*

The results prompted us to clone and sequence ANT of *Artemia franciscana*. In the literature, an incomplete 834-bp sequence has been reported (EF660895.1). Gene-specific primers for RACE PCR were designed on the basis of highly conserved regions of the known ANT nucleotide sequences from other species and the partial *A. franciscana* ANT sequence. RACE PCR products were sequenced, and the final assembled 1213-bp nucleotide sequence was submitted to GenBank (accession number: HQ228154). Alignment revealed 99% similarity to the partial *A. franciscana* ANT sequence (EF660895.1) and significant similarity (69–76%) to the sequences of human, bovine, rat, mouse, *Xenopus, Drosophila C.elegans, Branchiostoma, Crangon* and *Palaemon* isoforms (Fig. 34). The deduced amino acid sequence of the ORF comprises 301 amino acids and includes the signature of nucleotide carriers (RRRMMM) as well as 77–79% similarity to other species [115, 314].

6.4.2. Partial sequences of the ANT of *Crangon crangon* and *Palaemon serratus*

Initially the sequence of the Artemia ANT was compared to human, bovine, rat, mouse, *Xenopus*, *Drosophila Caenorhabditis, Branchiostoma, Crangon* and *Palaemon* isoforms. We are currently working on obtaining the ANT sequences of the investigated crustaceans. Partial sequences of the ANT of *Crangon crangon* and *Palaemon serratus* have already been successfully cloned. PCR products were sequenced and the final assembled nucleotide

sequences were submitted to GenBank (accession numbers: JQ269837 and JQ269838 for *Palaemon serratus* and *Crangon crangon*, respectively).

6.4.3. Comparison of the primary sequence of *Artemia* ANT with that of other species

On Fig. 34 the alignment of known protein sequences of isoforms of the ANT from different species are shown. Amino acids are represented by their single character code, a dot represents a deletion. Highly conserved regions are marked by yellow and fully conserved regions by red. To the best of our knowledge, the sequences of the ANTs expressed in organisms belonging to the same phylogenetic branch but other than *Artemia*, *Crangon* and *Palaemon*, are not known. Nonetheless, within a highly conserved region of amino acid sequence from position 188 to 260, the stretch 221-229 (PKQNLFI) exhibits a low degree of homology among the BKA-sensitive crustacean *Crangon crangon* and *Palaemon serratus* and the BKA-insensitive *Artemia franciscana*. It cannot be overemphasized that there can still be additional ANT isoforms in *Crangon crangon* and *Palaemon serratus*, since we used their abdominal muscles as a whole, and not an individual organ was dissected (for the purpose of bulk generation for obtaining sufficient yields for mitochondrial isolation). However, an exhaustive search of different primers based on multiple sequence alignment between *Artemia franciscana*, *Branchiostoma floridae*, *Caenorhabditis elegans* and *Drosophila melanogaster* homologues of ANT, yielded only one suitable transcript that was sufficiently long and contained the signature sequence RRRMMM [115, 314].

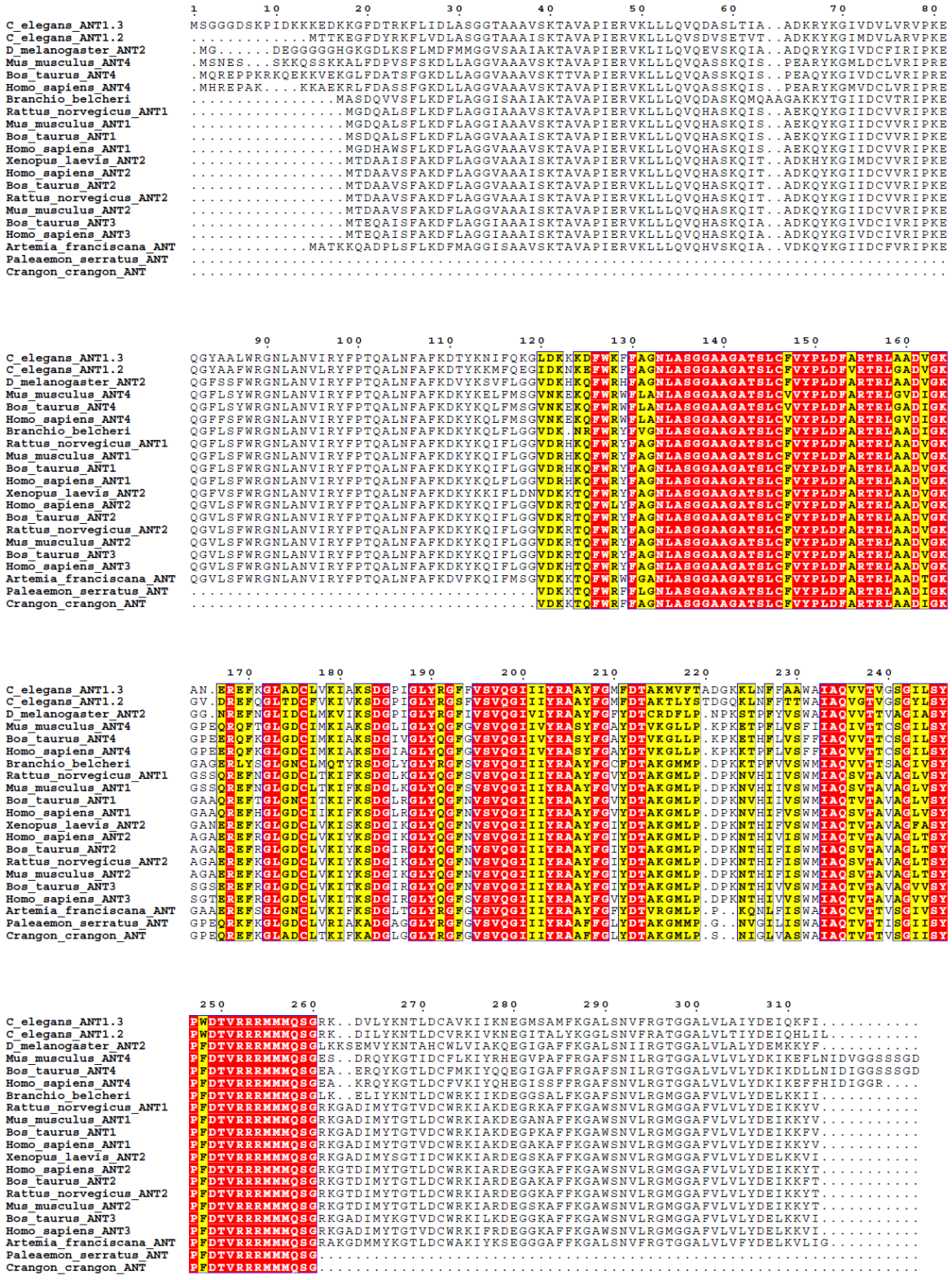

Figure 34: Multiple sequence alignments of known isoforms of the ANT expressed in different species.

6.4.4. Comparison of the predicted three-dimensional structure of *Artemia* ANT with that of bovine ANT

The structure of bovine ANT (isoform 1) is known (structure: pdb1okc) [115], and we were therefore able to compare it with the predicted structure of Artemia ANT, on the basis of its amino acid sequence. The two proteins are superimposed in Fig. 35. Bovine ANT is shown in red, and *Artemia* ANT in blue. It becomes immediately apparent that the two proteins are very similar, except for the three designated areas (a, b, and c). The part of bovine ANT that is different from *Artemia* ANT is colored yellow, and the corresponding part of Artemia ANT is colored magenta. In region a, this corresponds to the subsequence 228-237, in region b, to the subsequence 58-63 in and in region c, to the subsequence 22-23 of the multiple sequence alignments shown on Fig. 34.

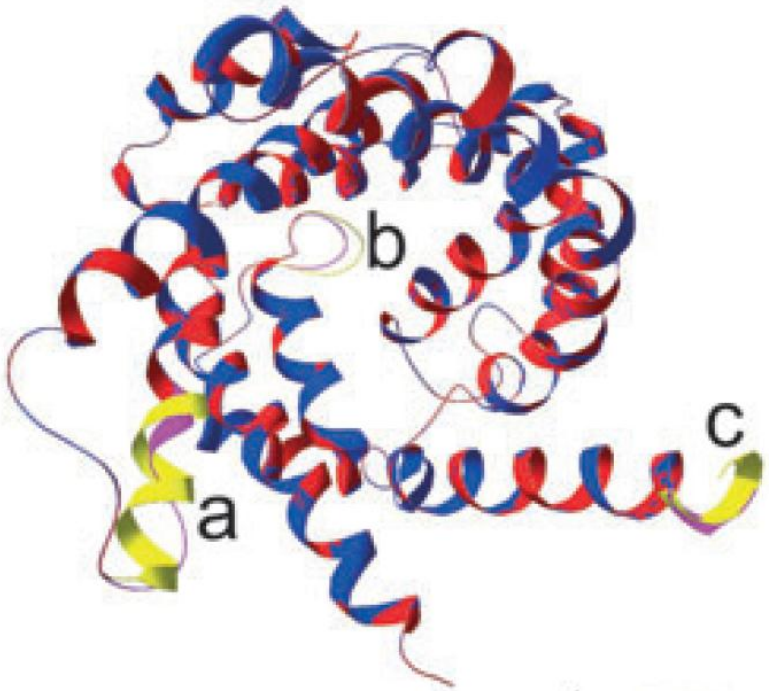

Figure 35: Predicted 3D structure of the *Artemia* ANT, overlapped by the known bovine structure.

6.4.5. The *Artemia* ANT expressed in yeast

The effort of the heterologus expression of *Artemia* ANT in yeast (*Saccharomyces cerevisiae*) was done in order to gain a good model for genetic manipulation that would allow identification of the BKA binding site. Because I was not involved in this study, it will be discussed briefly in this thesis, only to explain how its findings expand on the results of my PhD work.

Saccharomyces cerevisiae expresses three isoforms of ANT. Two strains were generated, in which the genes of the *Saccharomyces* ANT1 and ANT3 were inactivated and the ANT2 isoform was replaced with the *Artemia* ANT (ArANT) containing a hemagglutinin tag (ArANT-HA). Sal1p mediates a Ca^{2+}-dependent import of ATP-Mg from the cytosol to the mitochondria under conditions where these organelles are ATP consumers [315, 316], thereby maintaining or promoting cell survival. In one of the strains the suppressor of ΔANT2 (inactivated ANT2) lethality, SAL1, was inactivated but a plasmid coding for yeast ANT2 was included, because the ArANTΔsal1 strain was lethal. In both strains ArANT-HA was expressed and correctly localized to the mitochondria.

The most important findings were as follows: i) respiratory growth of yeasts expressing ArANT-HA was arrested by BKA only in the strain coexpressing SAL1; ii) fermentative growth of yeasts expressing ArANT-HA was arrested by BKA only in the strain in which SAL1 was absent, and iii) adenine nucleotide exchange mediated by ArANT-HA expressed in yeasts became sensitive to BKA, in a manner independent of SAL1.

Mindful of the fact that that *Artemia franciscana* is refractory to BKA and that BKA binds directly on the carrier [317, 318], (reviewed in [106]) one explanation could be a yet to be identified protein conferring ArANT resistance to BKA is present in mitochondria from *Artemia franciscana*. The generation of the database of the *Artemia* mitochondrial proteome would allow search for proteins that could play such a role.

Relevant to this, the lipid environment in which the ANT is embedded is a critical component for exchange activity in both yeast and mammals [319-321]. Indeed, a high

sensitivity of yeast ANT2 to the cardiolipin content has been previously demonstrated [322, 323]. The lipid composition of the inner mitochondrial membrane of *Artemia* in which ArANT is embedded may be very different from that in yeasts or any other organism to the extent that affords BKA resistance.

7. Discussion

Imbalance of cellular death by the opening of the permeability transition pore is thought to be an important player in untreatable diseases, such as different types of neurodegeneration, cancer and autoimmune diseases. The pore has been described almost 35 years ago, but the attempts aimed at identifying its molecular structure remained unsuccessful. Until recently, no animal species were known to lack the PTP. The finding that mitochondria from the embryo of the brine shrimp, *Artemia franciscana* do not undergo permeability transition upon treatment of well characterized inducers of the pore provides an opportunity for the identification of the PTP by novel approaches.

Our experiments on *Artemia* revealed a highly capable Ca^{2+} uptake machinery, that mechanistically resembled that of the mammalian consensus, but was different from it in some aspects. The Ca^{2+} uptake was sensitive to Ru 360, indicating the process is primarily executed by the Ca^{2+} uniporter. P_i was the necessary counter ion for Ca^{2+} uptake, which fact was also confirmed by EELS microscopy.

However, in contrast to mammals, ADP and ATP both decreased Ca^{2+} uptake capacity in *Artemia*. In the case of mammals the well-established explanation is the inhibitory effect of these nucleotides on the PTP. The inhibitory effect of ADP in *Artemia* could be abolished by blockage of ADP/ATP exchange either directly by inhibition of the ANT by cATR or indirectly, by inhibition of the F_oF_1 ATP-ase by oligomycin. Therefore ADP needs to enter the matrix in order to mediate its effect. Matrix ADP could cause this by two different mechanisms: I) by decreasing membrane potential or II) by binding to a specific matrix binding site. The two inhibitors, cATR and oligomycin have different effects on the matrix ADP pool: at sufficiently high membrane potential (both ANT and the F_oF_1 ATP-ase in forward mode), when cATR inhibits the ANT the ADP concentration slightly decreased (it is normally low even in phosphorylating mitochondria due to the higher flux control coefficient of the F_oF_1 ATP-ase compared to the ANT), as matrix ATP cannot be exchanged for ADP, however in the case of oligomycin, the matrix ADP level is increased, because ADP cannot be converted into ATP by oxidative phosphorylation (or substrate-

level phosphorylation in the matrix by succinyl-thiokinase, as we used succinate in our substrate combination, which disfavors the reaction). Therefore we conclude that Ca^{2+} uptake in *Artemia* is unaffected by matrix ADP concentration, and it is more likely that ADP inhibits Ca^{2+} uptake in *Artemia* mitochondria due to reducing membrane potential and thereby decreasing the driving force for Ca^{2+} uptake, rather than regulating Ca^{2+} dynamics by binding to a specific binding site inside the matrix.

ATP on the other hand does not need to enter the matrix and likely binds on the outer surface of mitochondria to affect Ca^{2+} uptake. This finding provides another possible explanation for the inhibitory effect of ADP: the inhibition is indirect and is in fact caused by the ATP produced by mitochondria, which can be abolished by the inhibition of ATP production by either cATR or oligomycin. These findings open up several new interesting questions regarding Ca^{2+} uptake in *Artemia*.

We investigated mitochondrial morphology of *Artemia* with transmission electron microscopy. *Artemia* mitochondria have a highly similar appearance to mammalian mitochondria regarding size and christae structure. However when loaded with high amounts of Ca^{2+}, needle like electron-dense formations appear in the matrix of *Artemia* mitochondria, whereas in mammals, Ca^{2+} sequestration results in ring-shaped or dotted structures. EELS was used to confirm the electron-dense structures to be rich in Ca and P. Similar morphology can be observed in mammals only when Mg^{2+} and ADP concentrations are low. In the presence of ADP Artemia mitochondria also showed dot like precipitates. We have not investigated whether the morphological change is due to the decreased Ca^{2+} uptake capacity caused by ADP or the direct effect of ADP on the precipitates, however the possibility that the needle-like structure of the precipitates is a contributor to the high Ca^{2+} uptake capacity in *Artemia* cannot be ruled out.

During our investigation we found that other classical PTP inhibitors that effectively increase Ca^{2+} uptake capacity on mammalian mitochondria had no effect on Ca^{2+} uptake in *Artemia*. A well-described inhibitor of the ANT, BKA is also such inhibitor of the PTP. We found *Artemia* to be insensitive to the ANT inhibitory effects of BKA: it failed to reverse

the depolarizing effect of ADP on ΔΨm experiments and in contrast to cATR, it did not affect ATP production. Inhibition by BKA on *Artemia* mitochondria could only be achieved by substantial decrease of the pH and the increase of BKA concentration. This finding is relevant, as the ANT is a known regulator of the PTP, but it is dispensable to the process. The possibility that these characteristics of *Artemia* mitochondria are connected to the absence of the PTP could not be overlooked, and we wished to test this hypothesis.

In order to do this we needed more closely related organisms to *Artemia* than vertebrates, so that a reliable comparison could be made. *Artemia* are extremophiles inhabiting harsh environments, with remarkable resilience to different kinds of physical and chemical stress. The absence of the PTP in these animals was originally investigated to provide an explanation for this resilience. Based on the fact that distinctly related eukaryotes such as fungi plants and all other animals that had been investigated by the time exhibited the PTP, the original authors assumed this was a unique trait of *Artemia* embryos. When we tested other non-extremophile, salt- and freshwater inhabiting crustaceans by similar methods, we surprisingly found that they all lacked the PTP without exception. Furthermore we observed no resistance to BKA in any of the newly investigated species, which falsified our early hypothesis regarding a connection between these two characteristics. Our new assumption was that the PTP was lost at some point in the evolution of the crustacean subphylum. We believed, that narrowing down at which point the mechanism of PT was lost in these animals would lead to clues about the molecular entity of the PTP. We therefore started characterizing species that branched off from crustaceans at different points during evolution. We were also interested if we would find species in other phyla that lacked PT.

To date we have not identified non-crustacean species without the PTP, and we found that the closest species to crustaceans exhibiting PTP are *Drosophila*. We conclude that the lack of PT is a unique trait of crustaceans. Fig. 36 is a taxonomic tree summarizing our findings: species in red exhibit permeability transition and species in green do not. The species which were first investigated by us for the presence of the PTP are marked by underline.

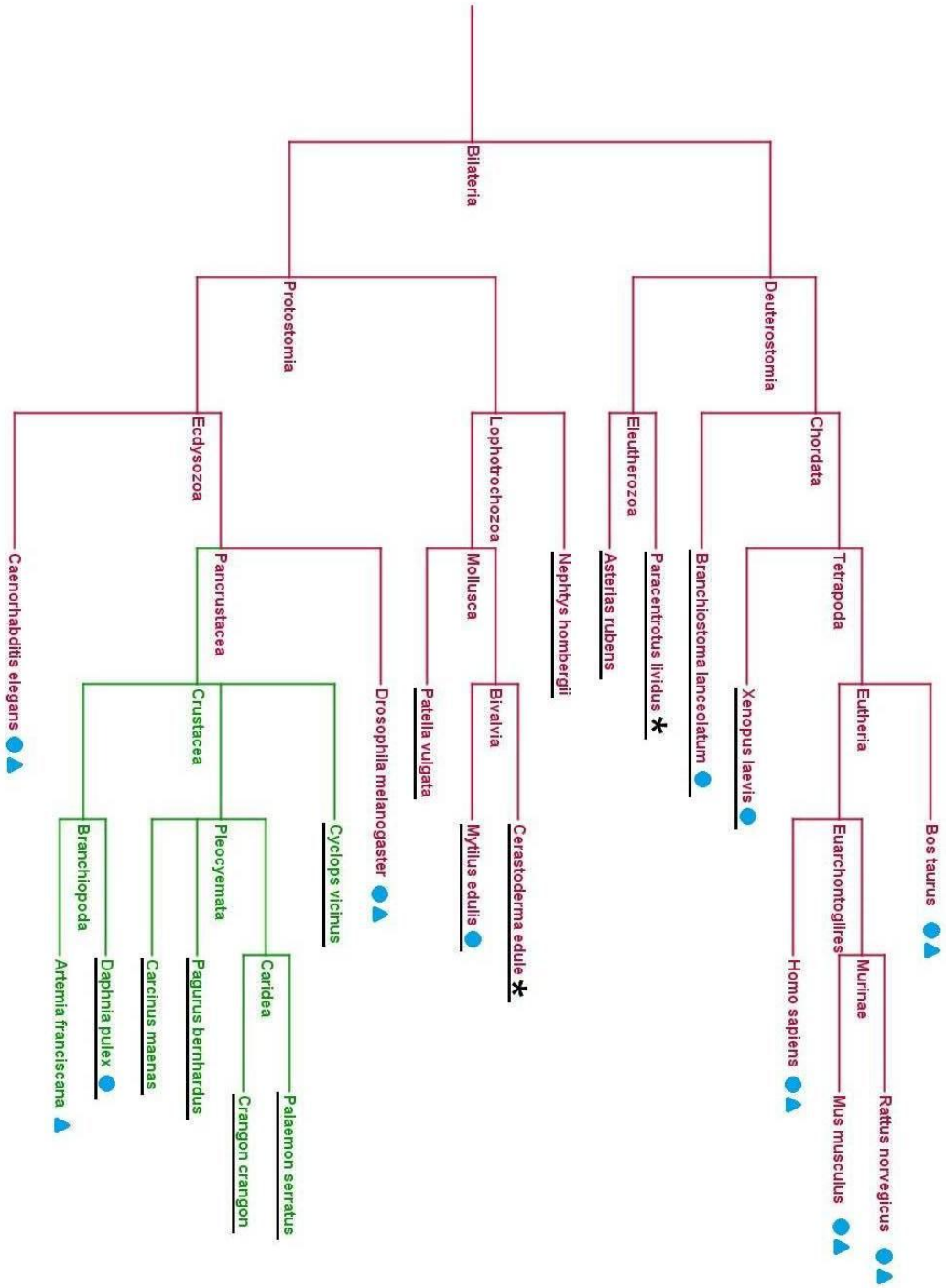

Figure 36: Taxonomic tree of the list of species that will be compared. Red: PTP exhibiting species, green: species without PTP, *: uncertain, more experiments are needed. Species that were first investigated by us are underlined. Blue triangle: mitochondrial proteome available, blue circle: transcriptome available.

Our future perspectives are to establish a database of mitochondrial proteomes and transcriptomes of these species. The analysis of such databases could pinpoint proteins that are absent in the non-PTP species and eventually lead to the identification of the PTP. In Fig. 36 the blue circle indicates species for which the transcriptome and the triangle for which the mitochondrial proteome is available.

Tough the BKA resistance of *Artemia* is unrelated to the absence of PTP, we believed that further investigation could lead to the identification of the bongkrekate binding site of the ANT. The BKA binding site is an unknown potential drug target for PTP inhibition and we sought to identify it by comparison of the *Artemia* ANT to multiple other sensitive ANT sequences. So far, our success in sequencing the full *Artemia* sequence, and the partial sequences of *Crangon crangon* and, *Palaemon serratus* highlights the amino acid sequence 221-229 (by the numbering of Fig. 34, PKQNLFI) to be possibly responsible for the BKA resistance of *Artemia*. A diminished effect of BKA has been demonstrated in yeast mutants [324, 325], but the site(s) of the mutation(s) have never been identified, although in another study mutations in transmembrane segments I, II, III and VI were reported to confer partial resistance to BKA [326]. With our collaborators, we were unsuccessful in demonstrating BKA insensitivity in yeast expressing the cloned *Artemia* ANT. This author has not contributed to the work of the ANT sequencing and the yeast studies.

8. Conclusions

Based on initial findings, we concluded that the Ca^{2+} uptake machinery in the primitive arthropod, *Artemia franciscana* is similar to the mammalian consensus in its basic principles of mechanism. We also confirmed that uptake capacity is higher and PT cannot be evoked in this species, furthermore we described unique traits of the Ca^{2+} uptake machinery and matrix Ca^{2+} precipitates. We found insensitivity to the inhibitory effect of bongkrekate on the adenine nucleotide translocator in isolated mitochondria from the embryos of *Artemia franciscana*. To us this finding was intriguing, because the ANT was previously proposed (and disproven) to be a structural component of the PTP. We later found no connection between the two phenomena and began investigating them separately.

To test if the bongkrekate resistance is in fact due to the unique ANT expressed in Artemia our collaborators attempted to express it in yeast cells while silencing the native yeast isoforms present. Growth of yeast expressing only the *Artemia* ANT remained sensitive to bongkrekate. Though these results are disappointing, some conclusions can be made: the insensitivity of *Artemia* to BKA might be due to some other protein entity either absent in mitochondria of the *Artemia* that is otherwise necessary for conferring sensitivity to BKA, or present that is masking the BKA binding site. Insensitivity could also be caused by unique physical properties of these mitochondria, such as differences in membrane characteristics.

To elaborate on the absence of PT in Artemia we decided to use new animal models. Testing several other crustaceans for the presence of the classical PTP yielded no species exhibiting it, regardless of the habitat or lifestyle. All other invertebrates we checked (as every non-crustacean animal ever described in the literature) were positive for the presence of the PTP. We propose that the subphylum of the crustaceans generally lack the pore.

We plan to expand the number of species investigated, primarily by the use of additional crustaceans. We will investigate the tadpole shrimp (*Triops canciformis*),which is the most ancient living crustacean, the fairy shrimp, which is the closest freshwater species available

relative to *Artemia*, and the common woodlouse (*Oniscus asellus*). Including other arthropods in the study would also be rational, because the closest species to crustaceans known to exhibit the PTP to date is an insect.

The extent of conservation of PT throughout the animal kingdom indicates it may have an important physiological role. Indeed, mice in which the PTP is inhibited greatly by the genetic ablation of CypD show a phenotype of cardiac hypertrophy and higher fatigue in response to exercise. The idea of PT being a Ca^{2+} release pathway in mitochondria is in agreement with the phenotype of the CypD KO mice, however it has not been experimentally proven. In light of this theory, one could expect to see adaptations of Ca^{2+} handling in crustacean mitochondria as a result of compensation for the loss of the PTP. Tough we found no fundamental differences in the mechanism in Artemia, quantitative analysis of Ca^{2+} handling kinetics could lead to a better understanding of the physiological role of the PTP.

We pursue our main goal of identification of the structural elements of the PTP by building a database of the mitochondrial proteomes of a number of selected species investigated and comparing of the proteomes of the two groups of PTP exhibiting and non-exhibiting species, searching for proteins absent in either group. As the PTP building proteins may only have lost their function and still be present in crustaceans, this approach has some inherent risk, however the PTP structure has been a puzzle for more than thirty years and has great scientific value.

9. Summary

Regulated permeabilization of the inner mitochondrial membrane through the opening of the permeability transition pore in response to stress stimuli is thought to play an important role in different neurodegenerative disorders and ischameia-reperfusion damage. The PTP is a highly conserved feature among eukaryotes, with only one exception described in the animal kingdom: the *Artemia franciscana*. In this study we attempted to find hints about the unknown protein entities serving as structural building blocks of the PTP, through the thorough biochemical characterization of *Artemia* mitochondria. We found that this species was resistant to the inhibitory effect of bongkrekate on its ANT. We hypothesized that this trait could be related to the lack of the PTP. Upon obtaining the primer sequence of the *Artemia* ANT and generating multiple sequence alignments against other ANT orthologs, we found the 221-229 (by the numbering of Fig. 34, PKQNLFI) region to be dissimilar in the *Artemia* sequence and deduced it was a possible BKA binding site.

In a collaboration we also intended to express the Artemia ANT in yeast, which we were expecting to confer BKA resistance, however the transfected yeast remained sensitive to BKA, the reason for which is currently under investigation.

We screened a number of invertebrates for the presence of PT at different phylogenetic proximities from *Artemia*, in order to clarify when it was lost. We identified six novel species that do not exhibit the permeability transition pore and showed that PT can be provoked in six other species, belonging to taxa, in which presence of PTP had not been studied previously. Our investigation utilized variable methods to test the functionality of the PTP in each of the species. Based on our results, we postulate that the PTP is a universal trait in the animal kingdom, except for the crustacean subphylum. We also clarified that bongkrekate insensitivity was not necessary for the lack of PTP. Our future plans are to attempt to find candidate proteins of PTP structure by compering PTP exhibiting and non-exhibiting species by a proteomics study on highly purified mitochondria from the selected species.

10. Összefoglalás

A belső mitokondriális membrán áteresztőképességének a permeabilitási tranzíciós póruson kertesztül szabályozottan történő megnövekedése fontos lépés lehet különböző neurodegeneratív betegségek és az ischaemia-reperfúziós károsodás patomechanizmusában. A PTP az eukarióták nagy többségében megörzött jelenség, ami alól az állatvilágban egyetlen kivétel került leírásra: az *Artemia franciscana*. A bemutatott tanulmány célja a PTP struktúrális elemeinek felderítése, aminek érdekében elsőként az *Artemiából* származó izolált mitokondriumok bioenergetikai vizsgálatát végeztük el. Ezen faj adenin nukleotid transzlokáza ellenáll a bongkrekiksav gátló hatásának, ami alapján feltételeztük, hogy ez a jelenség összefügghet a PTP hiányával. Az *Artemia* adenin nukleotid transzlokázának primer szekvenciáját vizsgálva felfigyeltünk egy kevéssé konzervált régióra, mely lehetséges, hogy a bongkrekát kötőhelye.

Egy kollaboráció keretein belül kísérletet tettünk az *Artemia* adenin nukleotid transzlokázának expresszálására élesztőben, annak reményében, hogy az ugyancsak ellenálló lesz bongkrekáttal szemben, azonban ez sikertelen volt, amire a magyarázatot jelenleg keressük.

Filogenetikailag változóan távoli fajok vizsgálatán keresztül kívántunk fényt deríteni arra, miként veszett el a PT jelensége az *Artemiából*. Sikerrel azonosítottunk hat gerictelen állatfajt melyekben a permeabilitás tranziciós pórus hiányzik, továbbá hat olyan taxához tartozó fajban írtuk le a pórus létezését, melyekben az korábban nem volt vizsgálat tárgya. Eredményeink hitelességének érdekében mindegyik fajban a pórus jelenlétét több különböző módszerrel is megvizsgáltuk. A leírtak alapján arra következtetünk, hogy a PTP az állatvilágban univerzális jelenség, mely valamikor a rákfélék altörzsének korai evolúciója során elveszett. Tisztáztuk továbbá, hogy a bongrekát érzéketlenség nem feltétele a tranzíciós pórus hiányának. A jövőben a PTP-vel rendelkező, és az azt nem mutató fajokból izolált tisztított mitokondriumpreparátumok proteomikai összehasonlításán keresztül reméljük a PTP struktúrális elemeit azonosítani.

11. References

1. Nicholls, D.G. and S.L. Budd. (2000) *Mitochondria and neuronal survival.* Physiol Rev. **80**(1): p. 315-60.
2. Chinopoulos, C. and V. Adam-Vizi. (2010) *Mitochondrial Ca2+ sequestration and precipitation revisited.* Febs J. **277**(18): p. 3637-51.
3. Nicholls, D.G. (1974) *The influence of respiration and ATP hydrolysis on the proton-electrochemical gradient across the inner membrane of rat-liver mitochondria as determined by ion distribution.* Eur J Biochem. **50**(1): p. 305-15.
4. Mitchell, P. and J. Moyle. (1969) *Estimation of membrane potential and pH difference across the cristae membrane of rat liver mitochondria.* Eur J Biochem. **7**(4): p. 471-84.
5. Gerencser, A.A., C. Chinopoulos, M.J. Birket, M. Jastroch, C. Vitelli, D.G. Nicholls, and M.D. Brand. (2012) *Quantitative measurement of mitochondrial membrane potential in cultured cells: calcium-induced de- and hyperpolarization of neuronal mitochondria.* J Physiol. **590**(Pt 12): p. 2845-71.
6. Mitchell, P. (1961) *Coupling of phosphorylation to electron and hydrogen transfer by a chemi-osmotic type of mechanism.* Nature. **191**: p. 144-8.
7. McCormack, J.G., A.P. Halestrap, and R.M. Denton. (1990) *Role of calcium ions in regulation of mammalian intramitochondrial metabolism.* Physiol Rev. **70**(2): p. 391-425.
8. Brustovetsky, N., T. Brustovetsky, K.J. Purl, M. Capano, M. Crompton, and J.M. Dubinsky. (2003) *Increased susceptibility of striatal mitochondria to calcium-induced permeability transition.* J Neurosci. **23**(12): p. 4858-67.
9. Deluca, H.F. and G.W. Engstrom. (1961) *Calcium uptake by rat kidney mitochondria.* Proc Natl Acad Sci U S A. **47**: p. 1744-50.
10. Vasington, F.D. and J.V. Murphy. (1962) *Ca^{2+} uptake by rat kidney mitochondria and its dependence on respiration and phosphorylation.* Journal of Biological Chemistry. **237**: p. 2670–2672.
11. Pizzo, P., I. Drago, R. Filadi, and T. Pozzan. (2012) *Mitochondrial Ca(2)(+) homeostasis: mechanism, role, and tissue specificities.* Pflugers Arch. **464**(1): p. 3-17.

12. Carafoli, E. and M. Crompton. (1978) *The regulation of intracellular calcium by mitochondria.* Ann N Y Acad Sci. **307**: p. 269-84.

13. Rossi, C.S. and A.L. Lehninger. (1964) *Stoichiometry of Respiratory Stimulation, Accumulation of Ca++ and Phosphate, and Oxidative Phosphorylation in Rat Liver Mitochondria.* J Biol Chem. **239**: p. 3971-80.

14. Rizzuto, R., A.W. Simpson, M. Brini, and T. Pozzan. (1992) *Rapid changes of mitochondrial Ca2+ revealed by specifically targeted recombinant aequorin.* Nature. **358**(6384): p. 325-7.

15. Ying, W.L., J. Emerson, M.J. Clarke, and D.R. Sanadi. (1991) *Inhibition of mitochondrial calcium ion transport by an oxo-bridged dinuclear ruthenium ammine complex.* Biochemistry. **30**(20): p. 4949-52.

16. Moore, C.L. (1971) *Specific inhibition of mitochondrial Ca++ transport by ruthenium red.* Biochem Biophys Res Commun. **42**(2): p. 298-305.

17. Kirichok, Y., G. Krapivinsky, and D.E. Clapham. (2004) *The mitochondrial calcium uniporter is a highly selective ion channel.* Nature. **427**(6972): p. 360-4.

18. Bragadin, M., T. Pozzan, and G.F. Azzone. (1979) *Activation energies and enthalpies during Ca2+ transport in rat liver mitochondria.* FEBS Lett. **104**(2): p. 347-51.

19. Perocchi, F., V.M. Gohil, H.S. Girgis, X.R. Bao, J.E. McCombs, A.E. Palmer, and V.K. Mootha. (2010) *MICU1 encodes a mitochondrial EF hand protein required for Ca(2+) uptake.* Nature. **467**(7313): p. 291-6.

20. De Stefani, D., A. Raffaello, E. Teardo, I. Szabo, and R. Rizzuto. (2011) *A forty-kilodalton protein of the inner membrane is the mitochondrial calcium uniporter.* Nature. **476**(7360): p. 336-40.

21. Baughman, J.M., F. Perocchi, H.S. Girgis, M. Plovanich, C.A. Belcher-Timme, Y. Sancak, X.R. Bao, L. Strittmatter, O. Goldberger, R.L. Bogorad, V. Koteliansky, and V.K. Mootha. (2011) *Integrative genomics identifies MCU as an essential component of the mitochondrial calcium uniporter.* Nature. **476**(7360): p. 341-5.

22. Chalmers, S. and D.G. Nicholls. (2003) *The relationship between free and total calcium concentrations in the matrix of liver and brain mitochondria.* J Biol Chem. **278**(21): p. 19062-70.

23. Sordahl, L.A. and B.B. Silver. (1975) *Pathological accumulation of calcium by mitochondria: modulation by magnesium.* Recent Adv Stud Cardiac Struct Metab. **6**: p. 85-93.
24. Weinbach, E.C. and T. Von Brand. (1967) *Formation, isolation and composition of dense granules from mitochondria.* Biochim Biophys Acta. **148**(1): p. 256-66.
25. Kristian, T., N.B. Pivovarova, G. Fiskum, and S.B. Andrews. (2007) *Calcium-induced precipitate formation in brain mitochondria: composition, calcium capacity, and retention.* J Neurochem. **102**(4): p. 1346-56.
26. Carafoli, E., C.S. Rossi, and A.L. Lehninger. (1965) *Uptake of Adenine Nucleotides by Respiring Mitochondria during Active Accumulation of Ca++ and Phosphate.* J Biol Chem. **240**: p. 2254-61.
27. Greenawalt, J.W., C.S. Rossi, and A.L. Lehninger. (1964) *Effect of Active Accumulation of Calcium and Phosphate Ions on the Structure of Rat Liver Mitochondria.* J Cell Biol. **23**: p. 21-38.
28. Zoccarato, F. and D. Nicholls. (1982) *The role of phosphate in the regulation of the independent calcium-efflux pathway of liver mitochondria.* Eur J Biochem. **127**(2): p. 333-8.
29. Vajda, S., M. Mandi, C. Konrad, G. Kiss, A. Ambrus, V. Adam-Vizi, and C. Chinopoulos. (2009) *A re-evaluation of the role of matrix acidification in uncoupler-induced Ca2+ release from mitochondria.* Febs J. **276**(10): p. 2713-24.
30. Tew, W.P., C.D. Malis, J.E. Howard, and A.L. Lehninger. (1981) *Phosphocitrate inhibits mitochondrial and cytosolic accumulation of calcium in kidney cells in vivo.* Proc Natl Acad Sci U S A. **78**(9): p. 5528-32.
31. Tew, W.P., C. Mahle, J. Benavides, J.E. Howard, and A.L. Lehninger. (1980) *Synthesis and characterization of phosphocitric acid, a potent inhibitor of hydroxylapatite crystal growth.* Biochemistry. **19**(9): p. 1983-8.
32. Moro, L., N. Stagni, E. Luxich, J.D. Sallis, and B. de Bernard. (1990) *Evidence in vitro for an enzymatic synthesis of phosphocitrate.* Biochem Biophys Res Commun. **170**(1): p. 251-8.
33. Williams, G.S., JD. (1987) *Urolithiasis, Clinical and Basic Research.* (L.H Smith, W.G. Robertson, and B. Finlayson Eds.).

34. Crompton, M., R. Moser, H. Ludi, and E. Carafoli. (1978) *The interrelations between the transport of sodium and calcium in mitochondria of various mammalian tissues.* Eur J Biochem. **82**(1): p. 25-31.

35. Pozzan, T., M. Bragadin, and G.F. Azzone. (1977) *Disequilibrium between steady-state Ca2+ accumulation ratio and membrane potential in mitochondria. Pathway and role of Ca2+ efflux.* Biochemistry. **16**(25): p. 5618-25.

36. Pozzan, T. and G.F. Azzone. (1976) *The coupling of electrical ion fluxes in rat liver mitochondria.* FEBS Lett. **72**(1): p. 62-6.

37. Gunter, T.E. and D.R. Pfeiffer. (1990) *Mechanisms by which mitochondria transport calcium.* Am J Physiol. **258**(5 Pt 1): p. C755-86.

38. Palty, R., W.F. Silverman, M. Hershfinkel, T. Caporale, S.L. Sensi, J. Parnis, C. Nolte, D. Fishman, V. Shoshan-Barmatz, S. Herrmann, D. Khananshvili, and I. Sekler. (2010) *NCLX is an essential component of mitochondrial Na+/Ca2+ exchange.* Proc Natl Acad Sci U S A. **107**(1): p. 436-41.

39. Nowikovsky, K., E.M. Froschauer, G. Zsurka, J. Samaj, S. Reipert, M. Kolisek, G. Wiesenberger, and R.J. Schweyen. (2004) *The LETM1/YOL027 gene family encodes a factor of the mitochondrial K+ homeostasis with a potential role in the Wolf-Hirschhorn syndrome.* J Biol Chem. **279**(29): p. 30307-15.

40. Jiang, D., L. Zhao, and D.E. Clapham. (2009) *Genome-wide RNAi screen identifies Letm1 as a mitochondrial Ca2+/H+ antiporter.* Science. **326**(5949): p. 144-7.

41. Villa, A., M.I. Garcia-Simon, P. Blanco, B. Sese, E. Bogonez, and J. Satrustegui. (1998) *Affinity chromatography purification of mitochondrial inner membrane proteins with calcium transport activity.* Biochim Biophys Acta. **1373**(2): p. 347-59.

42. Chinopoulos, C., A.A. Starkov, S. Grigoriev, L.M. Dejean, K.W. Kinnally, X. Liu, I.S. Ambudkar, and G. Fiskum. (2005) *Diacylglycerols activate mitochondrial cationic channel(s) and release sequestered Ca(2+).* J Bioenerg Biomembr. **37**(4): p. 237-47.

43. Szabadkai, G. and M.R. Duchen. (2008) *Mitochondria: the hub of cellular Ca2+ signaling.* Physiology (Bethesda). **23**: p. 84-94.

44. Rizzuto, R., P. Pinton, W. Carrington, F.S. Fay, K.E. Fogarty, L.M. Lifshitz, R.A. Tuft, and T. Pozzan. (1998) *Close contacts with the endoplasmic reticulum as determinants of mitochondrial Ca2+ responses.* Science. **280**(5370): p. 1763-6.

45. Csordas, G., P. Varnai, T. Golenar, S. Roy, G. Purkins, T.G. Schneider, T. Balla, and G. Hajnoczky. (2010) *Imaging interorganelle contacts and local calcium dynamics at the ER-mitochondrial interface.* Mol Cell. **39**(1): p. 121-32.

46. Babcock, D.F., J. Herrington, P.C. Goodwin, Y.B. Park, and B. Hille. (1997) *Mitochondrial participation in the intracellular Ca2+ network.* J Cell Biol. **136**(4): p. 833-44.

47. Landolfi, B., S. Curci, L. Debellis, T. Pozzan, and A.M. Hofer. (1998) *Ca2+ homeostasis in the agonist-sensitive internal store: functional interactions between mitochondria and the ER measured In situ in intact cells.* J Cell Biol. **142**(5): p. 1235-43.

48. Duchen, M.R. (1992) *Ca(2+)-dependent changes in the mitochondrial energetics in single dissociated mouse sensory neurons.* Biochem J. **283 (Pt 1)**: p. 41-50.

49. Breckenridge, D.G., M. Stojanovic, R.C. Marcellus, and G.C. Shore. (2003) *Caspase cleavage product of BAP31 induces mitochondrial fission through endoplasmic reticulum calcium signals, enhancing cytochrome c release to the cytosol.* J Cell Biol. **160**(7): p. 1115-27.

50. Fransson, S., A. Ruusala, and P. Aspenstrom. (2006) *The atypical Rho GTPases Miro-1 and Miro-2 have essential roles in mitochondrial trafficking.* Biochem Biophys Res Commun. **344**(2): p. 500-10.

51. Adam-Vizi, V. and A.A. Starkov. (2010) *Calcium and mitochondrial reactive oxygen species generation: how to read the facts.* J Alzheimers Dis. **20 Suppl 2**: p. S413-26.

52. Castilho, R.F., A.J. Kowaltowski, A.R. Meinicke, E.J. Bechara, and A.E. Vercesi. (1995) *Permeabilization of the inner mitochondrial membrane by Ca2+ ions is stimulated by t-butyl hydroperoxide and mediated by reactive oxygen species generated by mitochondria.* Free Radic Biol Med. **18**(3): p. 479-86.

53. Hansson, M.J., R. Mansson, S. Morota, H. Uchino, T. Kallur, T. Sumi, N. Ishii, M. Shimazu, M.F. Keep, A. Jegorov, and E. Elmer. (2008) *Calcium-induced generation of reactive oxygen species in brain mitochondria is mediated by permeability transition.* Free Radic Biol Med. **45**(3): p. 284-94.

54. Irigoin, F., N.M. Inada, M.P. Fernandes, L. Piacenza, F.R. Gadelha, A.E. Vercesi, and R. Radi. (2009) *Mitochondrial calcium overload triggers complement-dependent superoxide-mediated programmed cell death in Trypanosoma cruzi.* Biochem J. **418**(3): p. 595-604.

55. Kowaltowski, A.J., R.F. Castilho, and A.E. Vercesi. (1995) *Ca(2+)-induced mitochondrial membrane permeabilization: role of coenzyme Q redox state.* Am J Physiol. **269**(1 Pt 1): p. C141-7.

56. Gyulkhandanyan, A.V. and P.S. Pennefather. (2004) *Shift in the localization of sites of hydrogen peroxide production in brain mitochondria by mitochondrial stress.* J Neurochem. **90**(2): p. 405-21.

57. Komary, Z., L. Tretter, and V. Adam-Vizi. (2008) *H2O2 generation is decreased by calcium in isolated brain mitochondria.* Biochim Biophys Acta. **1777**(7-8): p. 800-7.

58. Starkov, A.A., B.M. Polster, and G. Fiskum. (2002) *Regulation of hydrogen peroxide production by brain mitochondria by calcium and Bax.* J Neurochem. **83**(1): p. 220-8.

59. Panov, A., S. Dikalov, N. Shalbuyeva, R. Hemendinger, J.T. Greenamyre, and J. Rosenfeld. (2007) *Species- and tissue-specific relationships between mitochondrial permeability transition and generation of ROS in brain and liver mitochondria of rats and mice.* Am J Physiol Cell Physiol. **292**(2): p. C708-18.

60. Schonfeld, P. and G. Reiser. (2007) *Ca2+ storage capacity of rat brain mitochondria declines during the postnatal development without change in ROS production capacity.* Antioxid Redox Signal. **9**(2): p. 191-9.

61. Votyakova, T.V. and I.J. Reynolds. (2005) *Ca2+-induced permeabilization promotes free radical release from rat brain mitochondria with partially inhibited complex I.* J Neurochem. **93**(3): p. 526-37.

62. Basso, E., L. Fante, J. Fowlkes, V. Petronilli, M.A. Forte, and P. Bernardi. (2005) *Properties of the permeability transition pore in mitochondria devoid of Cyclophilin D.* J Biol Chem. **280**(19): p. 18558-61.

63. Schinzel, A.C., O. Takeuchi, Z. Huang, J.K. Fisher, Z. Zhou, J. Rubens, C. Hetz, N.N. Danial, M.A. Moskowitz, and S.J. Korsmeyer. (2005) *Cyclophilin D is a component of mitochondrial permeability transition and mediates neuronal cell death after focal cerebral ischemia.* Proc Natl Acad Sci U S A. **102**(34): p. 12005-10.

64. Nakagawa, T., S. Shimizu, T. Watanabe, O. Yamaguchi, K. Otsu, H. Yamagata, H. Inohara, T. Kubo, and Y. Tsujimoto. (2005) *Cyclophilin D-dependent mitochondrial permeability transition regulates some necrotic but not apoptotic cell death.* Nature. **434**(7033): p. 652-8.

65. Baines, C.P., R.A. Kaiser, N.H. Purcell, N.S. Blair, H. Osinska, M.A. Hambleton, E.W. Brunskill, M.R. Sayen, R.A. Gottlieb, G.W. Dorn, J. Robbins, and J.D. Molkentin. (2005) *Loss of cyclophilin D reveals a critical role for mitochondrial permeability transition in cell death.* Nature. **434**(7033): p. 658-62.

66. Millay, D.P., M.A. Sargent, H. Osinska, C.P. Baines, E.R. Barton, G. Vuagniaux, H.L. Sweeney, J. Robbins, and J.D. Molkentin. (2008) *Genetic and pharmacologic inhibition of mitochondrial-dependent necrosis attenuates muscular dystrophy.* Nat Med. **14**(4): p. 442-7.

67. Du, H., L. Guo, F. Fang, D. Chen, A.A. Sosunov, G.M. McKhann, Y. Yan, C. Wang, H. Zhang, J.D. Molkentin, F.J. Gunn-Moore, J.P. Vonsattel, O. Arancio, J.X. Chen, and S.D. Yan. (2008) *Cyclophilin D deficiency attenuates mitochondrial and neuronal perturbation and ameliorates learning and memory in Alzheimer's disease.* Nat Med. **14**(10): p. 1097-105.

68. Gautier, C.A., E. Giaime, E. Caballero, L. Nunez, Z. Song, D. Chan, C. Villalobos, and J. Shen. (2012) *Regulation of mitochondrial permeability transition pore by PINK1.* Mol Neurodegener. **7**: p. 22.

69. Thomas, B., R. Banerjee, N.N. Starkova, S.F. Zhang, N.Y. Calingasan, L. Yang, E. Wille, B.J. Lorenzo, D.J. Ho, M.F. Beal, and A. Starkov. (2012) *Mitochondrial permeability transition pore component cyclophilin D distinguishes nigrostriatal dopaminergic death paradigms in the MPTP mouse model of Parkinson's disease.* Antioxid Redox Signal. **16**(9): p. 855-68.

70. Zhou, C., Y. Huang, and S. Przedborski. (2008) *Oxidative stress in Parkinson's disease: a mechanism of pathogenic and therapeutic significance.* Ann N Y Acad Sci. **1147**: p. 93-104.

71. Martin, L.J., B. Gertz, Y. Pan, A.C. Price, J.D. Molkentin, and Q. Chang. (2009) *The mitochondrial permeability transition pore in motor neurons: involvement in the pathobiology of ALS mice.* Exp Neurol. **218**(2): p. 333-46.

72. Ichas, F. and J.P. Mazat. (1998) *From calcium signaling to cell death: two conformations for the mitochondrial permeability transition pore. Switching from low- to high-conductance state.* Biochim Biophys Acta. **1366**(1-2): p. 33-50.

73. Starkov, A.A., G. Fiskum, C. Chinopoulos, B.J. Lorenzo, S.E. Browne, M.S. Patel, and M.F. Beal. (2004) *Mitochondrial alpha-ketoglutarate dehydrogenase complex generates reactive oxygen species.* J Neurosci. **24**(36): p. 7779-88.

74. Tretter, L. and V. Adam-Vizi. (2004) *Generation of reactive oxygen species in the reaction catalyzed by alpha-ketoglutarate dehydrogenase.* J Neurosci. **24**(36): p. 7771-8.

75. Rasola, A. and P. Bernardi. (2011) *Mitochondrial permeability transition in Ca(2+)-dependent apoptosis and necrosis.* Cell Calcium. **50**(3): p. 222-33.

76. Bernardi, P. and A. Rasola. (2007) *Calcium and cell death: the mitochondrial connection.* Subcell Biochem. **45**: p. 481-506.

77. Gramaglia, D., A. Gentile, M. Battaglia, L. Ranzato, V. Petronilli, M. Fassetta, P. Bernardi, and A. Rasola. (2004) *Apoptosis to necrosis switching downstream of apoptosome formation requires inhibition of both glycolysis and oxidative phosphorylation in a BCL-X(L)- and PKB/AKT-independent fashion.* Cell Death Differ. **11**(3): p. 342-53.

78. Carafoli, E. (2010) *The fateful encounter of mitochondria with calcium: how did it happen?* Biochim Biophys Acta. **1797**(6-7): p. 595-606.

79. Hunter, D.R., R.A. Haworth, and J.H. Southard. (1976) *Relationship between configuration, function, and permeability in calcium-treated mitochondria.* J Biol Chem. **251**(16): p. 5069-77.

80. Hunter, D.R. and R.A. Haworth. (1979) *The Ca2+-induced membrane transition in mitochondria. I. The protective mechanisms.* Arch Biochem Biophys. **195**(2): p. 453-9.

81. Haworth, R.A. and D.R. Hunter. (1979) *The Ca2+-induced membrane transition in mitochondria. II. Nature of the Ca2+ trigger site.* Arch Biochem Biophys. **195**(2): p. 460-7.

82. Hunter, D.R. and R.A. Haworth. (1979) *The Ca2+-induced membrane transition in mitochondria. III. Transitional Ca2+ release.* Arch Biochem Biophys. **195**(2): p. 468-77.

83. Zoratti, M. and I. Szabo. (1995) *The mitochondrial permeability transition.* Biochim Biophys Acta. **1241**(2): p. 139-76.

84. Petronilli, V., P. Costantini, L. Scorrano, R. Colonna, S. Passamonti, and P. Bernardi. (1994) *The voltage sensor of the mitochondrial permeability transition pore is tuned by the oxidation-reduction state of vicinal thiols. Increase of the gating potential by oxidants and its reversal by reducing agents.* J Biol Chem. **269**(24): p. 16638-42.

85. Valle, V.G., M.M. Fagian, L.S. Parentoni, A.R. Meinicke, and A.E. Vercesi. (1993) *The participation of reactive oxygen species and protein thiols in the mechanism of mitochondrial inner membrane permeabilization by calcium plus prooxidants.* Arch Biochem Biophys. **307**(1): p. 1-7.

86. Kowaltowski, A.J., R.F. Castilho, and A.E. Vercesi. (1996) *Opening of the mitochondrial permeability transition pore by uncoupling or inorganic phosphate in the presence of Ca2+ is dependent on mitochondrial-generated reactive oxygen species.* FEBS Lett. **378**(2): p. 150-2.

87. Scorrano, L., V. Petronilli, and P. Bernardi. (1997) *On the voltage dependence of the mitochondrial permeability transition pore. A critical appraisal.* J Biol Chem. **272**(19): p. 12295-9.

88. Kristian, T., T.M. Weatherby, T.E. Bates, and G. Fiskum. (2002) *Heterogeneity of the calcium-induced permeability transition in isolated non-synaptic brain mitochondria.* J Neurochem. **83**(6): p. 1297-308.

89. Chinopoulos, C., A.A. Starkov, and G. Fiskum. (2003) *Cyclosporin A-insensitive permeability transition in brain mitochondria: inhibition by 2-aminoethoxydiphenyl borate.* J Biol Chem. **278**(30): p. 27382-9.

90. Asimakis, G.K. and J.R. Aprille. (1980) *In vitro alteration of the size of the liver mitochondrial adenine nucleotide pool: correlation with respiratory functions.* Arch Biochem Biophys. **203**(1): p. 307-16.

91. Peng, C.F., D.W. Price, C. Bhuvaneswaran, and C.L. Wadkins. (1974) *Factors that influence phosphoenolpyruvate-induced calcium efflux from rat liver mitochondria.* Biochem Biophys Res Commun. **56**(1): p. 134-41.

92. Bernardi, P., S. Vassanelli, P. Veronese, R. Colonna, I. Szabo, and M. Zoratti. (1992) *Modulation of the mitochondrial permeability transition pore. Effect of protons and divalent cations.* J Biol Chem. **267**(5): p. 2934-9.

93. Bernardi, P., A. Krauskopf, E. Basso, V. Petronilli, E. Blachly-Dyson, F. Di Lisa, and M.A. Forte. (2006) *The mitochondrial permeability transition from in vitro artifact to disease target.* Febs J. **273**(10): p. 2077-99.

94. Nicolli, A., V. Petronilli, and P. Bernardi. (1993) *Modulation of the mitochondrial cyclosporin A-sensitive permeability transition pore by matrix pH. Evidence that the pore open-closed probability is regulated by reversible histidine protonation.* Biochemistry. **32**(16): p. 4461-5.

95. Bernardi, P. (1992) *Modulation of the mitochondrial cyclosporin A-sensitive permeability transition pore by the proton electrochemical gradient. Evidence that the pore can be opened by membrane depolarization.* J Biol Chem. **267**(13): p. 8834-9.

96. Novgorodov, S.A., T.I. Gudz, G.P. Brierley, and D.R. Pfeiffer. (1994) *Magnesium ion modulates the sensitivity of the mitochondrial permeability transition pore to cyclosporin A and ADP.* Arch Biochem Biophys. **311**(2): p. 219-28.

97. Liu, J., J.D. Farmer, Jr., W.S. Lane, J. Friedman, I. Weissman, and S.L. Schreiber. (1991) *Calcineurin is a common target of cyclophilin-cyclosporin A and FKBP-FK506 complexes.* Cell. **66**(4): p. 807-15.

98. Khauli, R.B., T. Strzelecki, S. Kumar, M. Fink, J. Stoff, and M. Menon. (1987) *Mitochondrial alterations after cyclosporine and ischemia: insights on the pathophysiology of nephrotoxicity.* Transplant Proc. **19**(1 Pt 2): p. 1395-7.

99. Jung, K., C. Reinholdt, and D. Scholz. (1987) *Inhibitory effect of cyclosporine on the respiratory efficiency of isolated human kidney mitochondria.* Transplantation. **43**(1): p. 162-3.

100. Fournier, N., G. Ducet, and A. Crevat. (1987) *Action of cyclosporine on mitochondrial calcium fluxes.* J Bioenerg Biomembr. **19**(3): p. 297-303.

101. Davidson, A.M. and A.P. Halestrap. (1990) *Partial inhibition by cyclosporin A of the swelling of liver mitochondria in vivo and in vitro induced by sub-micromolar [Ca2+], but not by butyrate. Evidence for two distinct swelling mechanisms.* Biochem J. **268**(1): p. 147-52.

102. Broekemeier, K.M., M.E. Dempsey, and D.R. Pfeiffer. (1989) *Cyclosporin A is a potent inhibitor of the inner membrane permeability transition in liver mitochondria.* J Biol Chem. **264**(14): p. 7826-30.

103. Crompton, M., H. Ellinger, and A. Costi. (1988) *Inhibition by cyclosporin A of a Ca2+-dependent pore in heart mitochondria activated by inorganic phosphate and oxidative stress.* Biochem J. **255**(1): p. 357-60.

104. Waldmeier, P.C., J.J. Feldtrauer, T. Qian, and J.J. Lemasters. (2002) *Inhibition of the mitochondrial permeability transition by the nonimmunosuppressive cyclosporin derivative NIM811.* Mol Pharmacol. **62**(1): p. 22-9.

105. Lapidus, R.G. and P.M. Sokolove. (1994) *The mitochondrial permeability transition. Interactions of spermine, ADP, and inorganic phosphate.* J Biol Chem. **269**(29): p. 18931-6.

106. Klingenberg, M. (2008) *The ADP and ATP transport in mitochondria and its carrier.* Biochim Biophys Acta. **1778**(10): p. 1978-2021.

107. Metelkin, E., O. Demin, Z. Kovacs, and C. Chinopoulos. (2009) *Modeling of ATP-ADP steady-state exchange rate mediated by the adenine nucleotide translocase in isolated mitochondria.* Febs J. **276**(23): p. 6942-55.

108. Boxer, D.H., J. Feckl, and M. Klingenberg. (1977) *Identity between the major protein located at the outer face of the inner mitochondrial membrane and carboxyatractylate binding protein.* FEBS Lett. **73**(1): p. 43-6.

109. Aquila, H., D. Misra, M. Eulitz, and M. Klingenberg. (1982) *Complete amino acid sequence of the ADP/ATP carrier from beef heart mitochondria.* Hoppe Seylers Z Physiol Chem. **363**(3): p. 345-9.

110. Saraste, M. and J.E. Walker. (1982) *Internal sequence repeats and the path of polypeptide in mitochondrial ADP/ATP translocase.* FEBS Lett. **144**(2): p. 250-4.

111. Block, M.R., G. Zaccai, G.J. Lauquin, and P.V. Vignais. (1982) *Small angle neutron scattering of the mitochondrial ADP/ATP carrier protein in detergent.* Biochem Biophys Res Commun. **109**(2): p. 471-7.

112. Majima, E., K. Ikawa, M. Takeda, M. Hashimoto, Y. Shinohara, and H. Terada. (1995) *Translocation of loops regulates transport activity of mitochondrial ADP/ATP carrier deduced from formation of a specific intermolecular disulfide bridge catalyzed by copper-o-phenanthroline.* J Biol Chem. **270**(49): p. 29548-54.

113. Crichton, P.G., M. Harding, J.J. Ruprecht, Y. Lee, and E.R. Kunji. (2013) *Lipid, detergent and Coomassie dye affect the migration of small membrane proteins in blue native gels: mitochondrial carriers migrate as monomers not dimers.* J Biol Chem.

114. Kunji, E.R. and P.G. Crichton. (2010) *Mitochondrial carriers function as monomers.* Biochim Biophys Acta. **1797**(6-7): p. 817-31.

115. Pebay-Peyroula, E., C. Dahout-Gonzalez, R. Kahn, V. Trezeguet, G.J. Lauquin, and G. Brandolin. (2003) *Structure of mitochondrial ADP/ATP carrier in complex with carboxyatractyloside.* Nature. **426**(6962): p. 39-44.

116. Powell, S.J., S.M. Medd, M.J. Runswick, and J.E. Walker. (1989) *Two bovine genes for mitochondrial ADP/ATP translocase expressed differences in various tissues.* Biochemistry. **28**(2): p. 866-73.

117. Stepien, G., A. Torroni, A.B. Chung, J.A. Hodge, and D.C. Wallace. (1992) *Differential expression of adenine nucleotide translocator isoforms in mammalian tissues and during muscle cell differentiation.* J Biol Chem. **267**(21): p. 14592-7.

118. Neckelmann, N., K. Li, R.P. Wade, R. Shuster, and D.C. Wallace. (1987) *cDNA sequence of a human skeletal muscle ADP/ATP translocator: lack of a leader peptide, divergence from a fibroblast translocator cDNA, and coevolution with mitochondrial DNA genes.* Proc Natl Acad Sci U S A. **84**(21): p. 7580-4.

119. Giraud, S., C. Bonod-Bidaud, M. Wesolowski-Louvel, and G. Stepien. (1998) *Expression of human ANT2 gene in highly proliferative cells: GRBOX, a new transcriptional element, is involved in the regulation of glycolytic ATP import into mitochondria.* J Mol Biol. **281**(3): p. 409-18.

120. Houldsworth, J. and G. Attardi. (1988) *Two distinct genes for ADP/ATP translocase are expressed at the mRNA level in adult human liver.* Proc Natl Acad Sci U S A. **85**(2): p. 377-81.

121. Dolce, V., P. Scarcia, D. Iacopetta, and F. Palmieri. (2005) *A fourth ADP/ATP carrier isoform in man: identification, bacterial expression, functional characterization and tissue distribution.* FEBS Lett. **579**(3): p. 633-7.

122. Aquila, H., T.A. Link, and M. Klingenberg. (1987) *Solute carriers involved in energy transfer of mitochondria form a homologous protein family.* FEBS Lett. **212**(1): p. 1-9.

123. Kemp, A., Jr. and E.C. Slater. (1964) *The Site of Action of Atractyloside.* Biochim Biophys Acta. **92**: p. 178-80.

124. Klingenberg, M., K. Grebe, and B. Scherer. (1975) *The binding of atractylate and carboxy-atractylate to mitochondria.* Eur J Biochem. **52**(2): p. 351-63.

125. Klingenberg, M., K. Grebe, and G. Falkner. (1971) *Interaction between the binding of 35S-atractyloside and bongkrekic acid at mitochondrial membranes.* FEBS Lett. **16**(4): p. 301-303.

126. Welling, W., J.A. Cohen, and W. Berends. (1960) *Disturbance of oxidative phosphorylation by an antibioticum produced by Pseudomonas cocovenenans.* Biochem Pharmacol. **3**: p. 122-35.

127. Henderson, P.J. and H.A. Lardy. (1970) *Bongkrekic acid. An inhibitor of the adenine nucleotide translocase of mitochondria.* J Biol Chem. **245**(6): p. 1319-26.

128. Kemp, A., Jr., T.A. Out, H.F. Guiot, and J.H. Souverijn. (1970) *The effect of adenine nucleotides and pH on the inhibition of oxidative phosphorylation by bongkrekic acid.* Biochim Biophys Acta. **223**(2): p. 460-2.

129. Scherer, B. and M. Klingenberg. (1974) *Demonstration of the relationship between the adenine nucleotide carrier and the structural changes of mitochondria as induced by adenosine 5'-diphosphate.* Biochemistry. **13**(1): p. 161-70.

130. Klingenberg, M., K. Grebe, and H.W. Heldt. (1970) *On the inhibition of the adenine nucleotide translocation by bongkrekic acid.* Biochem Biophys Res Commun. **39**(3): p. 344-51.

131. Henderson, P.J., H.A. Lardy, and E. Dorschner. (1970) *Factors affecting the inhibition of adenine nucleotide translocase by bongkrekic acid.* Biochemistry. **9**(17): p. 3453-7.

132. Halestrap, A.P. and C. Brenner. (2003) *The adenine nucleotide translocase: a central component of the mitochondrial permeability transition pore and key player in cell death.* Curr Med Chem. **10**(16): p. 1507-25.

133. Novgorodov, S.A., T.I. Gudz, Y.E. Kushnareva, O. Eriksson, and Y.N. Leikin. (1991) *Effects of the membrane potential upon the Ca(2+)- and cumene hydroperoxide-induced permeabilization of the inner mitochondrial membrane.* FEBS Lett. **295**(1-3): p. 77-80.

134. Woldegiorgis, G., E. Shrago, J. Gipp, and M. Yatvin. (1981) *Fatty acyl coenzyme A-sensitive adenine nucleotide transport in a reconstituted liposome system.* J Biol Chem. **256**(23): p. 12297-300.

135. Furuno, T., T. Kanno, K. Arita, M. Asami, T. Utsumi, Y. Doi, M. Inoue, and K. Utsumi. (2001) *Roles of long chain fatty acids and carnitine in mitochondrial membrane permeability transition.* Biochem Pharmacol. **62**(8): p. 1037-46.

136. Lauquin, G.J., A.M. Duplaa, G. Klein, A. Rousseau, and P.V. Vignais. (1976) *Isobongkrekic acid, a new inhibitor of mitochondrial ADP-ATP transport: radioactive labeling and chemical and biological properties.* Biochemistry. **15**(11): p. 2323-7.

137. Fiore, C., V. Trezeguet, A. Le Saux, P. Roux, C. Schwimmer, A.C. Dianoux, F. Noel, G.J. Lauquin, G. Brandolin, and P.V. Vignais. (1998) *The mitochondrial ADP/ATP carrier: structural, physiological and pathological aspects.* Biochimie. **80**(2): p. 137-50.

138. Haworth, R.A. and D.R. Hunter. (2000) *Control of the mitochondrial permeability transition pore by high-affinity ADP binding at the ADP/ATP translocase in permeabilized mitochondria.* J Bioenerg Biomembr. **32**(1): p. 91-6.

139. Powers, M.F., L.L. Smith, and A.D. Beavis. (1994) *On the relationship between the mitochondrial inner membrane anion channel and the adenine nucleotide translocase.* J Biol Chem. **269**(14): p. 10614-20.

140. Szabo, I. and M. Zoratti. (1991) *The giant channel of the inner mitochondrial membrane is inhibited by cyclosporin A.* J Biol Chem. **266**(6): p. 3376-9.

141. Petronilli, V., I. Szabo, and M. Zoratti. (1989) *The inner mitochondrial membrane contains ion-conducting channels similar to those found in bacteria.* FEBS Lett. **259**(1): p. 137-43.

142. Brustovetsky, N. and M. Klingenberg. (1996) *Mitochondrial ADP/ATP carrier can be reversibly converted into a large channel by Ca2+.* Biochemistry. **35**(26): p. 8483-8.

143. Brustovetsky, N., M. Tropschug, S. Heimpel, D. Heidkamper, and M. Klingenberg. (2002) *A large Ca2+-dependent channel formed by recombinant ADP/ATP carrier from Neurospora crassa resembles the mitochondrial permeability transition pore.* Biochemistry. **41**(39): p. 11804-11.

144. Kokoszka, J.E., K.G. Waymire, S.E. Levy, J.E. Sligh, J. Cai, D.P. Jones, G.R. MacGregor, and D.C. Wallace. (2004) *The ADP/ATP translocator is not essential for the mitochondrial permeability transition pore.* Nature. **427**(6973): p. 461-5.

145. Griffiths, E.J. and A.P. Halestrap. (1991) *Further evidence that cyclosporin A protects mitochondria from calcium overload by inhibiting a matrix peptidyl-prolyl cis-trans isomerase. Implications for the immunosuppressive and toxic effects of cyclosporin.* Biochem J. **274 (Pt 2)**: p. 611-4.

146. Halestrap, A.P. and A.M. Davidson. (1990) *Inhibition of Ca2(+)-induced large-amplitude swelling of liver and heart mitochondria by cyclosporin is probably caused by the inhibitor binding to mitochondrial-matrix peptidyl-prolyl cis-trans isomerase and preventing it interacting with the adenine nucleotide translocase.* Biochem J. **268**(1): p. 153-60.

147. Luvisetto, S., E. Basso, V. Petronilli, P. Bernardi, and M. Forte. (2008) *Enhancement of anxiety, facilitation of avoidance behavior, and occurrence of adult-onset obesity in mice lacking mitochondrial cyclophilin D.* Neuroscience. **155**(3): p. 585-96.

148. Elrod, J.W., R. Wong, S. Mishra, R.J. Vagnozzi, B. Sakthievel, S.A. Goonasekera, J. Karch, S. Gabel, J. Farber, T. Force, J.H. Brown, E. Murphy, and J.D. Molkentin. (2010) *Cyclophilin D controls mitochondrial pore-dependent Ca(2+) exchange, metabolic flexibility, and propensity for heart failure in mice.* J Clin Invest. **120**(10): p. 3680-7.

149. Giorgio, V., E. Bisetto, M.E. Soriano, F. Dabbeni-Sala, E. Basso, V. Petronilli, M.A. Forte, P. Bernardi, and G. Lippe. (2009) *Cyclophilin D modulates mitochondrial F0F1-ATP synthase by interacting with the lateral stalk of the complex.* J Biol Chem. **284**(49): p. 33982-8.

150. Chinopoulos, C. and V. Adam-Vizi. (2012) *Modulation of the mitochondrial permeability transition by cyclophilin D: moving closer to F(0)-F(1) ATP synthase?* Mitochondrion. **12**(1): p. 41-5.

151. Chinopoulos, C., C. Konrad, G. Kiss, E. Metelkin, B. Torocsik, S.F. Zhang, and A.A. Starkov. (2011) *Modulation of F0F1-ATP synthase activity by cyclophilin D regulates matrix adenine nucleotide levels.* Febs J. **278**(7): p. 1112-25.

152. Szabo, I. and M. Zoratti. (1993) *The mitochondrial permeability transition pore may comprise VDAC molecules. I. Binary structure and voltage dependence of the pore.* FEBS Lett. **330**(2): p. 201-5.

153. Szabo, I., V. De Pinto, and M. Zoratti. (1993) *The mitochondrial permeability transition pore may comprise VDAC molecules. II. The electrophysiological properties of VDAC are compatible with those of the mitochondrial megachannel.* FEBS Lett. **330**(2): p. 206-10.

154. Crompton, M., S. Virji, and J.M. Ward. (1998) *Cyclophilin-D binds strongly to complexes of the voltage-dependent anion channel and the adenine nucleotide translocase to form the permeability transition pore.* Eur J Biochem. **258**(2): p. 729-35.

155. Sampson, M.J., W.K. Decker, A.L. Beaudet, W. Ruitenbeek, D. Armstrong, M.J. Hicks, and W.J. Craigen. (2001) *Immotile sperm and infertility in mice lacking mitochondrial voltage-dependent anion channel type 3.* J Biol Chem. **276**(42): p. 39206-12.

156. Anflous, K., D.D. Armstrong, and W.J. Craigen. (2001) *Altered mitochondrial sensitivity for ADP and maintenance of creatine-stimulated respiration in oxidative striated muscles from VDAC1-deficient mice.* J Biol Chem. **276**(3): p. 1954-60.

157. Weeber, E.J., M. Levy, M.J. Sampson, K. Anflous, D.L. Armstrong, S.E. Brown, J.D. Sweatt, and W.J. Craigen. (2002) *The role of mitochondrial porins and the permeability transition pore in learning and synaptic plasticity.* J Biol Chem. **277**(21): p. 18891-7.

158. Cheng, E.H., T.V. Sheiko, J.K. Fisher, W.J. Craigen, and S.J. Korsmeyer. (2003) *VDAC2 inhibits BAK activation and mitochondrial apoptosis.* Science. **301**(5632): p. 513-7.

159. Baines, C.P., R.A. Kaiser, T. Sheiko, W.J. Craigen, and J.D. Molkentin. (2007) *Voltage-dependent anion channels are dispensable for mitochondrial-dependent cell death.* Nat Cell Biol. **9**(5): p. 550-5.

160. Anholt, R.R., P.L. Pedersen, E.B. De Souza, and S.H. Snyder. (1986) *The peripheral-type benzodiazepine receptor. Localization to the mitochondrial outer membrane.* J Biol Chem. **261**(2): p. 576-83.

161. Papadopoulos, V., H. Amri, N. Boujrad, C. Cascio, M. Culty, M. Garnier, M. Hardwick, H. Li, B. Vidic, A.S. Brown, J.L. Reversa, J.M. Bernassau, and K. Drieu. (1997) *Peripheral benzodiazepine receptor in cholesterol transport and steroidogenesis.* Steroids. **62**(1): p. 21-8.

162. Pastorino, J.G., G. Simbula, E. Gilfor, J.B. Hoek, and J.L. Farber. (1994) *Protoporphyrin IX, an endogenous ligand of the peripheral benzodiazepine receptor, potentiates induction of the*

mitochondrial permeability transition and the killing of cultured hepatocytes by rotenone. J Biol Chem. **269**(49): p. 31041-6.

163. Verma, A. and S.H. Snyder. (1988) *Characterization of porphyrin interactions with peripheral type benzodiazepine receptors.* Mol Pharmacol. **34**(6): p. 800-5.

164. Verma, A., J.S. Nye, and S.H. Snyder. (1987) *Porphyrins are endogenous ligands for the mitochondrial (peripheral-type) benzodiazepine receptor.* Proc Natl Acad Sci U S A. **84**(8): p. 2256-60.

165. Hirsch, T., D. Decaudin, S.A. Susin, P. Marchetti, N. Larochette, M. Resche-Rigon, and G. Kroemer. (1998) *PK11195, a ligand of the mitochondrial benzodiazepine receptor, facilitates the induction of apoptosis and reverses Bcl-2-mediated cytoprotection.* Exp Cell Res. **241**(2): p. 426-34.

166. Le Fur, G., M.L. Perrier, N. Vaucher, F. Imbault, A. Flamier, J. Benavides, A. Uzan, C. Renault, M.C. Dubroeucq, and C. Gueremy. (1983) *Peripheral benzodiazepine binding sites: effect of PK 11195, 1-(2-chlorophenyl)-N-methyl-N-(1-methylpropyl)-3-isoquinolinecarboxamide. I. In vitro studies.* Life Sci. **32**(16): p. 1839-47.

167. Ricchelli, F., J. Sileikyte, and P. Bernardi. (2011) *Shedding light on the mitochondrial permeability transition.* Biochim Biophys Acta. **1807**(5): p. 482-90.

168. Sileikyte, J., V. Petronilli, A. Zulian, F. Dabbeni-Sala, G. Tognon, P. Nikolov, P. Bernardi, and F. Ricchelli. (2011) *Regulation of the inner membrane mitochondrial permeability transition by the outer membrane translocator protein (peripheral benzodiazepine receptor).* J Biol Chem. **286**(2): p. 1046-53.

169. McGeoch, J.E., M.W. McGeoch, R. Mao, and G. Guidotti. (2000) *Opposing actions of cGMP and calcium on the conductance of the F(0) subunit c pore.* Biochem Biophys Res Commun. **274**(3): p. 835-40.

170. Bonora, M., A. Bononi, E. De Marchi, C. Giorgi, M. Lebiedzinska, S. Marchi, S. Patergnani, A. Rimessi, J.M. Suski, A. Wojtala, M.R. Wieckowski, G. Kroemer, L. Galluzzi, and P. Pinton. (2013) *Role of the c subunit of the FO ATP synthase in mitochondrial permeability transition.* Cell Cycle. **12**(4): p. 674-83.

171. Giorgio, V., S. von Stockum, M. Antoniel, A. Fabbro, F. Fogolari, M. Forte, G.D. Glick, V. Petronilli, M. Zoratti, I. Szabo, G. Lippe, and P. Bernardi. (2013) *Dimers of mitochondrial*

ATP synthase form the permeability transition pore. Proc Natl Acad Sci U S A. **110**(15): p. 5887-92.

172. Bernardi, P. (2013) *The mitochondrial permeability transition pore: a mystery solved?* Front Physiol. **4**: p. 95.

173. Szabadkai, G. and C. Chinopoulos. (2013) *What Makes You Can Also Break You, Part II: Mitochondrial Permeability Transition Pore Formation by Dimers of the F1FO ATP-Synthase?* Front Oncol. **3**: p. 140.

174. Chinopoulos, C. and G. Szabadkai. (2013) *What makes you can also break you: mitochondrial permeability transition pore formation by the c subunit of the F(1)F(0) ATP-synthase?* Front Oncol. **3**: p. 25.

175. Azzolin, L., S. von Stockum, E. Basso, V. Petronilli, M.A. Forte, and P. Bernardi. (2010) *The mitochondrial permeability transition from yeast to mammals.* FEBS Lett. **584**(12): p. 2504-9.

176. Bernardi, P. and S. von Stockum. (2012) *The permeability transition pore as a Ca(2+) release channel: new answers to an old question.* Cell Calcium. **52**(1): p. 22-7.

177. Huser, J. and L.A. Blatter. (1999) *Fluctuations in mitochondrial membrane potential caused by repetitive gating of the permeability transition pore.* Biochem J. **343 Pt 2**: p. 311-7.

178. Petronilli, V., G. Miotto, M. Canton, M. Brini, R. Colonna, P. Bernardi, and F. Di Lisa. (1999) *Transient and long-lasting openings of the mitochondrial permeability transition pore can be monitored directly in intact cells by changes in mitochondrial calcein fluorescence.* Biophys J. **76**(2): p. 725-34.

179. Altschuld, R.A., C.M. Hohl, L.C. Castillo, A.A. Garleb, R.C. Starling, and G.P. Brierley. (1992) *Cyclosporin inhibits mitochondrial calcium efflux in isolated adult rat ventricular cardiomyocytes.* Am J Physiol. **262**(6 Pt 2): p. H1699-704.

180. Koulintchenko, M., Y. Konstantinov, and A. Dietrich. (2003) *Plant mitochondria actively import DNA via the permeability transition pore complex.* Embo J. **22**(6): p. 1245-54.

181. Gibson, G.E., A. Starkov, J.P. Blass, R.R. Ratan, and M.F. Beal. (2010) *Cause and consequence: mitochondrial dysfunction initiates and propagates neuronal dysfunction, neuronal death and behavioral abnormalities in age-associated neurodegenerative diseases.* Biochim Biophys Acta. **1802**(1): p. 122-34.

182. Johri, A. and M.F. Beal. (2012) *Mitochondrial dysfunction in neurodegenerative diseases.* J Pharmacol Exp Ther. **342**(3): p. 619-30.

183. Petrasch-Parwez, E., H.P. Nguyen, M. Lobbecke-Schumacher, H.W. Habbes, S. Wieczorek, O. Riess, K.H. Andres, R. Dermietzel, and S. Von Horsten. (2007) *Cellular and subcellular localization of Huntingtin [corrected] aggregates in the brain of a rat transgenic for Huntington disease.* The Journal of comparative neurology. **501**(5): p. 716-30.

184. Panov, A.V., C.A. Gutekunst, B.R. Leavitt, M.R. Hayden, J.R. Burke, W.J. Strittmatter, and J.T. Greenamyre. (2002) *Early mitochondrial calcium defects in Huntington's disease are a direct effect of polyglutamines.* Nature neuroscience. **5**(8): p. 731-6.

185. Orr, A.L., S. Li, C.E. Wang, H. Li, J. Wang, J. Rong, X. Xu, P.G. Mastroberardino, J.T. Greenamyre, and X.J. Li. (2008) *N-terminal mutant huntingtin associates with mitochondria and impairs mitochondrial trafficking.* The Journal of neuroscience : the official journal of the Society for Neuroscience. **28**(11): p. 2783-92.

186. Choo, Y.S., G.V. Johnson, M. MacDonald, P.J. Detloff, and M. Lesort. (2004) *Mutant huntingtin directly increases susceptibility of mitochondria to the calcium-induced permeability transition and cytochrome c release.* Human molecular genetics. **13**(14): p. 1407-20.

187. Oliveira, J.M., M.B. Jekabsons, S. Chen, A. Lin, A.C. Rego, J. Goncalves, L.M. Ellerby, and D.G. Nicholls. (2007) *Mitochondrial dysfunction in Huntington's disease: the bioenergetics of isolated and in situ mitochondria from transgenic mice.* Journal of neurochemistry. **101**(1): p. 241-9.

188. Oliveira, J.M., S. Chen, S. Almeida, R. Riley, J. Goncalves, C.R. Oliveira, M.R. Hayden, D.G. Nicholls, L.M. Ellerby, and A.C. Rego. (2006) *Mitochondrial-dependent Ca2+ handling in Huntington's disease striatal cells: effect of histone deacetylase inhibitors.* The Journal of neuroscience : the official journal of the Society for Neuroscience. **26**(43): p. 11174-86.

189. Lim, D., L. Fedrizzi, M. Tartari, C. Zuccato, E. Cattaneo, M. Brini, and E. Carafoli. (2008) *Calcium homeostasis and mitochondrial dysfunction in striatal neurons of Huntington disease.* The Journal of biological chemistry. **283**(9): p. 5780-9.

190. Cui, L., H. Jeong, F. Borovecki, C.N. Parkhurst, N. Tanese, and D. Krainc. (2006) *Transcriptional repression of PGC-1alpha by mutant huntingtin leads to mitochondrial dysfunction and neurodegeneration.* Cell. **127**(1): p. 59-69.

191. Thomas, B. and M.F. Beal. (2007) *Parkinson's disease.* Human molecular genetics. **16 Spec No. 2**: p. R183-94.

192. Liu, W., C. Vives-Bauza, R. Acin-Perez, A. Yamamoto, Y. Tan, Y. Li, J. Magrane, M.A. Stavarache, S. Shaffer, S. Chang, M.G. Kaplitt, X.Y. Huang, M.F. Beal, G. Manfredi, and C. Li. (2009) *PINK1 defect causes mitochondrial dysfunction, proteasomal deficit and alpha-synuclein aggregation in cell culture models of Parkinson's disease.* PLoS One. **4**(2): p. e4597.

193. Wang, H.L., A.H. Chou, T.H. Yeh, A.H. Li, Y.L. Chen, Y.L. Kuo, S.R. Tsai, and S.T. Yu. (2007) *PINK1 mutants associated with recessive Parkinson's disease are defective in inhibiting mitochondrial release of cytochrome c.* Neurobiology of disease. **28**(2): p. 216-26.

194. Wang, H.L., A.H. Chou, A.S. Wu, S.Y. Chen, Y.H. Weng, Y.C. Kao, T.H. Yeh, P.J. Chu, and C.S. Lu. (2011) *PARK6 PINK1 mutants are defective in maintaining mitochondrial membrane potential and inhibiting ROS formation of substantia nigra dopaminergic neurons.* Biochimica et biophysica acta. **1812**(6): p. 674-84.

195. Choubey, V., D. Safiulina, A. Vaarmann, M. Cagalinec, P. Wareski, M. Kuum, A. Zharkovsky, and A. Kaasik. (2011) *Mutant A53T alpha-synuclein induces neuronal death by increasing mitochondrial autophagy.* The Journal of biological chemistry. **286**(12): p. 10814-24.

196. Song, D.D., C.W. Shults, A. Sisk, E. Rockenstein, and E. Masliah. (2004) *Enhanced substantia nigra mitochondrial pathology in human alpha-synuclein transgenic mice after treatment with MPTP.* Experimental neurology. **186**(2): p. 158-72.

197. Hsu, L.J., Y. Sagara, A. Arroyo, E. Rockenstein, A. Sisk, M. Mallory, J. Wong, T. Takenouchi, M. Hashimoto, and E. Masliah. (2000) *alpha-synuclein promotes mitochondrial deficit and oxidative stress.* The American journal of pathology. **157**(2): p. 401-10.

198. Alobuia, W.M., W. Xia, and B.P. Vohra. (2013) *Axon degeneration is key component of neuronal death in amyloid - beta toxicity.* Neurochemistry international.

199. Du, H., L. Guo, S. Yan, A.A. Sosunov, G.M. McKhann, and S.S. Yan. (2010) *Early deficits in synaptic mitochondria in an Alzheimer's disease mouse model.* Proceedings of the National Academy of Sciences of the United States of America. **107**(43): p. 18670-5.

200. Pooler, A.M., W. Noble, and D.P. Hanger. (2013) *A role for tau at the synapse in Alzheimer's disease pathogenesis.* Neuropharmacology.

201. Wirz, K.T., S. Keitel, D.F. Swaab, J. Verhaagen, and K. Bossers. (2013) *Early Molecular Changes in Alzheimer's Disease: Can We Catch the Disease in its Presymptomatic Phase?* Journal of Alzheimer's disease : JAD.

202. Johri, A. and M.F. Beal. (2012) *Mitochondrial dysfunction in neurodegenerative diseases.* The Journal of pharmacology and experimental therapeutics. **342**(3): p. 619-30.

203. Dumont, M. and M.F. Beal. (2011) *Neuroprotective strategies involving ROS in Alzheimer disease.* Free radical biology & medicine. **51**(5): p. 1014-26.

204. Chaturvedi, R.K. and M.F. Beal. (2008) *Mitochondrial approaches for neuroprotection.* Annals of the New York Academy of Sciences. **1147**: p. 395-412.

205. Guo, L., H. Du, S. Yan, X. Wu, G.M. McKhann, J.X. Chen, and S.S. Yan. (2013) *Cyclophilin D deficiency rescues axonal mitochondrial transport in Alzheimer's neurons.* PloS one. **8**(1): p. e54914.

206. Hervias, I., M.F. Beal, and G. Manfredi. (2006) *Mitochondrial dysfunction and amyotrophic lateral sclerosis.* Muscle & nerve. **33**(5): p. 598-608.

207. Wiedemann, F.R., K. Winkler, A.V. Kuznetsov, C. Bartels, S. Vielhaber, H. Feistner, and W.S. Kunz. (1998) *Impairment of mitochondrial function in skeletal muscle of patients with amyotrophic lateral sclerosis.* Journal of the neurological sciences. **156**(1): p. 65-72.

208. Wiedemann, F.R., G. Manfredi, C. Mawrin, M.F. Beal, and E.A. Schon. (2002) *Mitochondrial DNA and respiratory chain function in spinal cords of ALS patients.* Journal of neurochemistry. **80**(4): p. 616-25.

209. Vielhaber, S., D. Kunz, K. Winkler, F.R. Wiedemann, E. Kirches, H. Feistner, H.J. Heinze, C.E. Elger, W. Schubert, and W.S. Kunz. (2000) *Mitochondrial DNA abnormalities in skeletal muscle of patients with sporadic amyotrophic lateral sclerosis.* Brain : a journal of neurology. **123 (Pt 7)**: p. 1339-48.

210. Borthwick, G.M., M.A. Johnson, P.G. Ince, P.J. Shaw, and D.M. Turnbull. (1999) *Mitochondrial enzyme activity in amyotrophic lateral sclerosis: implications for the role of mitochondria in neuronal cell death.* Annals of neurology. **46**(5): p. 787-90.

211. Byrne, S., C. Walsh, C. Lynch, P. Bede, M. Elamin, K. Kenna, R. McLaughlin, and O. Hardiman. (2011) *Rate of familial amyotrophic lateral sclerosis: a systematic review and meta-analysis.* Journal of neurology, neurosurgery, and psychiatry. **82**(6): p. 623-7.

212. Andersen, P.M. and A. Al-Chalabi. (2011) *Clinical genetics of amyotrophic lateral sclerosis: what do we really know?* Nature reviews. Neurology. **7**(11): p. 603-15.

213. Cozzolino, M., A. Ferri, C. Valle, and M.T. Carri. (2013) *Mitochondria and ALS: implications from novel genes and pathways.* Molecular and cellular neurosciences. **55**: p. 44-9.

214. Rosen, D.R., T. Siddique, D. Patterson, D.A. Figlewicz, P. Sapp, A. Hentati, D. Donaldson, J. Goto, J.P. O'Regan, H.X. Deng, and et al. (1993) *Mutations in Cu/Zn superoxide dismutase gene are associated with familial amyotrophic lateral sclerosis.* Nature. **362**(6415): p. 59-62.

215. Andersen, P.M., P. Nilsson, V. Ala-Hurula, M.L. Keranen, I. Tarvainen, T. Haltia, L. Nilsson, M. Binzer, L. Forsgren, and S.L. Marklund. (1995) *Amyotrophic lateral sclerosis associated with homozygosity for an Asp90Ala mutation in CuZn-superoxide dismutase.* Nature genetics. **10**(1): p. 61-6.

216. Reaume, A.G., J.L. Elliott, E.K. Hoffman, N.W. Kowall, R.J. Ferrante, D.F. Siwek, H.M. Wilcox, D.G. Flood, M.F. Beal, R.H. Brown, Jr., R.W. Scott, and W.D. Snider. (1996) *Motor neurons in Cu/Zn superoxide dismutase-deficient mice develop normally but exhibit enhanced cell death after axonal injury.* Nature genetics. **13**(1): p. 43-7.

217. Vijayvergiya, C., M.F. Beal, J. Buck, and G. Manfredi. (2005) *Mutant superoxide dismutase 1 forms aggregates in the brain mitochondrial matrix of amyotrophic lateral sclerosis mice.* The Journal of neuroscience : the official journal of the Society for Neuroscience. **25**(10): p. 2463-70.

218. Vande Velde, C., T.M. Miller, N.R. Cashman, and D.W. Cleveland. (2008) *Selective association of misfolded ALS-linked mutant SOD1 with the cytoplasmic face of mitochondria.* Proceedings of the National Academy of Sciences of the United States of America. **105**(10): p. 4022-7.

219. Pasinelli, P., M.E. Belford, N. Lennon, B.J. Bacskai, B.T. Hyman, D. Trotti, and R.H. Brown, Jr. (2004) *Amyotrophic lateral sclerosis-associated SOD1 mutant proteins bind and aggregate with Bcl-2 in spinal cord mitochondria.* Neuron. **43**(1): p. 19-30.

220. Liu, J., C. Lillo, P.A. Jonsson, C. Vande Velde, C.M. Ward, T.M. Miller, J.R. Subramaniam, J.D. Rothstein, S. Marklund, P.M. Andersen, T. Brannstrom, O. Gredal, P.C. Wong, D.S. Williams, and D.W. Cleveland. (2004) *Toxicity of familial ALS-linked SOD1 mutants from selective recruitment to spinal mitochondria.* Neuron. **43**(1): p. 5-17.

221. Jaarsma, D., F. Rognoni, W. van Duijn, H.W. Verspaget, E.D. Haasdijk, and J.C. Holstege. (2001) *CuZn superoxide dismutase (SOD1) accumulates in vacuolated mitochondria in transgenic mice expressing amyotrophic lateral sclerosis-linked SOD1 mutations.* Acta neuropathologica. **102**(4): p. 293-305.

222. Israelson, A., N. Arbel, S. Da Cruz, H. Ilieva, K. Yamanaka, V. Shoshan-Barmatz, and D.W. Cleveland. (2010) *Misfolded mutant SOD1 directly inhibits VDAC1 conductance in a mouse model of inherited ALS.* Neuron. **67**(4): p. 575-87.

223. Higgins, C.M., C. Jung, H. Ding, and Z. Xu. (2002) *Mutant Cu, Zn superoxide dismutase that causes motoneuron degeneration is present in mitochondria in the CNS.* The Journal of neuroscience : the official journal of the Society for Neuroscience. **22**(6): p. RC215.

224. Ferri, A., M. Cozzolino, C. Crosio, M. Nencini, A. Casciati, E.B. Gralla, G. Rotilio, J.S. Valentine, and M.T. Carri. (2006) *Familial ALS-superoxide dismutases associate with mitochondria and shift their redox potentials.* Proceedings of the National Academy of Sciences of the United States of America. **103**(37): p. 13860-5.

225. Deng, H.X., Y. Shi, Y. Furukawa, H. Zhai, R. Fu, E. Liu, G.H. Gorrie, M.S. Khan, W.Y. Hung, E.H. Bigio, T. Lukas, M.C. Dal Canto, T.V. O'Halloran, and T. Siddique. (2006) *Conversion to the amyotrophic lateral sclerosis phenotype is associated with intermolecular linked insoluble aggregates of SOD1 in mitochondria.* Proceedings of the National Academy of Sciences of the United States of America. **103**(18): p. 7142-7.

226. Bergemalm, D., P.A. Jonsson, K.S. Graffmo, P.M. Andersen, T. Brannstrom, A. Rehnmark, and S.L. Marklund. (2006) *Overloading of stable and exclusion of unstable human superoxide dismutase-1 variants in mitochondria of murine amyotrophic lateral sclerosis*

models. The Journal of neuroscience : the official journal of the Society for Neuroscience. **26**(16): p. 4147-54.

227. Wong, P.C., C.A. Pardo, D.R. Borchelt, M.K. Lee, N.G. Copeland, N.A. Jenkins, S.S. Sisodia, D.W. Cleveland, and D.L. Price. (1995) *An adverse property of a familial ALS-linked SOD1 mutation causes motor neuron disease characterized by vacuolar degeneration of mitochondria.* Neuron. **14**(6): p. 1105-16.

228. Dal Canto, M.C. and M.E. Gurney. (1994) *Development of central nervous system pathology in a murine transgenic model of human amyotrophic lateral sclerosis.* The American journal of pathology. **145**(6): p. 1271-9.

229. Dal Canto, M.C. (1995) *Comparison of pathological alterations in ALS and a murine transgenic model: pathogenetic implications.* Clinical neuroscience. **3**(6): p. 332-7.

230. Carri, M.T., A. Ferri, A. Battistoni, L. Famhy, R. Gabbianelli, F. Poccia, and G. Rotilio. (1997) *Expression of a Cu,Zn superoxide dismutase typical of familial amyotrophic lateral sclerosis induces mitochondrial alteration and increase of cytosolic Ca2+ concentration in transfected neuroblastoma SH-SY5Y cells.* FEBS letters. **414**(2): p. 365-8.

231. Chinopoulos, C. (2011) *Mitochondrial consumption of cytosolic ATP: not so fast.* FEBS Lett. **585**(9): p. 1255-9.

232. Rona, G., M. Boutet, and I. Huttner. (1983) *Reperfusion injury. A possible link between catecholamine-induced and ischemic myocardial alterations.* Advances in myocardiology. **4**: p. 427-39.

233. Griffiths, E.J. and A.P. Halestrap. (1995) *Mitochondrial non-specific pores remain closed during cardiac ischaemia, but open upon reperfusion.* Biochem J. **307 (Pt 1)**: p. 93-8.

234. Fiskum, G. (1983) *Involvement of mitochondria in ischemic cell injury and in regulation of intracellular calcium.* The American journal of emergency medicine. **1**(2): p. 147-53.

235. Schaper, J., F. Schwarz, H. Kittstein, G. Stammler, B. Winkler, H. Scheld, and F. Hehrlein. (1982) *The effects of global ischemia and reperfusion on human myocardium: quantitative evaluation by electron microscopic morphometry.* The Annals of thoracic surgery. **33**(2): p. 116-22.

236. Jenkins, L.W., J.T. Povlishock, W. Lewelt, J.D. Miller, and D.P. Becker. (1981) *The role of postischemic recirculation in the development of ischemic neuronal injury following complete cerebral ischemia.* Acta neuropathologica. **55**(3): p. 205-20.

237. Lindenau, K.F., J. Bohm, H. Warnke, H. David, K. Sajkiewicz, A. Hecht, and D. Berisch. (1978) *[Reperfusion of the myocardium after acute ischemic lesion].* Zeitschrift fur experimentelle Chirurgie. **11**(5): p. 303-11.

238. Bond, J.M., E. Chacon, B. Herman, and J.J. Lemasters. (1993) *Intracellular pH and Ca2+ homeostasis in the pH paradox of reperfusion injury to neonatal rat cardiac myocytes.* Am J Physiol. **265**(1 Pt 1): p. C129-37.

239. Bond, J.M., B. Herman, and J.J. Lemasters. (1991) *Protection by acidotic pH against anoxia/reoxygenation injury to rat neonatal cardiac myocytes.* Biochem Biophys Res Commun. **179**(2): p. 798-803.

240. Argaud, L., O. Gateau-Roesch, O. Raisky, J. Loufouat, D. Robert, and M. Ovize. (2005) *Postconditioning inhibits mitochondrial permeability transition.* Circulation. **111**(2): p. 194-7.

241. Javadov, S.A., S. Clarke, M. Das, E.J. Griffiths, K.H. Lim, and A.P. Halestrap. (2003) *Ischaemic preconditioning inhibits opening of mitochondrial permeability transition pores in the reperfused rat heart.* J Physiol. **549**(Pt 2): p. 513-24.

242. Matsumoto, S., H. Friberg, M. Ferrand-Drake, and T. Wieloch. (1999) *Blockade of the mitochondrial permeability transition pore diminishes infarct size in the rat after transient middle cerebral artery occlusion.* Journal of cerebral blood flow and metabolism : official journal of the International Society of Cerebral Blood Flow and Metabolism. **19**(7): p. 736-41.

243. Nakai, A., Y. Shibazaki, Y. Taniuchi, H. Miyake, A. Oya, and T. Takeshita. (2004) *Role of mitochondrial permeability transition in fetal brain damage in rats.* Pediatric neurology. **30**(4): p. 247-53.

244. Uchino, H., E. Elmer, K. Uchino, P.A. Li, Q.P. He, M.L. Smith, and B.K. Siesjo. (1998) *Amelioration by cyclosporin A of brain damage in transient forebrain ischemia in the rat.* Brain research. **812**(1-2): p. 216-26.

245. Yoshimoto, T. and B.K. Siesjo. (1999) *Posttreatment with the immunosuppressant cyclosporin A in transient focal ischemia.* Brain research. **839**(2): p. 283-91.

246. Hausenloy, D.J., S.Y. Lim, S.G. Ong, S.M. Davidson, and D.M. Yellon. (2010) *Mitochondrial cyclophilin-D as a critical mediator of ischaemic preconditioning.* Cardiovasc Res. **88**(1): p. 67-74.

247. Li, P.A., H. Uchino, E. Elmer, and B.K. Siesjo. (1997) *Amelioration by cyclosporin A of brain damage following 5 or 10 min of ischemia in rats subjected to preischemic hyperglycemia.* Brain Res. **753**(1): p. 133-40.

248. Folbergrova, J., P.A. Li, H. Uchino, M.L. Smith, and B.K. Siesjo. (1997) *Changes in the bioenergetic state of rat hippocampus during 2.5 min of ischemia, and prevention of cell damage by cyclosporin A in hyperglycemic subjects.* Exp Brain Res. **114**(1): p. 44-50.

249. Ferrand-Drake, M., H. Friberg, and T. Wieloch. (1999) *Mitochondrial permeability transition induced DNA-fragmentation in the rat hippocampus following hypoglycemia.* Neuroscience. **90**(4): p. 1325-38.

250. Friberg, H., M. Ferrand-Drake, F. Bengtsson, A.P. Halestrap, and T. Wieloch. (1998) *Cyclosporin A, but not FK 506, protects mitochondria and neurons against hypoglycemic damage and implicates the mitochondrial permeability transition in cell death.* J Neurosci. **18**(14): p. 5151-9.

251. Sullivan, P.G., M. Thompson, and S.W. Scheff. (2000) *Continuous infusion of cyclosporin A postinjury significantly ameliorates cortical damage following traumatic brain injury.* Exp Neurol. **161**(2): p. 631-7.

252. Scheff, S.W. and P.G. Sullivan. (1999) *Cyclosporin A significantly ameliorates cortical damage following experimental traumatic brain injury in rodents.* J Neurotrauma. **16**(9): p. 783-92.

253. Okonkwo, D.O. and J.T. Povlishock. (1999) *An intrathecal bolus of cyclosporin A before injury preserves mitochondrial integrity and attenuates axonal disruption in traumatic brain injury.* J Cereb Blood Flow Metab. **19**(4): p. 443-51.

254. Okonkwo, D.O., A. Buki, R. Siman, and J.T. Povlishock. (1999) *Cyclosporin A limits calcium-induced axonal damage following traumatic brain injury.* Neuroreport. **10**(2): p. 353-8.

255. Alessandri, B., A.C. Rice, J. Levasseur, M. DeFord, R.J. Hamm, and M.R. Bullock. (2002) *Cyclosporin A improves brain tissue oxygen consumption and learning/memory performance after lateral fluid percussion injury in rats.* J Neurotrauma. **19**(7): p. 829-41.

256. Vanderluit, J.L., L.T. McPhail, K.J. Fernandes, N.R. Kobayashi, and W. Tetzlaff. (2003) *In vivo application of mitochondrial pore inhibitors blocks the induction of apoptosis in axotomized neonatal facial motoneurons.* Cell Death Differ. **10**(9): p. 969-76.

257. Fox, D.A., A.T. Poblenz, L. He, J.B. Harris, and C.J. Medrano. (2003) *Pharmacological strategies to block rod photoreceptor apoptosis caused by calcium overload: a mechanistic target-site approach to neuroprotection.* Eur J Ophthalmol. **13 Suppl 3**: p. S44-56.

258. Du, Q., X.L. Bian, X.L. Xu, B. Zhu, B. Yu, and Q. Zhai. (2013) *Role of mitochondrial permeability transition in human hepatocellular carcinoma Hep-G2 cell death induced by rhein.* Fitoterapia. **91C**: p. 68-73.

259. Via, L.D., A.N. Garcia-Argaez, M. Martinez-Vazquez, S. Grancara, S. Grancara, P. Martinis, and A. Toninello. (2013) *Mitochondrial Permeability Transition as Target of Anticancer Drugs.* Current pharmaceutical design.

260. Silva-Platas, C., N. Garcia, E. Fernandez-Sada, D. Davila, C. Hernandez-Brenes, D. Rodriguez, and G. Garcia-Rivas. (2012) *Cardiotoxicity of acetogenins from Persea americana occurs through the mitochondrial permeability transition pore and caspase-dependent apoptosis pathways.* Journal of bioenergetics and biomembranes. **44**(4): p. 461-71.

261. Cardoso, S., R.X. Santos, C. Carvalho, S. Correia, G.C. Pereira, S.S. Pereira, P.J. Oliveira, M.S. Santos, T. Proenca, and P.I. Moreira. (2008) *Doxorubicin increases the susceptibility of brain mitochondria to Ca(2+)-induced permeability transition and oxidative damage.* Free radical biology & medicine. **45**(10): p. 1395-402.

262. Montaigne, D., C. Hurt, and R. Neviere. (2012) *Mitochondria death/survival signaling pathways in cardiotoxicity induced by anthracyclines and anticancer-targeted therapies.* Biochemistry research international. **2012**: p. 951539.

263. Gharanei, M., A. Hussain, O. Janneh, and H.L. Maddock. (2013) *Doxorubicin induced myocardial injury is exacerbated following ischaemic stress via opening of the*

mitochondrial permeability transition pore. Toxicology and applied pharmacology. **268**(2): p. 149-56.

264. Montaigne, D., X. Marechal, S. Preau, R. Baccouch, T. Modine, G. Fayad, S. Lancel, and R. Neviere. (2011) *Doxorubicin induces mitochondrial permeability transition and contractile dysfunction in the human myocardium.* Mitochondrion. **11**(1): p. 22-6.

265. Ascensao, A., J. Lumini-Oliveira, N.G. Machado, R.M. Ferreira, I.O. Goncalves, A.C. Moreira, F. Marques, V.A. Sardao, P.J. Oliveira, and J. Magalhaes. (2011) *Acute exercise protects against calcium-induced cardiac mitochondrial permeability transition pore opening in doxorubicin-treated rats.* Clinical science. **120**(1): p. 37-49.

266. Montaigne, D., X. Marechal, R. Baccouch, T. Modine, S. Preau, K. Zannis, P. Marchetti, S. Lancel, and R. Neviere. (2010) *Stabilization of mitochondrial membrane potential prevents doxorubicin-induced cardiotoxicity in isolated rat heart.* Toxicology and applied pharmacology. **244**(3): p. 300-7.

267. Toninello, A., M. Salvi, and L. Colombo. (2000) *The membrane permeability transition in liver mitochondria of the great green goby Zosterisessor ophiocephalus (Pallas).* J Exp Biol. **203**(Pt 22): p. 3425-34.

268. Krumschnabel, G., C. Manzl, C. Berger, and B. Hofer. (2005) *Oxidative stress, mitochondrial permeability transition, and cell death in Cu-exposed trout hepatocytes.* Toxicol Appl Pharmacol. **209**(1): p. 62-73.

269. Savina, M.V., L.V. Emelyanova, and E.A. Belyaeva. (2006) *Bioenergetic parameters of lamprey and frog liver mitochondria during metabolic depression and activity.* Comp Biochem Physiol B Biochem Mol Biol. **145**(3-4): p. 296-305.

270. Hanada, H., K. Katsu, T. Kanno, E.F. Sato, A. Kashiwagi, J. Sasaki, M. Inoue, and K. Utsumi. (2003) *Cyclosporin A inhibits thyroid hormone-induced shortening of the tadpole tail through membrane permeability transition.* Comp Biochem Physiol B Biochem Mol Biol. **135**(3): p. 473-83.

271. von Stockum, S., E. Basso, V. Petronilli, P. Sabatelli, M.A. Forte, and P. Bernardi. (2011) *Properties of Ca(2+) transport in mitochondria of Drosophila melanogaster.* J Biol Chem. **286**(48): p. 41163-70.

272. Manon, S., X. Roucou, M. Guerin, M. Rigoulet, and B. Guerin. (1998) *Characterization of the yeast mitochondria unselective channel: a counterpart to the mammalian permeability transition pore?* J Bioenerg Biomembr. **30**(5): p. 419-29.

273. Vianello, A., F. Macri, E. Braidot, and E.N. Mokhova. (1995) *Effect of cyclosporin A on energy coupling in pea stem mitochondria.* FEBS Lett. **371**(3): p. 258-60.

274. Saviani, E.E., C.H. Orsi, J.F. Oliveira, C.A. Pinto-Maglio, and I. Salgado. (2002) *Participation of the mitochondrial permeability transition pore in nitric oxide-induced plant cell death.* FEBS Lett. **510**(3): p. 136-40.

275. Fortes, F., R.F. Castilho, R. Catisti, E.G. Carnieri, and A.E. Vercesi. (2001) *Ca2+ induces a cyclosporin A-insensitive permeability transition pore in isolated potato tuber mitochondria mediated by reactive oxygen species.* J Bioenerg Biomembr. **33**(1): p. 43-51.

276. Arpagaus, S., A. Rawyler, and R. Braendle. (2002) *Occurrence and characteristics of the mitochondrial permeability transition in plants.* J Biol Chem. **277**(3): p. 1780-7.

277. Virolainen, E., O. Blokhina, and K. Fagerstedt. (2002) *Ca(2+)-induced high amplitude swelling and cytochrome c release from wheat (Triticum aestivum L.) mitochondria under anoxic stress.* Ann Bot. **90**(4): p. 509-16.

278. Tiwari, B.S., B. Belenghi, and A. Levine. (2002) *Oxidative stress increased respiration and generation of reactive oxygen species, resulting in ATP depletion, opening of mitochondrial permeability transition, and programmed cell death.* Plant Physiol. **128**(4): p. 1271-81.

279. Scott, I. and D.C. Logan. (2008) *Mitochondrial morphology transition is an early indicator of subsequent cell death in Arabidopsis.* New Phytol. **177**(1): p. 90-101.

280. Petrussa, E., V. Casolo, C. Peresson, E. Braidot, A. Vianello, and F. Macri. (2004) *The K(ATP)+ channel is involved in a low-amplitude permeability transition in plant mitochondria.* Mitochondrion. **3**(5): p. 297-307.

281. Lin, J., Y. Wang, and G. Wang. (2006) *Salt stress-induced programmed cell death in tobacco protoplasts is mediated by reactive oxygen species and mitochondrial permeability transition pore status.* J Plant Physiol. **163**(7): p. 731-9.

282. Kim, M., J.H. Lim, C.S. Ahn, K. Park, G.T. Kim, W.T. Kim, and H.S. Pai. (2006) *Mitochondria-associated hexokinases play a role in the control of programmed cell death in Nicotiana benthamiana.* Plant Cell. **18**(9): p. 2341-55.

283. Curtis, M.J. and T.J. Wolpert. (2004) *The victorin-induced mitochondrial permeability transition precedes cell shrinkage and biochemical markers of cell death, and shrinkage occurs without loss of membrane integrity.* Plant J. **38**(2): p. 244-59.

284. Curtis, M.J. and T.J. Wolpert. (2002) *The oat mitochondrial permeability transition and its implication in victorin binding and induced cell death.* Plant J. **29**(3): p. 295-312.

285. Yamada, A., T. Yamamoto, Y. Yoshimura, S. Gouda, S. Kawashima, N. Yamazaki, K. Yamashita, M. Kataoka, T. Nagata, H. Terada, D.R. Pfeiffer, and Y. Shinohara. (2009) *Ca2+-induced permeability transition can be observed even in yeast mitochondria under optimized experimental conditions.* Biochim Biophys Acta. **1787**(12): p. 1486-91.

286. Jung, D.W., P.C. Bradshaw, and D.R. Pfeiffer. (1997) *Properties of a cyclosporin-insensitive permeability transition pore in yeast mitochondria.* J Biol Chem. **272**(34): p. 21104-12.

287. Kovaleva, M.V., E.I. Sukhanova, T.A. Trendeleva, M.V. Zyl'kova, L.A. Ural'skaya, K.M. Popova, N.E. Saris, and R.A. Zvyagilskaya. (2009) *Induction of a non-specific permeability transition in mitochondria from Yarrowia lipolytica and Dipodascus (Endomyces) magnusii yeasts.* J Bioenerg Biomembr. **41**(3): p. 239-49.

288. Deryabina, Y.I., E.P. Isakova, E.I. Shurubor, and R.A. Zvyagilskaya. (2004) *Calcium-dependent nonspecific permeability of the inner mitochondrial membrane is not induced in mitochondria of the yeast Endomyces magnusii.* Biochemistry (Mosc). **69**(9): p. 1025-33.

289. Kovaleva, M.V., E.I. Sukhanova, T.A. Trendeleva, K.M. Popova, M.V. Zylkova, L.A. Uralskaya, and R.A. Zvyagilskaya. (2010) *Induction of permeability of the inner membrane of yeast mitochondria.* Biochemistry (Mosc). **75**(3): p. 297-303.

290. Holman, J.D. and S.C. Hand. (2009) *Metabolic Depression is Delayed and Mitochondrial Impairment Averted during Prolonged Anoxia in the ghost shrimp, Lepidophthalmus louisianensis (Schmitt, 1935).* J Exp Mar Bio Ecol. **376**(2): p. 85-93.

291. Menze, M.A., K. Hutchinson, S.M. Laborde, and S.C. Hand. (2005) *Mitochondrial permeability transition in the crustacean Artemia franciscana: absence of a calcium-regulated pore in the face of profound calcium storage.* Am J Physiol Regul Integr Comp Physiol. **289**(1): p. R68-76.

292. Chen, C.H., J.W. Greenawalt, and A.L. Lehninger. (1974) *Biochemical and ultrastructural aspects of Ca2+ transport by mitochondria of the hepatopancreas of the blue crab Callinectes sapidus.* J Cell Biol. **61**(2): p. 301-15.

293. Munday, K.A. and B.D. Thompson. (1962) *The preparation and properties of sub-cellular respiring particles (mitochonria) from the hepatopancreas of Carcinus maenas.* Comp Biochem Physiol. **5**: p. 95-112.

294. Tsokos, J., R. Kreisberg, A. Michaels, B. Komm, and J. Linton. (1983) *Respiratory and calcium transport properties of spiny lobster hepatopancreas mitochondria.* Arch Biochem Biophys. **224**(2): p. 707-17.

295. Belyaeva, E.A., V.V. Glazunov, and S.M. Korotkov. (2002) *Cyclosporin A-sensitive permeability transition pore is involved in Cd(2+)-induced dysfunction of isolated rat liver mitochondria: doubts no more.* Arch Biochem Biophys. **405**(2): p. 252-64.

296. Lei, W., L. Wang, D. Liu, T. Xu, and J. Luo. (2011) *Histopathological and biochemical alternations of the heart induced by acute cadmium exposure in the freshwater crab Sinopotamon yangtsekiense.* Chemosphere. **84**(5): p. 689-94.

297. Bubel, A. (1976) *Histological and electron microscopical observations on the effects of different salinities and heavy metal ions, on the gills of Jaera nordmanni (Rathke) (Crustacea, Isopoda).* Cell Tissue Res. **167**(1): p. 65-95.

298. Konrad, C., G. Kiss, B. Torocsik, V. Adam-Vizi, and C. Chinopoulos. (2012) *Absence of Ca2+-induced mitochondrial permeability transition but presence of bongkrekate-sensitive nucleotide exchange in C. crangon and P. serratus.* PLoS One. **7**(6): p. e39839.

299. Konrad, C., G. Kiss, B. Torocsik, J.L. Labar, A.A. Gerencser, M. Mandi, V. Adam-Vizi, and C. Chinopoulos. (2011) *A distinct sequence in the adenine nucleotide translocase from Artemia franciscana embryos is associated with insensitivity to bongkrekate and atypical effects of adenine nucleotides on Ca2+ uptake and sequestration.* Febs J. **278**(5): p. 822-36.

300. Reynolds, J.A. and S.C. Hand. (2004) *Differences in isolated mitochondria are insufficient to account for respiratory depression during diapause in artemia franciscana embryos.* Physiol Biochem Zool. **77**(3): p. 366-77.

301. Kwast, K.E. and S.C. Hand. (1993) *Regulatory features of protein synthesis in isolated mitochondria from Artemia embryos.* Am J Physiol. **265**(6 Pt 2): p. R1238-46.

302. Smith, P.K., R.I. Krohn, G.T. Hermanson, A.K. Mallia, F.H. Gartner, M.D. Provenzano, E.K. Fujimoto, N.M. Goeke, B.J. Olson, and D.C. Klenk. (1985) *Measurement of protein using bicinchoninic acid.* Anal Biochem. **150**(1): p. 76-85.

303. Chinopoulos, C., S. Vajda, L. Csanady, M. Mandi, K. Mathe, and V. Adam-Vizi. (2009) *A novel kinetic assay of mitochondrial ATP-ADP exchange rate mediated by the ANT.* Biophys J. **96**(6): p. 2490-504.

304. Zuasti, A., C. Jimenez-Cervantes, J.C. Garcia-Borron, and C. Ferrer. (1998) *The melanogenic system of Xenopus laevis.* Arch Histol Cytol. **61**(4): p. 305-16.

305. Miwa, S. and M.D. Brand. (2005) *The topology of superoxide production by complex III and glycerol 3-phosphate dehydrogenase in Drosophila mitochondria.* Biochim Biophys Acta. **1709**(3): p. 214-9.

306. Akerman, K.E. and M.K. Wikstrom. (1976) *Safranine as a probe of the mitochondrial membrane potential.* FEBS Lett. **68**(2): p. 191-7.

307. Csanady, L. and B. Torocsik. (2009) *Four Ca2+ ions activate TRPM2 channels by binding in deep crevices near the pore but intracellularly of the gate.* J Gen Physiol. **133**(2): p. 189-203.

308. RF, E. (1986) *Electron Energy-loss Spectroscopy in the Electron Microscope, 1st edn.* . Plenum Press, New York.

309. Zolkiewska, A., A. Czyz, J. Duszynski, and L. Wojtczak. (1993) *Continuous recording of intramitochondrial pH with fluorescent pH indicators: novel probes and limitations of the method.* Acta Biochim Pol. **40**(2): p. 241-50.

310. Sievers, F., A. Wilm, D. Dineen, T.J. Gibson, K. Karplus, W. Li, R. Lopez, H. McWilliam, M. Remmert, J. Soding, J.D. Thompson, and D.G. Higgins. (2011) *Fast, scalable generation of high-quality protein multiple sequence alignments using Clustal Omega.* Mol Syst Biol. **7**: p. 539.

311. Gouet, P., E. Courcelle, D.I. Stuart, and F. Metoz. (1999) *ESPript: analysis of multiple sequence alignments in PostScript.* Bioinformatics. **15**(4): p. 305-8.

312. Shibuya, T. and Y. Tsujimoto. (2012) *Deleterious effects of mitochondrial ROS generated by KillerRed photodynamic action in human cell lines and C. elegans.* J Photochem Photobiol B. **117**: p. 1-12.

313. Giacomotto, J., N. Brouilly, L. Walter, M.C. Mariol, J. Berger, L. Segalat, T.S. Becker, P.D. Currie, and K. Gieseler. (2013) *Chemical genetics unveils a key role of mitochondrial dynamics, cytochrome c release and IP3R activity in muscular dystrophy.* Hum Mol Genet.

314. Nury, H., C. Dahout-Gonzalez, V. Trezeguet, G.J. Lauquin, G. Brandolin, and E. Pebay-Peyroula. (2006) *Relations between structure and function of the mitochondrial ADP/ATP carrier.* Annu Rev Biochem. **75**: p. 713-41.

315. Traba, J., E.M. Froschauer, G. Wiesenberger, J. Satrustegui, and A. Del Arco. (2008) *Yeast mitochondria import ATP through the calcium-dependent ATP-Mg/Pi carrier Sal1p, and are ATP consumers during aerobic growth in glucose.* Mol Microbiol. **69**(3): p. 570-85.

316. Cavero, S., J. Traba, A. Del Arco, and J. Satrustegui. (2005) *The calcium-dependent ATP-Mg/Pi mitochondrial carrier is a target of glucose-induced calcium signalling in Saccharomyces cerevisiae.* Biochem J. **392**(Pt 3): p. 537-44.

317. Kramer, R. and M. Klingenberg. (1977) *Reconstitution of inhibitor binding properties of the isolated adenosine 5'-diphosphate,adenosine 5'-triphosphate carrier-linked binding protein.* Biochemistry. **16**(23): p. 4954-61.

318. Aquila, H., W. Eiermann, W. Babel, and M. Klingenberg. (1978) *Isolation of the ADP/ATP translocator from beef heart mitochondria as the bongkrekate-protein complex.* Eur J Biochem. **85**(2): p. 549-60.

319. Woldegiorgis, G. and E. Shrago. (1985) *Adenine nucleotide translocase activity and sensitivity to inhibitors in hepatomas. Comparison of the ADP/ATP carrier in mitochondria and in a purified reconstituted liposome system.* J Biol Chem. **260**(12): p. 7585-90.

320. Brandolin, G., J. Doussiere, A. Gulik, T. Gulik-Krzywicki, G.J. Lauquin, and P.V. Vignais. (1980) *Kinetic, binding and ultrastructural properties of the beef heart adenine nucleotide carrier protein after incorporation into phospholipid vesicles.* Biochim Biophys Acta. **592**(3): p. 592-614.

321. Jiang, F., M.T. Ryan, M. Schlame, M. Zhao, Z. Gu, M. Klingenberg, N. Pfanner, and M.L. Greenberg. (2000) *Absence of cardiolipin in the crd1 null mutant results in decreased mitochondrial membrane potential and reduced mitochondrial function.* J Biol Chem. **275**(29): p. 22387-94.

322. Hoffmann, B., A. Stockl, M. Schlame, K. Beyer, and M. Klingenberg. (1994) *The reconstituted ADP/ATP carrier activity has an absolute requirement for cardiolipin as shown in cysteine mutants.* J Biol Chem. **269**(3): p. 1940-4.

323. Beyer, K. and M. Klingenberg. (1985) *ADP/ATP carrier protein from beef heart mitochondria has high amounts of tightly bound cardiolipin, as revealed by 31P nuclear magnetic resonance.* Biochemistry. **24**(15): p. 3821-6.

324. Perkins, M.E., J.M. Haslam, H.R. Klyce, and A.W. Linnane. (1973) *Bongkrekic acid resistant mutants of Saccharomyces cerevisiae.* FEBS Lett. **36**(2): p. 137-42.

325. Lauquin, G., P.V. Vignais, and J.R. Mattoon. (1973) *Yeast mutants resistant to bongkrekic acid, an inhibitor of mitochondrial adenine nucleotide translocation.* FEBS Lett. **35**(2): p. 198-200.

326. Zeman, I., C. Schwimmer, V. Postis, G. Brandolin, C. David, V. Trezeguet, and G.J. Lauquin. (2003) *Four mutations in transmembrane domains of the mitochondrial ADP/ATP carrier increase resistance to bongkrekic acid.* J Bioenerg Biomembr. **35**(3): p. 243-56.

12. Publications

12.1. Related to the thesis

Konrad, C., G. Kiss, B. Torocsik, V. Adam-Vizi, and C. Chinopoulos, *Absence of Ca2+-induced mitochondrial permeability transition but presence of bongkrekate-sensitive nucleotide exchange in C. crangon and P. serratus.* PloS one, 2012. **7**(6): p. e39839.

Konrad, C., G. Kiss, B. Torocsik, J.L. Labar, A.A. Gerencser, M. Mandi, V. Adam-Vizi, and C. Chinopoulos, *A distinct sequence in the adenine nucleotide translocase from Artemia franciscana embryos is associated with insensitivity to bongkrekate and atypical effects of adenine nucleotides on Ca2+ uptake and sequestration.* The FEBS journal, 2011. 278(5): p. 822-36.

12.2. Independent from the thesis

Kiss, G., C. Konrad, I. Pour-Ghaz, J.J. Mansour, B. Nemeth, A.A. Starkov, V. Adam-Vizi, and C. Chinopoulos, Mitochondrial diaphorases as NAD(+) donors to segments of the citric acid cycle that support substrate-level phosphorylation yielding ATP during respiratory inhibition. Faseb J, 2014. 28(4): p. 1682-97.

Kiss, G., C. Konrad, J. Doczi, A.A. Starkov, H. Kawamata, G. Manfredi, S.F. Zhang, G.E. Gibson, M.F. Beal, V. Adam-Vizi, and C. Chinopoulos, The negative impact of alpha-ketoglutarate dehydrogenase complex deficiency on matrix substrate-level phosphorylation. Faseb J, 2013. 27(6): p. 2392-406.

Doczi, J., L. Turiak, S. Vajda, M. Mandi, B. Torocsik, A.A. Gerencser, G. Kiss, C. Konrad, V. Adam-Vizi, and C. Chinopoulos, Complex contribution of cyclophilin D to Ca2+-induced permeability transition in brain mitochondria, with relation to the bioenergetic state. J Biol Chem, 2011. 286(8): p. 6345-53.

Chinopoulos, C., C. Konrad, G. Kiss, E. Metelkin, B. Torocsik, S.F. Zhang, and A.A. Starkov, Modulation of F0F1-ATP synthase activity by cyclophilin D regulates matrix adenine nucleotide levels. Febs J, 2011. 278(7): p. 1112-25.

Chinopoulos, C., A.A. Gerencser, M. Mandi, K. Mathe, B. Torocsik, J. Doczi, L. Turiak, G. Kiss, C. Konrad, S. Vajda, V. Vereczki, R.J. Oh, and V. Adam-Vizi, Forward operation of adenine nucleotide translocase during F0F1-ATPase reversal: critical role of matrix substrate-level phosphorylation. Faseb J, 2010. 24(7): p. 2405-16.

Vajda, S., M. Mandi, C. Konrad, G. Kiss, A. Ambrus, V. Adam-Vizi, and C. Chinopoulos, A re-evaluation of the role of matrix acidification in uncoupler-induced Ca2+ release from mitochondria. Febs J, 2009. 276(10): p. 2713-24.

13. Acknowledgements

Most importantly I would like to express my gratitude to my supervisor and tutor, Dr. Christos Chinopoulos. I know Christos as an energetic, open-minded, enthusiastic, patient, skeptical character, who has a deep knowledge in the literature and techniques in a broad spectrum of science. I recognize him as both an excellent scientist and mentor, and am thankful for the time I had spent as his student in the Department of medical Biochemistry.

I also wish to thank Gergely Kiss, with whom we become friends during our graduate years. We both had an interest for science, and he had convinced me to join the laboratory of Christos together. Keeping up with Gergely, as he is extremely fast learning, precise and creative did prove to be a challenge from time to time. His help and input was always valuable for my work.

I would like to express my gratitude to Professor Veronika Ádám, who provided me the opportunity for carrying out experiments in the Department of Medical Biochemistry, and also to all my colleagues in the Department, especially to Professor László Tretter and his group for the helpful discussions, and to Dr. Beáta Törőcsik, who did all the molecular biology work presented in this thesis.

Finally, I would like to thank my loving parents and my friends for the support they provided throughout my PhD studies.